

KSU PILE STANDARDIZATION AND STUDY OF
SLOWING DOWN AND DIFFUSION MODELS

by

LARRY RAY FOULKE

B. S., Kansas State University, 1960

A THESIS

submitted in partial fulfillment of the

requirements for the degree

MASTER OF SCIENCE

Department of Nuclear Engineering

KANSAS STATE UNIVERSITY
Manhattan, Kansas

1961

LD
2668
T4
1961
F68
C.2
Document

TABLE OF CONTENTS

INTRODUCTION	1
THEORY	4
Thermal Neutron Diffusion	4
Neutron Slowing Down	6
Solutions for Particular Conditions	8
EXPERIMENTAL FACILITIES	16
General Pile Description	16
Standard Pile Configuration	19
Finite Pile Configuration	19
Foil Counting Facilities	22
Neutron Probe Facilities	27
Traversing Mechanism	29
EXPERIMENTAL PROCEDURE	34
Foil Measurements	34
Neutron Probe Measurements in Standard Pile	36
Neutron Probe Measurements in Finite Pile	38
DATA PRESENTATION AND ANALYSIS	38
Pile Standardization Data Treatment	38
Empirical Fit of Indium Resonance Data	44
DISCUSSION AND RESULTS	50
Standardization Constants	50
Confidence Limits on Flux Assignment	57

TABLE OF CONTENTS (concl.)

Intercalibration with Argonne Standard Pile and Hanford Standard Pile	65
Theoretical Standardization of BF_3 Neutron Probe	69
Scintillation Probe Standardization	70
The Use of Gaussian Ranges and the Fermi Age to Describe Slowing Down	71
Study of Source Boundary Condition in Finite Pile	73
Suggestions for Further Work	89
ACKNOWLEDGMENT	91
LITERATURE CITED	92
APPENDICES	96
APPENDIX A: Solutions to the Fermi Age Equation and the Thermal Diffusion Equation for the Standard Pile Analysis....	97
APPENDIX B: Finite Pile Solution to the Thermal Diffusion Equation Using the Distributed Thermal Source Found from the Solution to the Fermi Age Equation...	102
APPENDIX C: Finite Pile Solution to the Thermal Diffusion Equa- tion Using a Point Source of Thermal Neutrons.....	106
APPENDIX D: Description and Explanation of the IBM-650 Compu- ter Program Used to Calculate the Flux in the Standard Pile	109
APPENDIX E: Description and Explanation of the IBM-650 Compu- ter Program Used to Calculate the Thermal Flux from a Fast Point Neutron Source in a Finite Pile...	117
APPENDIX F: Description and Explanation of the IBM-650 Compu- ter Program Used to Calculate the Thermal Flux from a Thermal Point Neutron Source in a Finite Pile. 127	
APPENDIX G: Description and Explanation of the IBM-650 Compu- ter Program Used for Empirically Fitting Experi- mental Data with the Sum of Several Terms of Gaussian Form	137
APPENDIX H: Considerations of Perturbations and Corrections Encountered in Experiments Using Finite Foils and Sources	146

INTRODUCTION

In investigations concerned with neutrons and their behavior, there is often a need for accurate measurement of a laboratory standard of absolute thermal neutron flux. In 1941, Anderson and Fermi (3) outlined a method of determining an absolute thermal neutron flux in a laboratory pile, based on theoretical and semi-empirical considerations. Seren (35) seems to have been the first to do the experimental work in his calibration of the Argonne Standard Pile in 1943. This pile was dismantled in 1946 and Redman (32) recalibrated what is now the Argonne Standard Pile. In 1954, Hanford Laboratories (11) published a report on the standardization of indium foils and gold foils in the Hanford Standard Pile. It is reasonable to think that other piles have been standardized as this method of pile standardization has been outlined in many references (11, 16, 20, 30).

A standardized pile is a large stack of graphite in which a neutron source of known strength has been placed, and an absolute thermal neutron flux has been defined. The spatial distribution of the slowing down density, q , at indium resonance energy can be measured with cadmium-covered indium foils. Assuming no leakage of epithermal neutrons in the z direction of the assumed infinite column and no absorption of epithermal neutrons, absolute values can be assigned to this measured distribution of the slowing down density since the volume integral of this slowing down density must equal the known neutron emission rate of the source, Q_0 . Empirically fitting the absolute slowing down density leads to an analytical expression which may be evaluated at thermal energy, and which then can

be used as a source term in the one velocity thermal diffusion equation. The solution to this equation is then taken to define the absolute flux. It is customary to use the neutron velocity of 2,200 meters per second (m/sec) in the calculation of the flux in a standard pile (20).

The confidence limits of such an absolute flux assignment are determined primarily by the accuracy of the source strength and the diffusion coefficient. It is reported by Hughes (20) that this method of flux assignment is within the error in the knowledge of the absolute source strength. Previous investigators (11, 35) seemed to have no question about uncertainty of the diffusion coefficient. However, recent measurements of the transport mean free path and the diffusion coefficient in graphite introduce additional uncertainty about assignments of absolute flux (6, 29)

The National Bureau of Standards (7) has made provision for producing a constant thermal neutron flux of 4,000 neutrons per square centimeter per second (n/cm^2 -sec) in a particular moderating geometry. This calibration has been made to an accuracy of ± 2 per cent by the absolute counting of α particles from the $B^{10}(n,\alpha)Li$ (7) reaction. It has been verified to within the limits of experimental accuracy by a comparison with an independent calibration by Oak Ridge National Laboratories. The National Bureau of Standards invites the exchange of activated gold foils between it and other national laboratories for the purpose of intercomparison of absolute flux. This has not been done at Kansas State University; however intercomparisons have been completed with Hanford Laboratories, and with Argonne National Laboratory.

Glasstone and Edlund (15) have assumed that for the experimental determination of the diffusion length, extraneous sources to the thermal

diffusion equation emit only thermal neutrons. This development appears to be adequate for describing what happens to the thermal flux near a concentrated source. The method of assuming that the source emits epithermal neutrons of age zero, and allowing their distribution in space and energy to be determined by the Fermi age equation, leads to the more accurate expression of a distributed thermal source for use in the thermal diffusion equation.

Some work with this coupling of the Fermi age equation and the thermal diffusion equation in addition to pile standardization has been done. A group at Hanford (10) used this method in an investigation of the diffusion length. They concluded that generally this fast source theory was preferable, but only in the case of a single source did the diffusion length obtained from thermal source theory differ appreciably from that obtained from fast source theory. A paper by Anselone (4) at Hanford in 1954 outlines the use of the "method of images" in determining theoretically the distribution of thermal neutrons from fast sources in exponential piles. A publication by Wallace and LeCaine (42) has an extensive compilation of these coupled solutions for various geometries.

Previous work at Kansas State University leading to this work has been the determination of the Fermi age both from theory and experiment by Steichen (39) and the determination of diffusion length in the KSU pile by Kaiser (22).

THEORY

Thermal Neutron Diffusion

Extensive treatment of the theory of thermal neutron diffusion can be found in many references (2, 15, 24, 43). It will be considered sufficient for this work to outline the basic theory of neutron diffusion and point out the assumptions and approximations involved.

The rate of change of the number of thermal neutrons in an elemental volume equals the number which flow in through the boundary of the elemental volume plus the number produced by sources minus the number captured per unit time. The equation expressing this principle of continuity at a steady state condition is

$$-\nabla \cdot \vec{j} + S(\vec{r}) - \Sigma_a n(\vec{r}) v = 0, \quad (1)$$

where n is the density of the thermal neutrons, v is their representative velocity. Σ_a is the absorption cross section of the medium, and S is the number of thermal neutrons produced per unit time per unit volume. The net number of neutrons, \vec{j} , flowing in unit time through a unit area normal to the direction of flow is the neutron current given by Fick's law of diffusion, the characteristic assumption of elementary diffusion theory

$$\vec{j} = -D \nabla n v. \quad (2)$$

In this, D is the diffusion coefficient for the monoenergetic flux, having the dimensions of length.

Using Eq. 2 in Eq. 1 gives the thermal diffusion equation, Eq. 3. Since for monoenergetic neutrons the neutron flux, ϕ , is equal to $n\nu$, this equation will be written

$$D \nabla^2 \phi - \Sigma_a \phi + S = 0 \quad (3)$$

where an isotropic medium has been assumed.

The conditions for the justification of diffusion theory and the diffusion equation include the following considerations:

(a) Collisions between neutrons do not occur, making the probability of collisions proportional only to ϕ . This results in linear equations describing the neutron diffusion. Weinberg and Wigner (43) point this out as the most important mathematical property of the diffusion equation. This makes superposition of solutions possible.

(b) The neutron scattering is spherically symmetric or isotropic. The isotropic distribution allows the velocity vector to be treated as a scalar in the equation of continuity. This assumption places a limitation on the diffusion equation near sources, boundaries, and absorbers since near them, the scattering is not isotropic.

(c) The nuclei of the isotropic, homogeneous moderator are at rest and of such high mass number with respect to a neutron that they do not recoil appreciably under the impact of neutrons (43).

(d) The neutrons are monoenergetic for which scattering occurs without energy loss. This allows the diffusion equation to be energy independent.

(e) The fractional change in the neutron flux and the mean free path over a distance of two or three mean-free paths is small (15). It can be shown on the basis of transport theory that Fick's law is not valid if this condition does not hold (15). Thus in regions near a concentrated source, absorber or boundary where the flux changes rapidly or the mean-free path is discontinuous, the neutron current cannot be represented as being proportional to the gradient of the flux.

(f) The diffusion medium is a weak absorber so that the scattering cross section can represent the total cross section, and therefore $\Sigma_a / \Sigma_s \ll 1$. This is tied in with condition (e) in that if the absorption cross section is appreciable, the neutron density may vary substantially within a mean-free path.

(g) The diffusion coefficient is independent of position. This allows D to be factored out of the term for divergence of the current in Eq. 3 leaving $D \nabla^2 \phi$ for $\nabla \cdot D \nabla \phi$.

(h) The general dimensions of the moderator are much larger than characteristic lengths such as the diffusion length in diffusion theory or the slowing down length in slowing down theory.

Neutron Slowing Down

The problem of neutron slowing down must be considered in order to determine the effective source to the thermal diffusion equation. The accurate theory here is quite complicated (43). For this treatment it will be sufficiently accurate to consider the slowing down process to be described by an approximate, continuous slowing down model given by

Fermi. It is based on the assumption of a functional relationship between a neutron's energy and its age, i. e., the time elapsed since its birth at a primary source.

The approximation is that for large neutron populations the neutrons lose energy in a continuous fashion rather than in discontinuous, discrete jumps as with a single neutron. This approximation cannot be valid in the event that a neutron may lose its entire energy in a single collision which is the case with moderators of low mass number.

The development of the Fermi age equation which describes the neutron slowing down process is given in considerable detail in a number of works (2, 15, 43). Assuming no capture of neutrons during slowing down, the Fermi age equation is

$$\nabla^2 q(\vec{r}, \tau) = \frac{\partial q(\vec{r}, \tau)}{\partial \tau} . \quad (4)$$

A new variable, the Fermi age has been introduced and is defined by

$$\tau(E_0, E) = \int_E^{E_0} \frac{D(E) dE}{\xi \Sigma_s(E) E} . \quad (5)$$

In the above expression, the slowing down density $q(\vec{r}, \tau)$ can be defined as the number of neutrons/cm³-sec which slow down past a given energy E , corresponding to the age τ , at a given point \vec{r} . E_0 is the energy of the source neutrons, E is the energy to which τ is measured and ξ is the average logarithmic energy decrement per collision. D is the diffusion coefficient, and Σ_s is the macroscopic scattering cross section.

Solutions for Particular Conditions

The solution to the Fermi age equation for a point neutron source emitting Q_0 monoenergetic neutrons per second in a finite parallelepiped of sides $2a$, $2b$, and $2c$ is derived in Appendix B, and given here as

$$q(x, y, z, \tau) = \sum_{m=1}^{\infty} \sum_{n=1}^{\infty} \sum_{0=1}^{\infty} Q_0 F_m(x) F_m(x_0) G_n(y) G_n(y_0) H_0(z) H_0(z_0) e^{-(\alpha_m^2 + \beta_n^2 + \gamma_0^2)\tau} \quad (6)$$

where

$$\begin{aligned} F_m(x) &= \frac{1}{\sqrt{a}} \cos \alpha_m x && \text{for } m \text{ odd} \\ F_m(x) &= \frac{1}{\sqrt{a}} \sin \alpha_m x && \text{for } m \text{ even} \\ F_m(x_0) &= \frac{1}{\sqrt{a}} \cos \alpha_m x_0 && \text{for } m \text{ odd} \\ F_m(x_0) &= \frac{1}{\sqrt{a}} \sin \alpha_m x_0 && \text{for } m \text{ even} \\ \alpha_m &= \frac{m\pi}{2a} . \end{aligned} \quad (7)$$

$G_n(y)$, $G_n(y_0)$, $H_0(z_0)$ are defined in the same manner, with the dimensions b and c corresponding to directions y and z , respectively. This solution will be referred to as the slowing down density in a finite pile from a fast source. It will be evaluated at the age corresponding to thermal energy and used as the distributed thermal neutron source in the thermal diffusion equation.

The one-dimensional solution to the Fermi age equation for a point source of monoenergetic neutrons at the origin of an infinite column of rectangular sides a and b is derived in Appendix A and given here as

$$q(z, \tau) = \frac{4Q_0}{ab\sqrt{4\pi\tau}} \sum_{j=1}^{\infty} \sum_{k=1}^{\infty} e^{-\pi^2\tau(j^2/a^2 + k^2/b^2)} e^{-z^2/4\tau}. \quad (8)$$

In this, z represents the distance from the source along the central Z axis of the infinite column, and j and k are summed over odd integers.

The $\sqrt{\tau}$ is often called the slowing down length or characteristic length. The quantity $2\sqrt{\tau}$ will be referred to as the Gaussian range and denoted by

$$r = 2\sqrt{\tau}. \quad (9)$$

Defining

$$c = \frac{4}{ab\sqrt{\pi}r} \sum_{j=1}^{\infty} \sum_{k=1}^{\infty} e^{-\frac{\pi^2 r^2}{4}(j^2/a^2 + k^2/b^2)}, \quad (10)$$

Eq. 8 becomes

$$q(z, \tau) = Q_0 c e^{-z^2/r^2}. \quad (11)$$

A quantity which is proportional to the slowing down density may be measured with some accuracy with cadmium-covered indium foils. There are some correction factors that must be applied to this measured distribution which will be introduced in the analytical part of this work. The cadmium covering filters out most of the neutrons with energies of 0.4 eV and below so that the activation of the indium foil is due primarily to neutrons with an energy of 1.44 eV,

corresponding to the energy of the resonance cross section of indium.

From the solution to the Fermi age equation in the infinite column, Eq. 11, it can be seen that the natural logarithm of the activity of cadmium-covered indium foils plotted against z^2 should yield a straight line with a slope of $-1/r^2$. However, the neutrons from a Pu-Be source are not monoenergetic but have a wide energy distribution as shown in Fig. 1. Hence, it is not unreasonable to find a curved line for this plot in Fig. 14. This curve might be considered to represent the superposition of the solutions for an infinite number of sources, each having a different monoenergy and thus a different Gaussian range. Thus Eq. 11 should be written

$$q(z, \tau) = Q_0 \sum_{i=1}^{\infty} f_i C_i e^{-z^2/r_i^2} \quad (12)$$

where f_i represents the fraction of the Q_0 neutrons emitted per second that are in the i^{th} energy group and r_i represents the Gaussian range from the energy level of the i^{th} group to the energy level of 1.44 ev.

Another solution for such a source distribution shown for the Pu-Be source in Fig. 1 would be found from a numerical integration of the point kernel over the source spectrum (43),

$$q(\vec{r}, \tau) = \sum_{i=1}^N \int_0^{\tau} d\tau_s S_i(\tau_s) \Psi_i(\vec{r}) e^{-B_i^2(\tau - \tau_s)} \quad (13)$$

$S_i(\tau)$ is the amplitude of the i^{th} harmonic from a source of age τ_s . $\Psi_i(\vec{r})$ represents the wave function satisfying the age

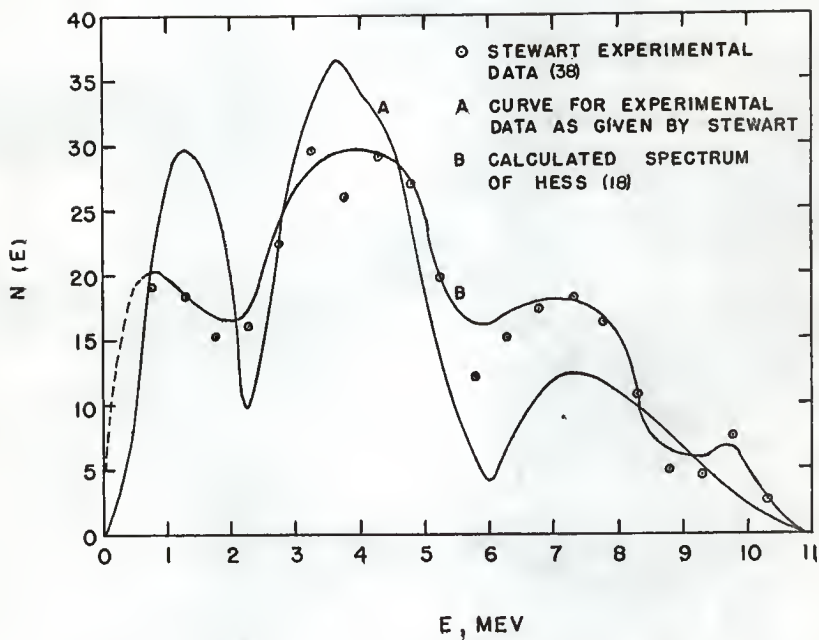


Fig. 1. Calculated and measured neutron energy spectrum for a Pu-Be neutron source.

equation and the boundary conditions, and B_i^2 represents the buckling of the distribution $\Psi_i(\vec{r})$.

An approximate fit of the quantity proportional to the slowing down density at indium resonance energy may be made with a finite number of the terms in Eq. 12.

$$q = Q_0 \sum_{i=1}^N f_i C_i e^{-z^2/r_i^2} \quad (14)$$

In terms of the experimental distribution, Eq. 14 is

$$A_{res} = \sum_{i=1}^N B_i e^{-z^2/r_i^2} \quad (15)$$

The f_i may be found from the experimentally determined amplitudes, B_i , and the constants C_i may be determined by Eq. 10. B_i is proportional to $f_i C_i$ and $\sum_{i=1}^N f_i = 1$. The combination of these relationships gives

$$f_i = \frac{B_i/C_i}{\sum_{i=1}^N B_i/C_i} \quad (16)$$

The result of this analysis gives an analytical expression, Eq. 14, for the absolute slowing down density to indium resonance energy if the absolute source strength Q_0 is known.

An experimentally determined Gaussian range to indium resonance energy may be extended to represent the Gaussian range to thermal energy by use of the definition of the age, Eq. 5, and by use of the relationship between age and Gaussian range, Eq. 9.

$$\tau(E_{oi}, E_{th}) = \tau(E_{oi}, E_{In}) + \tau(E_{In}, E_{th}) \quad (17)$$

or

$$\frac{r_{th-i}^2}{4} = \frac{r_{In-i}^2}{4} + \int_{E_{th}}^{E_{In}} \frac{D}{\xi \Sigma_s} \frac{dE}{E} \quad (18)$$

Using the Gaussian ranges to thermal energy, the absolute expression for slowing down density, Eq. 14, gives the number of neutrons slowing down to thermal energy per unit volume per second, i. e.,

$$q_{th}(z) = Q_0 \sum_{i=1}^N f_i C_i e^{-z^2/r_{th-i}^2} \quad (19)$$

This extrapolation of the resonance energy Gaussian ranges to thermal energy assumes that the moderating process described by the age equation applies until the neutron energy corresponds to thermal energy. At this point slowing down stops and the neutron is considered to diffuse at a constant thermal energy.

The solution to the thermal diffusion equation in the infinite column of rectangular sides a and b , using as a source term Eq. 19, the expression for absolute slowing down density to thermal energy, is derived in Appendix A and given here as

$$\begin{aligned} \phi(z) = & \sum_{i=1}^N \sum_{j,k=1}^{\infty} \frac{f_i Q_0 b_{jk}}{D a b} e^{-(\alpha_j^2 + \beta_k^2) \frac{r_{th-i}^2}{4}} e^{\frac{r_{th-i}^2}{4 b_{jk}}} \left\{ e^{-z/b_{jk}} \left[1 + \operatorname{erf} \left(\frac{z}{r_{th-i}} - \frac{r_{th-i}}{2 b_{jk}} \right) \right] \right. \\ & \left. + e^{z/b_{jk}} \left[1 - \operatorname{erf} \left(\frac{z}{r_{th-i}} + \frac{r_{th-i}}{2 b_{jk}} \right) \right] \right\} \quad (20) \end{aligned}$$

where

$$\frac{1}{b_{jk}^2} = \frac{1}{L^2} + \frac{\pi^2 j^2}{a^2} + \frac{\pi^2 k^2}{b^2} = \kappa^2 + \alpha_j^2 + \beta_k^2 \quad (21)$$

and

$$\text{erf}(x) = \frac{2}{\sqrt{\pi}} \int_0^x e^{-u^2} du \quad (22)$$

It is evident that if the nuclear constants of the moderator are known, the absolute neutron flux along the Z axis may be defined from Eq. 20. Once this absolute flux is defined, various thermal neutron detectors can be standardized against it so that a normalization factor will convert from count rate to flux. Such detectors will be referred to as standardized detectors.

To correct for the fact that neutron measurements cannot actually be made in a column of infinite height, the experimental thermal measurements must be adjusted so that it appears that they were made in a pile of infinite height. Actually the neutron flux goes to zero at the upper extrapolated boundary, h , of the actual finite column. Actual pile measurements may be adjusted by the familiar fundamental mode end correction factor used in diffusion length measurements (11),

$$C_e = \left[1 - e^{-2(h-z)/b} \right]^{-1} \quad (23)$$

The solution to the diffusion equation in a finite medium of sides $2a$, $2b$, and $2c$, using as a source term the distributed thermal source given by Eq. 6, is derived in Appendix B and given here as

$$\phi(x, y, z) = \sum_{m=1}^{\infty} \sum_{n=1}^{\infty} \sum_{0=1}^{\infty} \frac{Q_0 F_m(x) F_m(x_0) G_n(y) G_n(y_0) H_0(z) H_0(z_0)}{D(\alpha_m^2 + \beta_n^2 + \gamma_0^2 + \kappa^2)} e^{-(\alpha_m^2 + \beta_n^2 + \gamma_0^2)\tau} \text{th} \quad (24)$$

In this solution $F_m(x)$, $F_m(x_0)$, $G_n(y)$, $G_n(y_0)$, $H_0(z)$, $H_0(z_0)$ are given in Eqs. 7.

If the thermal diffusion equation in this geometry is sourced by a thermal point source the solution, derived in Appendix C, is

$$\phi(x, y, z) = \sum_m \sum_n \frac{Q_0}{D \gamma_{mn}} F_m(x) F_m(x_0) G_n(y) G_n(y_0) \frac{\sinh \gamma_{mn} (2c - z) \sinh \gamma_{mn} z_0}{\sinh 2\gamma_{mn} c} \quad (25)$$

Some note should be made of the inaccuracy in the assumption of a physical point neutron source. The source to the age equation should actually be given by the distribution of first collisions (27). It would be introduced into the age equation as a function of the mean free path and the distance from the source location

$$f_i Q_0 = \frac{f_i Q_0 e^{-z/\lambda_i}}{4 \pi z^2} \quad (26)$$

In this equation, λ_i represents the first collision mean free path of the neutrons in the i^{th} energy group. λ_i may be determined according to an equation given on page 200 of Reference 43.

EXPERIMENTAL FACILITIES

General Pile Description

The Kansas State University Standard Graphite Pile, shown in Fig. 2, in which all measurements were made, consisted of a rectangular parallelepiped, 68 inches square and 100 inches high, resting on a concrete foundation. The column was constructed by stacking layers of machined reactor grade graphite blocks, approximately 4 inches in cross section and of various lengths. In stacking, the long dimension of the graphite blocks was altered by 90° cross-lapping from layer to layer. As seen in Fig. 2, certain of the graphite blocks were drilled to a diameter of 1.75 inches along the lengths of the blocks. For this work, in the effort to make a homogeneous, solid moderator, each of the fuel ports contained graphite cylinders measuring 1.625 inches in diameter with each being 22.68 inches in length, and of the same material as the graphite blocks.

The graphite cylinders rested on the bottoms of the fuel ports, leaving crescent shaped air gaps between the tops of the cylinders and the tops of the fuel ports. The distance between the tops of the cylinders and the tops of the fuel ports was 0.125 inches. The blocks along the central vertical axis of the column contained horizontal foil slots with a cross section of 1.281 inches by 0.343 inches. These slots were such that graphite foil stringers, shown in Fig. 3, containing indium foils with their covering material, could be placed at approximately 4-inch intervals up the central axis of the column. The density of the solid

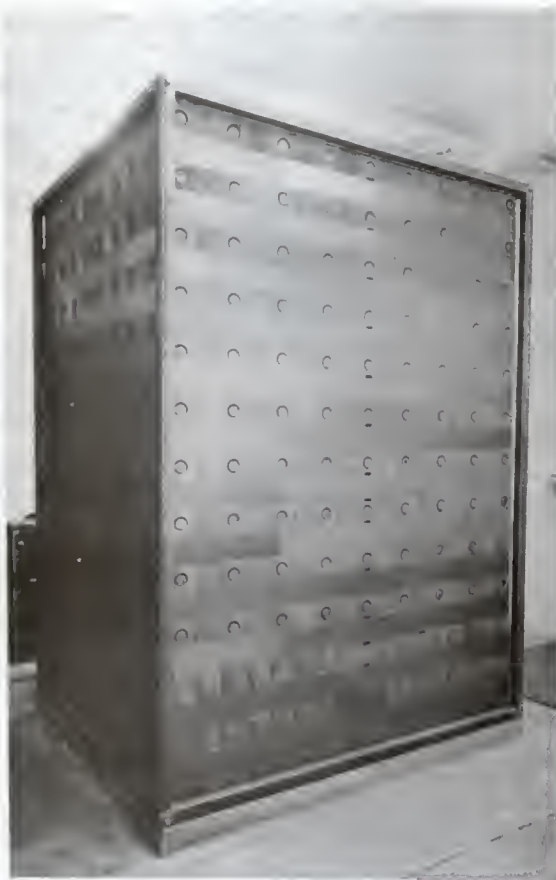


Fig. 2. KSU Standard Graphite Pile.

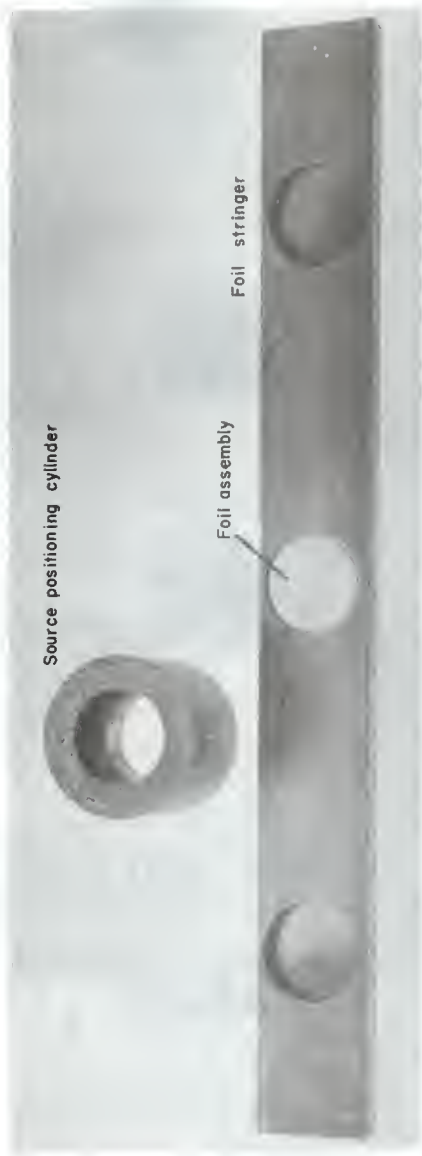


Fig. 3. Source positioning cylinder and foil stringer with foil assembly.

graphite blocks was 1.683 gm/cm^3 . Steichen (39) calculated the percentage of air voids to be approximately 0.3 per cent. The resulting effective density of the pile was 1.678 gm/cm^3 .

A summary of the physical specifications of the one curie Pu-Be neutron sources is given in Table 1.

A source was held in a graphite positioning cylinder, shown in Fig. 3, of inner diameter such that the sources fit snugly in the cylinders and of outer diameter such that the cylinders fit closely in the fuel ports of the graphite pile.

Standard Pile Configuration

For the standard pile analysis, a source in its graphite positioning cylinder, was located in the column in the bottom row of fuel ports (just above the pedestal) such that the central axis along the length of the source containers coincided with the horizontal central axis of the fuel port, and also so that the center of the source coincided with the vertical central axis of the pile. In this position, the center point of the source arrangement was 26 inches from the bottom, 74 inches from the top, and 34 inches from any side of the column.

A schematic diagram of the standard pile showing the various detector locations in relation to the source is shown in Fig. 4.

Finite Pile Configuration

For the finite pile analysis, a source was positioned in the plane of the fifth layer of fuel ports, in the same centering arrangement within the

Table 1. Summary of physical specifications of Plutonium-Beryllium neutron sources (8).

Source number	Grams Pu	Grams Be	Neutron emission rate (n/sec)
365	7.87	15.99	1.54×10^6
366	7.87	16.01	1.61×10^6
367	7.86	15.89	1.71×10^6
368	7.86	15.88	1.58×10^6
369	7.86	16.09	1.60×10^6

The inner container of each source is 0.85 inches in diameter, 0.90 inches in height, and is made of tantalum. The outside container of each source is 1.02 inches in diameter, 1.30 inches in height, and is made of stainless steel. All sources are sealed by welding. The melting point of tantalum is $5,425^{\circ}$ F. The melting point of 18-8 stainless steel is $2,600^{\circ}$ F.

The sources were calibrated by comparison to within ± 2 per cent of standards calibrated at the Los Alamos Scientific Laboratory. The absolute accuracy of the Los Alamos standard is reported as ± 5 per cent (7), thus giving an absolute accuracy of ± 7 per cent to the sources listed above.

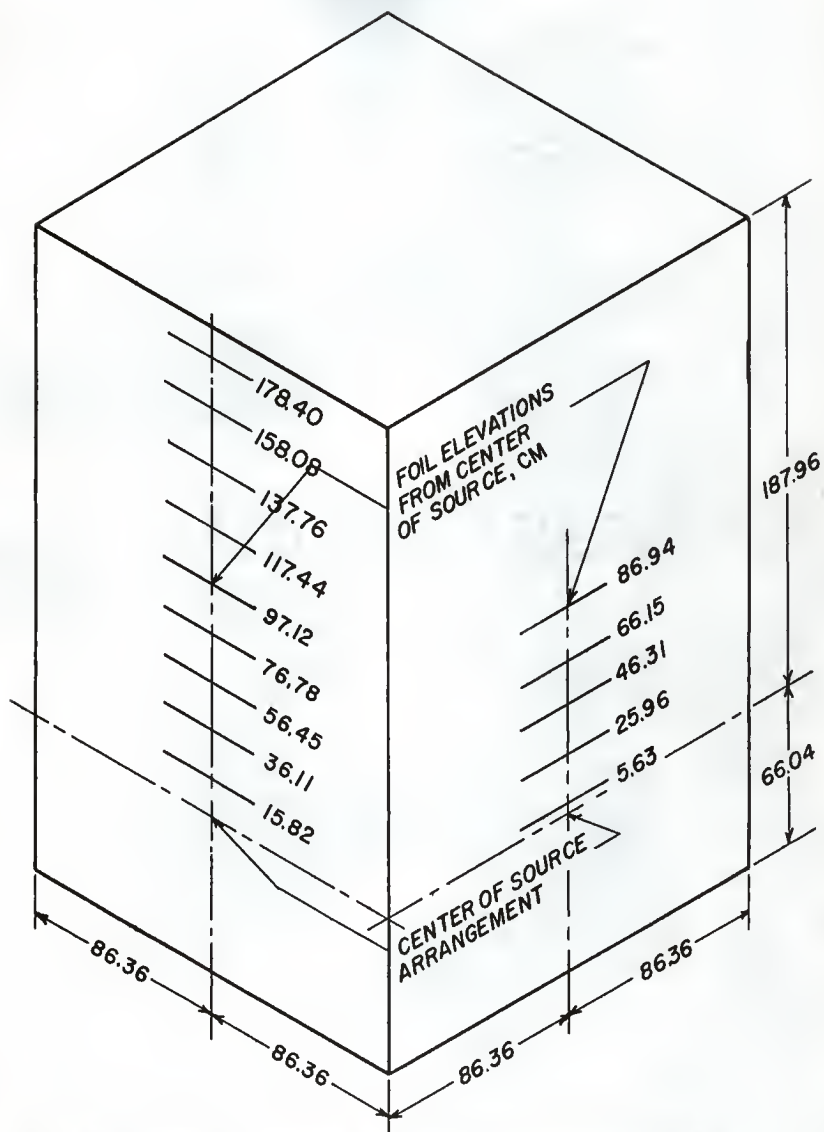


Fig. 4. Schematic diagram of KSU Standard Graphite Pile.

plane as was used with the standard pile arrangement. Cadmium sheets, approximately 0.020 inches thick were inserted in the plane separating the pedestal from the first row of fuel port blocks in order to create an artificial boundary at that point. Provision for this arrangement was made at the time of the original construction of the pile by inserting strips of 1100 aluminum alloy having a width of 0.50 inch and a thickness of 0.032 inch. The aluminum strips were spaced such that sheets of cadmium approximately 8 inches wide could be inserted easily.

The two uppermost layers of graphite were removed from the pile for the finite geometry measurements. This left the pile in such a state that it approximated a cube with sides of 68 inches, and with one source in the center of this cube. A schematic view of this pile arrangement is shown in Fig. 5.

Foil Counting Facilities

The indium foils, shown in Fig. 6, were 1.00 inches in diameter, had a thickness of approximately 0.005 inches, and weighed an average of 0.4592 gm, giving a mg/cm^2 thickness of 92.7. The foils were chosen such that their weights did not differ by more than one per cent.

The cadmium covers, shown in Fig. 6, were constructed by pressing them from a cadmium sheet. The covers had an inside diameter of slightly more than one inch and a wall thickness ranging from 0.021 inches to 0.022 inches. In addition to the cover, the foils were covered on both sides with cadmium disks of the same thickness as the covers, giving an overall average cadmium covering thickness of 0.043 inches.

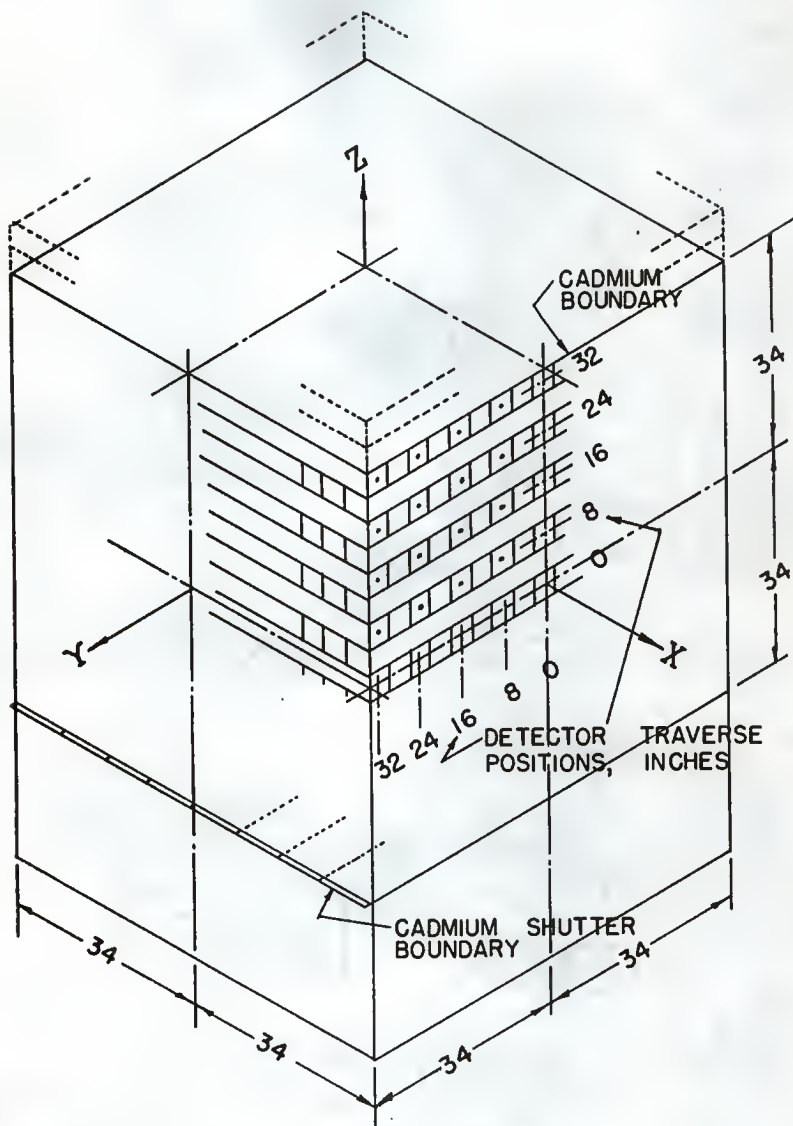


Fig. 5. Schematic diagram of finite pile.



Fig. 6. Cadmium covered foil assembly.

Aluminum covers were made in the same manner for the purpose of protecting and supporting the foil during bare foil measurements. Aluminum disks were inserted between the foil and the cover in order to duplicate the irradiation geometry used in the cadmium covered foil measurements.

The foil stringers, 0.125 inches by 0.325 inches by 12 inches, shown in Fig. 3, were constructed from the same material as the graphite blocks. The stringers were recessed so that the foils with their covering material could be positively positioned in the center of each stringer.

The foil counting system shown in Fig. 7 consisted of a B. J. Electronics Model DD7. continuous flow proportional counter, a Baird Atomic Model 255 proportional counter preamplifier, a Baird Atomic Model 132 scaler, and a Baird Atomic Model 322 timer. The KSU Nuclear Engineering Inventory No. of the scaler was 145, and the proportional counter, 369. The local identification of the preamplifier was KSU Nuclear Laboratory Inventory No. 10025. The proportional counter had a tungsten collector wire with a one half inch loop. The counting gas was Olin-Matheson P-10, a mixture of 10 per cent methane and 90 per cent argon.

The proportional counter was housed in a lead brick shield such that the minimum shield thickness at any point was at least 2 inches. A 0.020 inch thick aluminum tray was constructed to facilitate the removal and the positioning of the foil in the counter well.

The major portion of the foil counting system just described was due to the efforts of Steichen (39).

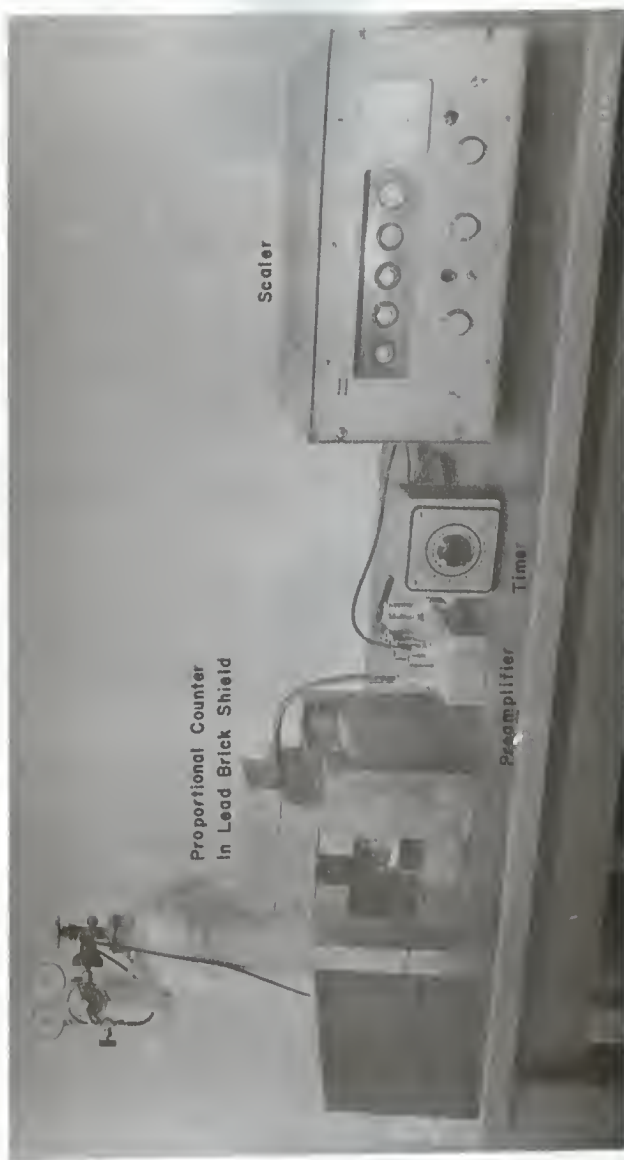


Fig. 2. Foil counting system.

Neutron Probe Facilities

The counting system used in the neutron probe measurements is shown in Fig. 8. Measurements were made with both a BF_3 probe, Nuclear Engineering Inventory No. 97, and a Scintillation probe, N. E. No. 99. The BF_3 probe counting system consisted of a Nuclear Chicago Model NC-202 BF_3 neutron probe, a Nuclear Chicago Model 1062 preamplifier, a Baird Atomic Model 132 scaler, a John Fluke Model 400 BDA high voltage power supply, a B. J. Electronics Model DM1-D count rate meter, and an Esterline Angus Model A.W. strip chart recorder.

The scintillation probe counting system was identical except that a Nuclear Chicago, Model DS8-10, scintillation detector, was substituted for the NC-202 BF_3 probe and its Model 1062 preamplifier.

The basic detector portion of the DS8-10 scintillation probe had a transistorized preamplifier and a 10-stage photomultiplier with cesium antimony dynodes, housed in a container 9-1/4 inches long by 1 inch diameter. The SN-6 neutron probe portion had a thermal neutron crystal which was a phosphor of silver activated zinc sulfide, 95 per cent enriched with boron-10. It was attached at the end of an aluminum covered lucite light pipe, 42 inches long by 5/16 inch outside diameter.

The BF_3 probe active volume, with length of 1/2 inch and diameter of 3/16 inch, contained B^{10}F_3 gas at a pressure of 70 cm Hg and at an enrichment of 96 per cent. The Model 1062 transistorized preamplifier had a length of 6.25 inches and a diameter of 1.5 inches.

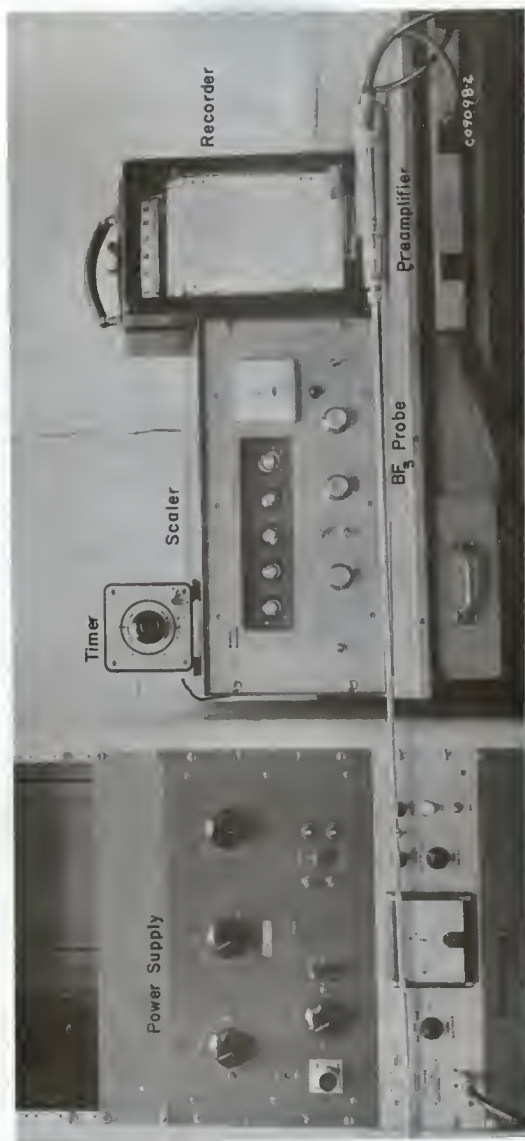


Fig. 8. Neutron probe counting system.

The BF_3 probe is shown with the counting system in Fig. 8; the scintillation probe is shown in Fig. 12.

Traversing Mechanism

For the purpose of supporting these two detectors in a variety of positions in the pile, a traversing mechanism was designed and built. A drawing of this mechanism is displayed as Fig. 9. Figures 10 and 11 include photographs of the complete assembly, and Fig. 12 shows a close-up view of the positioning device of the mechanism.

The mechanism was designed such that the detector could be positioned positively at any elevation between the limits of 19 inches and 101 inches. The detector could be positioned horizontally into the pile either by hand adjustment or motor powered adjustment. A cam action engaging device allowed the detector to be moved horizontally at the rate of one inch per minute by the motor and lead screw, or it allowed the detector to be positioned freely by hand. The mechanism was designed such that a maximum horizontal traverse of 40 inches was available.

The complete traversing mechanism could be moved to a different horizontal position on the face of the pile as a result of caster wheels mounted on the base. The base of the mechanism could be positioned firmly in a desired position with respect to the floor by use of the leveling screws at each corner of the base, which allowed the caster wheels to be raised from the floor.

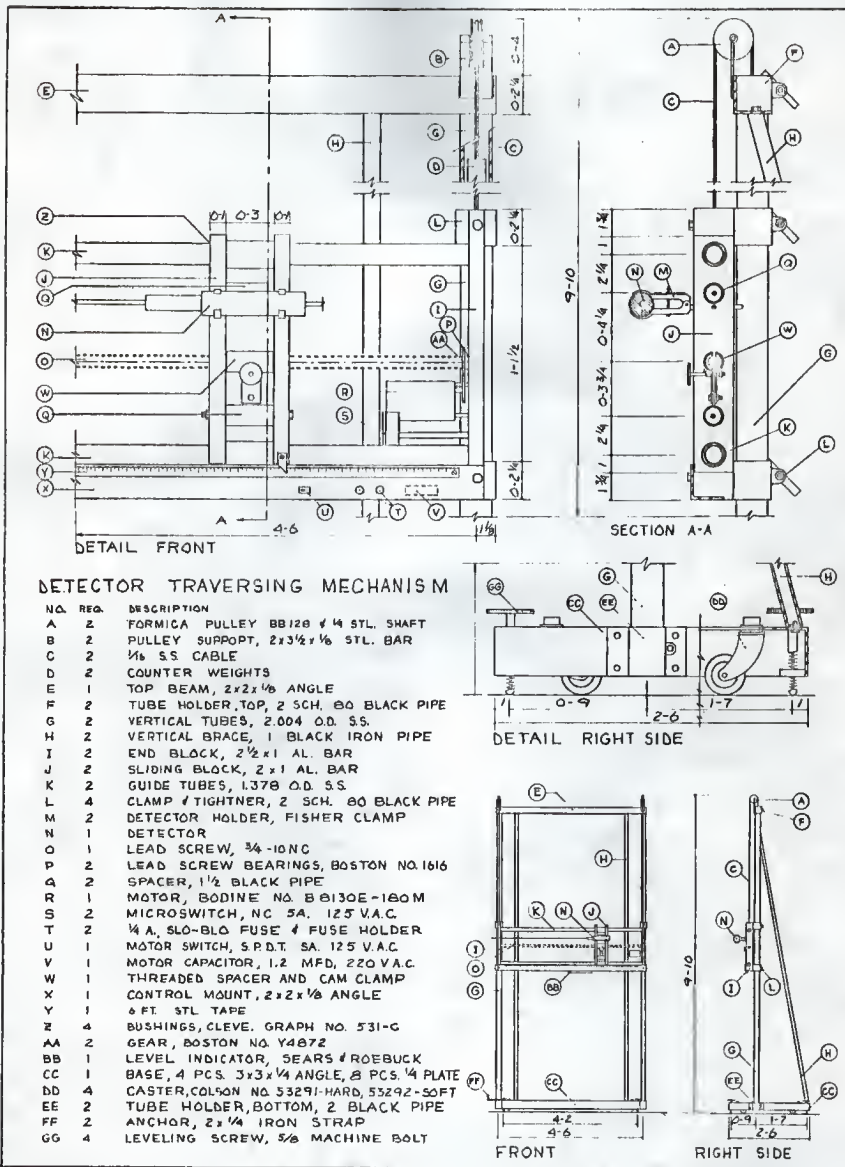


Fig. 9. Traversing mechanism for graphite pile, assembly drawing.



Fig. 10. Traversing mechanism and standard pile.



Fig. 11. Traversing mechanism and finite pile.

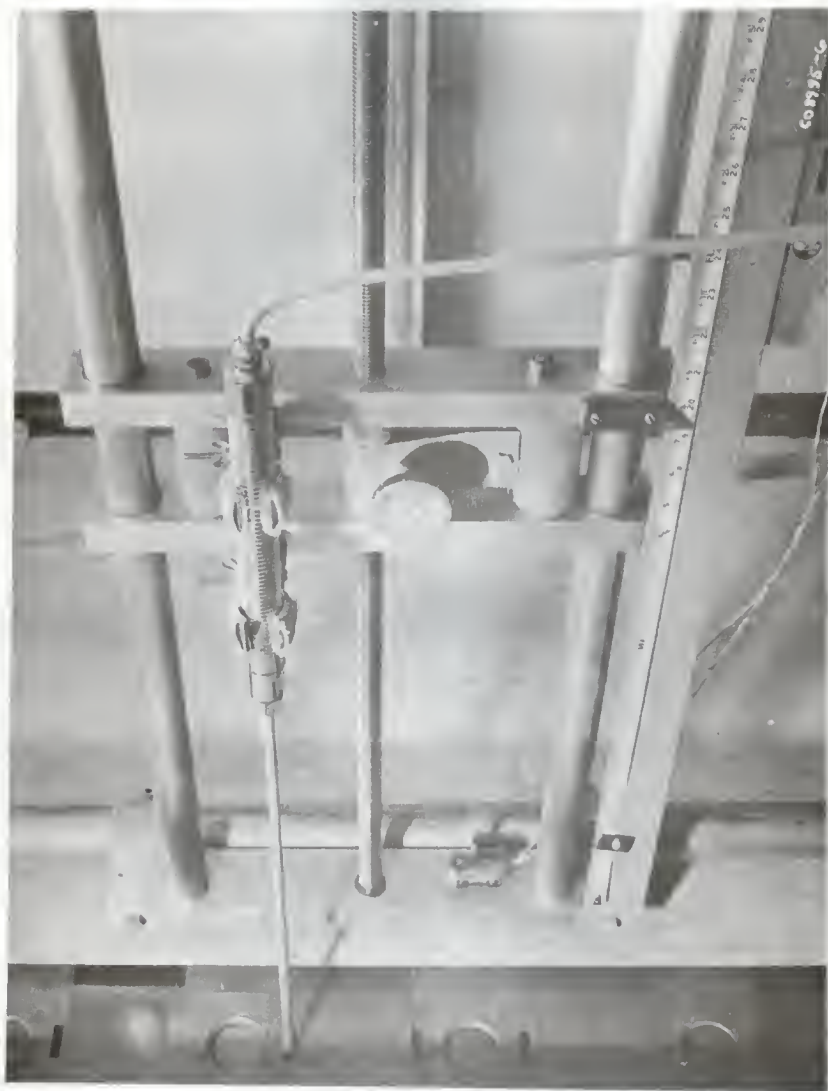


Fig. 12. Sliding assembly of traversing mechanism with scintillation probe.

In order to accommodate these neutron probes in a maximum number of positions and with the minimum amount of created void space, the three 1.652 inch diameter graphite cylinders, shown in Fig. 13, were drilled along their central axis to a diameter of 3/8-inch. Their use to accommodate a probe may be seen in Fig. 11.

EXPERIMENTAL PROCEDURE

Foil Measurements

All foil experiments were performed using one of the neutron sources described in Table 1. The source was placed in position in the pile as described in the section on experimental facilities. The foils in their appropriate covering material were placed in the foil stringer. The foil stringers were then placed in the pile such that the indium foils were centered on a line along the vertical axis of the column, directly above the center of the neutron source.

The foils were allowed to remain in the pile at least 7 hours until they reached equilibrium saturation activity with respect to the 54 minute half-life isotope. The foil nearest to the source was removed and a spare foil in an identical covering material was placed in the vacated position. The removed foil was allowed to "cool" for 3 minutes to assure the decay of the 13 second half-life isotope, and was then counted for a period of 27 minutes. At the end of the counting period, the foil second closest to the source was removed and the foil which had just been counted was immediately placed in the vacated position. This procedure was followed until all foils in the pile had been counted. A



Fig.13. Special graphite cylinders for accommodation of neutron probes.

total of eleven sets of data using cadmium covered indium foils were taken using this procedure. Of these eleven trials, 5 were made counting the activity of the source side of the foil, and 6 were made counting the side of the foil away from the source. A total of 4 sets of data were taken using aluminum covered indium foils. Of these 4 trials, 2 were made on each side of the foil. The background count was taken for a period of 27 minutes before and after the counting periods for each of the sets of data. The data for cadmium covered indium foils were taken by Steichen (39).

The counter was operated at 1,950 volts, and with a pulse height sensitivity setting of 0.2. A number of trials were made by Steichen using various sensitivity settings, foil-collector wire spacings, and sizes of collector wire loops, to obtain an optimum operating plateau and minimum counter background.

The counting system was checked for stability before and after each trial with standard Ra-D-E source, Nuclear-Chicago Serial No. 2354. All foil data used in pile standardization were taken with the counting system in such a condition that the count rate from the standard Ra-D-E source was within 200 counts of 17,048 counts per minute.

Neutron Probe Measurements in Standard Pile

All experiments with the neutron probes were performed using one of the neutron sources described in Table 1. Probe measurements were made in both the foil slots and the fuel ports. Measurements in the fuel

ports were made using the special graphite cylinders described in the section entitled "EXPERIMENTAL FACILITIES."

Probe data for the standard pile analysis were taken such that 10,000 counts were obtained in each selected position. For the BF_3 probe, this was done with 7 series of runs getting 1,000 counts in each position, and one run getting 3,000 counts in each position. For the scintillation probe, this was done with a series of 10 runs, getting 1,000 in each selected position.

BF_3 probe data were taken at an operating voltage of 1,450 volts, and a pulse height sensitivity setting of 0.8. Scintillation probe data was taken at the same pulse height sensitivity but with an operating voltage of 11,000 volts.

Before each series of runs, 10 one-minute counts were taken in a standard position to check for proper distribution and counter reproducibility. All BF_3 probe measurements were taken at an operating condition such that a count rate of $1,764 \pm 25$ counts per minute was obtained at a position 15.82 cm directly above source number 368 in the standard pile configuration. All scintillation probe measurements were taken at an operating condition such that a count rate of 2533 ± 57 counts per minute was obtained in this same standard position. The variance reported on these count ranges is the standard deviation of a single observation.

The count rate meter and the strip chart recorder were used to monitor the counting during periods of operator absence, thus insuring that no erratic data were recorded.

Neutron Probe Measurements in Finite Pile

All measurements for the experiment in the finite geometry which compared the various source conditions to the thermal diffusion equation were made with the standardized BF_3 probe operating at the conditions described in the previous section.

The medium was mapped by means of the special graphite cylinders placed in the five hole by five hole array of fuel ports of the upper, northwest $1/8$ th of the finite medium (see Fig. 5). By selecting positions at 4-inch intervals along the horizontal traverse into the special graphite cylinders, 9 positions were available in each of 24 fuel ports, and 8 positions were available in the one fuel port containing the source, thus making a total of 224 positions to be counted for each pile mapping. This procedure resulted in a 3-dimensional mapping using a net dimension of 4 inches by 8 inches by 8 inches.

The data were taken such that in each position, either 1,000 counts were obtained or 10 minutes counting time had elapsed, depending on which condition was met first. Each selected position was counted for at least 2 minutes. Four complete traverses of the 224 positions were made to get the average at each position as reported in the results.

DATA PRESENTATION AND ANALYSIS

Pile Standardization Data Treatment

The raw data averages used in the standard pile analysis were corrected for background and tabulated in Table 2. All data used in the pile

standardization were based on source No. 368 used by Steichen, having an emission rate of 1.58×10^6 neutrons per second (see Table 1). It is important to note that A_{In} , the activity of an aluminum covered or bare indium foil and A_{CdInCd} , the activity of a cadmium covered indium foil, has always been reported in this work as the total counts over the 27 minute counting period.

The foil data may be adjusted to give activity at the time of removal by well known decay laws which results in the equation,

$$\begin{array}{l} \text{Total counts in} \\ \text{27 minute counting} \\ \text{period} \end{array} = \int_{3 \text{ min}}^{30 \text{ min}} A_{Sat} e^{-\lambda_d t} dt. \quad (27)$$

Using λ_d as $0.012815 \text{ min}^{-1}$ for the appropriate decay constant of indium, the saturation activity at the time of removal from the pile may be found from

$$A_{Sat} = \left(\frac{\text{Total counts in 27 min-}}{\text{ute counting period}} \right) (0.0422). \quad (28)$$

This may be considered to be the saturation activity since the foils were always irradiated for seven half-lives or more.

Column 2 of Table 2 lists the cadmium covered indium foil data as measured by Steichen in his determination of the age of neutrons from a Pu-Be source in graphite (39). Columns 4 and 5 list the counts per minute obtained from BF_3 probe measurements and scintillation probe measurements. The error quoted in all cases is the standard deviation of the mean. It includes only the statistical

Table 2. Summary of standard raw data.

z	A_{CdInCd}	A_{In}	A_{BF_3}	A_{Sc}
cm	total counts in 27 minute count period	total counts in 27 minute count period	counts per minute	counts per minute
5.63	35,199.0 \pm 92.0	201,715 \pm 3,367	1,856.00 \pm 14.0	2,823.0 \pm 19.0
15.82	27,668.0 \pm 101.0	184,099 \pm 604	1,764.00 \pm 8.0	2,501.0 \pm 18.0
25.96	18,543.0 \pm 42.0	152,790 \pm 368	1,528.00 \pm 14.0	2,217.0 \pm 25.0
36.11	10,752.0 \pm 34.0		1,228.00 \pm 10.0	1,716.0 \pm 14.0
46.31	5,686.0 \pm 35.0	89,840 \pm 317	973.00 \pm 8.2	1,341.0 \pm 16.0
56.45	2,558.0 \pm 12.0	62,977 \pm 1,057	700.00 \pm 6.1	948.9 \pm 8.7
66.15	1,174.0 \pm 8.0		515.90 \pm 6.9	692.0 \pm 6.1
76.78	468.5 \pm 6.4	32,437 \pm 286	371.60 \pm 2.5	509.6 \pm 4.2
86.94	209.8 \pm 6.4	23,661 \pm 116	272.90 \pm 2.5	374.2 \pm 4.3
97.12	93.1 \pm 6.1		196.40 \pm 2.2	256.7 \pm 2.5
117.44		8,763 \pm 148	100.40 \pm 2.0	132.4 \pm 1.8
137.76		4,287 \pm 95	51.30	66.5 \pm 1.1
158.08			24.63	32.0 \pm 0.9
178.40			7.54	

error of the experimental data. Steichen's data for A_{CdInCd} were a combination of data taken with four sources and data taken with one source. The corrected activities for four source geometry were normalized to the one source geometry at 46.31 cm. Steichen felt that the four source data gave better statistics than the one source data at points far from the source. At these points, the correction for the finite size of the four sources became small.

The purpose of the foil measurements was to get quantities proportional to the thermal flux and the slowing down density at indium resonance energy. The activity due to thermal neutrons only was determined by means of a cadmium difference method. The foil was exposed to neutrons at a given position, first uncovered and then covered with a layer of cadmium 0.043 inches thick. Since cadmium absorbs the thermal neutrons, the activation of the cadmium covered indium foil was due primarily to epithermal neutrons while the uncovered indium foil activation was due to both thermal and epithermal neutrons. The difference in these two activations, the cadmium difference, after account was taken of the epithermal neutron absorption in the cadmium cover by the factor F_{Cd} (40), was taken to be proportional to the thermal flux.

$$(nv)_{\text{th}} = K_{\text{th}} A_{\text{th}} = K_{\text{th}}^0 F' (A_{\text{In}} - F_{\text{Cd}} A_{\text{CdInCd}}) \quad (29)$$

In this expression, K_{th} is the constant of proportionality between flux and cadmium difference activation which standardizes the detector. F' is a term containing considerations of perturba-

tions and corrections introduced through experimental limitations and finite foils. K_{th}^0 is the constant of proportionality which is independent of these corrections and perturbations.

The term F' may include the following considerations:

- a) activation of indium by higher energy resonance neutrons
- b) absorption of epithermal neutrons in the cadmium filter
- c) finite size of source and detector
- d) difference in foil weights and size
- e) unequal activation of two sides of foil
- f) flux depression in vicinity of foil
- g) self-shielding of the center of the foil by its outer layers
- h) mutual shadowing of neighboring foils
- i) hardening of the neutron spectrum through the foil
- j) obliquity of foil with respect to the source.

These correction factors are discussed further in Appendix H.

Reasons for consideration or rejection of individual correction factors are given, and the correction factors (a) through (e) which were used in this work are discussed quantitatively. The standardization constants determined in this thesis may be used only in graphite since many of the neglected correction factors depend upon the diffusing medium.

As outlined in the theory, the slowing down density at indium resonance energy may be taken to be proportional to the activation of a cadmium covered indium foil.

$$q_{\text{res}} = K_{\text{res}} A_{\text{res}} = K_{\text{res}}^0 F' A_{\text{CdInCd}} \quad (30)$$

F' again represents appropriate correction factors that may be applied to the foil activations.

It must be kept in mind that for a $1/v$ absorber such as indium in the thermal range and for a resonance absorber in the epithermal range, the foil activation is more correctly proportional to the density of thermal neutrons or to the density of resonance neutrons (16). Hence, for a foil of $1/v$ cross section, A_{th} is proportional to n_{th} , not $(nv)_{\text{th}}$, making K_{th} depend upon the energy distribution of the thermal neutrons. Thus, foils standardized in graphite for thermal flux cannot readily be extrapolated for use in any other medium where the energy distribution of the thermal neutrons may be different.

In the case of a slowing down density standardization, where A_{res} is proportional to n_{res} and q_{res} , the standardization constant for converting A_{res} to q_{res} cannot be directly used in media other than graphite (16) since

$$q_{\text{res}} = \frac{n_{\text{res}} v_{\text{res}} \xi}{\lambda} = K_{\text{res}} A_{\text{res}} \quad (31)$$

where λ represents the scattering mean free path. To convert from graphite to water, the slowing down density standardization constant in water would have to be expressed (16) as

$$K_{\text{res}}(\text{water}) = K_{\text{res}}(\text{graphite}) \frac{\lambda(\text{graphite}) \xi(\text{water})}{\lambda(\text{water}) \xi(\text{graphite})} \quad (32)$$

Table 3 presents the corrected foil activations A_{res} and A_{th} which are considered to be proportional to the slowing down density at indium resonance energy and the thermal neutron flux, respectively. The end correction factor given by Eq. 23 in the theory, which adjusts the finite pile measurements to make them appear as if they had been taken in an infinite pile, is given in Column 4 of Table 3. Columns 5, 6, and 7 give the adjusted infinite pile measurements with foils, the BF_3 probe and the scintillation probe. Perturbations of the thermal flux by the two probes have not been considered. The count rates from these two instruments have been assumed to be proportional to the thermal neutron density, so that they are subject to the restriction that the standardization constant found in graphite is not useable in a medium where the energy distribution of the thermal neutrons may be different. The thermal standardization constants for these detectors will be found from the relationships

$$(nv)_{\text{th}} = K_{\text{th}} (\text{BF}_3) R_{\text{BF}_3} \quad (33)$$

and

$$(nv)_{\text{th}} = K_{\text{th}} (\text{Sc}) R_{\text{Sc}} \quad (34)$$

where R signifies count rate.

Empirical Fit of Indium Resonance Data

It may be recalled from the theoretical development of the standard pile analysis that an empirical fit of the quantity proportional to the slowing down density at indium resonance was

Table 3. Summary of experimental measurements for standard pile analysis.

Distance from source cm	A _{res} Counts in 27 minute counting period	A _{th} Counts in 27 minute counting period	C _e	A _{th} C _e Counts in 27 minute counting period	R _{BF₃e} Counts/min.	R _{Sc e} Counts/min.
5.63	32,623.0 ± 92	164,820 ± 3,370	1.0000	164,820	1,856.0	2,823
15.82	26,738.0 ± 101	153,967 ± 612	1.0000	153,967	1,764.0	2,501
25.96	18,335.0 ± 42	132,239 ± 470	1.0000	132,239	1,528	2,217
36.11	10,817.0 ± 34		1.0000		1,228	1,716
46.31	5,673.0 ± 35	83,546 ± 319	1.0000	83,546	973.7	1,341
56.45	2,576.0 ± 12	60,109 ± 1,056	1.0000	60,109	700.0	948.9
66.15	1,159.0 ± 8		1.0000		515.9	692.0
76.78	470.7 ± 6.4	31,914 ± 286	1.0000	31,914	371.6	509.6
86.94	212.5 ± 6.4	23,415 ± 116	1.0000	23,415	272.9	374.2
97.12	92.9 ± 6.1		1.0030		197.0	257.5
117.44		8,763 ± 148	1.0110	8,859	101.5	133.9
137.76		4,287 ± 95	1.0400	4,458	53.35	69.2
158.08			1.1570		28.50	37.02
178.40			1.9608		14.78	

required in order to express the slowing down density in the analytical form of Eq. 14. An IBM-650 code was developed for this purpose of fitting the data with a function of Gaussian form. It is given in Appendix G.

This fit was made by a trial and error procedure which strived to minimize the sum of the weighted squares of the residuals between the experimental values and the values calculated from the empirical expression. Tables 4 and 5 summarize these efforts to fit empirically the resonance data. The effect of various correction factors applied to the resonance data, the effect of the number of terms used in the finite summation, and the effect of a weighting function were studied.

The best fit may be considered on the basis of two different criteria; one, that the sum of the weighted residuals squared be a minimum; or two, that the residual between the calculated and experimental value at any point should lie within the statistical standard deviation of the experimental measurement. A weighting function of unity allows the former criterion to be satisfied more satisfactorily. Scarborough (33) points out that the residuals squared are best weighted with the reciprocal of the standard deviation squared $1/\sigma^2$. This weighting function allows the latter criterion to be satisfied more completely.

A consideration of interest was the necessary number of terms needed in Eq. 14 to fit adequately the resonance data. Since the fit was made to only ten data points, there was some limitation on the number of terms which could be used, each term having two parameters.

Table 4. Summary of resonance data fits.

Distance from source in cm	5.63	15.82	25.96	36.11	46.31	56.45	66.15	76.78	86.94	97.12	Sum of squares of residuals	
												Experimental deviations
No. of terms	Weight function	Residuals between experimental values and calculated values										
Raw	3	1	(-4.3)	(12.3)	-43.0	93.7	-107.7	34.3	(-1.2)	19.5	(4.6)	(1.5) 2.40x10 ⁴
G	3	1	(-5.6)	(18.1)	-47.5	89.3	-105.0	37.3	(0.2)	18.3	(3.3)	(0.3) 2.35x10 ⁴
W	3	1	(-4.0)	(11.3)	(-29.7)	49.8	-62.2	24.5	9.4	7.4	-7.0	(-4.1) 8.17x10 ³
R	3	1	(37.0)	(-66.4)	(5.1)	81.8	-99.6	56.6	(-3.1)	(-1.8)	-11.8	(-1.6) 2.58x10 ⁴
GW	3	1	(-3.3)	(9.2)	(-26.5)	47.8	-63.5	24.2	11.0	7.9	-6.7	(-4.4) 7.94x10 ³
GR	3	1	(37.2)	(-67.5)	(5.8)	81.6	-99.6	56.5	(-2.6)	(-2.1)	-11.8	(-1.9) 2.59x10 ⁴
RW	3	1	(14.4)	(-30.9)	(21.4)	(17.7)	-63.8	49.6	15.6	-6.7	-19.4	(-6.1) 9.17x10 ³
GWR	3	1	(13.0)	(-31.1)	(23.5)	(15.5)	-64.6	48.3	16.1	(-6.2)	-18.0	(-4.9) 9.08x10 ³
GWR	4	1	(15.8)	(-37.2)	(24.9)	(22.4)	-66.8	41.8	14.9	(-2.8)	-15.2	(-2.8) 9.43x10 ³
GWR	2	1	(-56.5)	(30.9)	102.1	(-16.3)	-150.0	19.2	55.2	52.4	18.1	(4.6) 4.39x10 ⁴
GWR	1	1	289.5	110.0	391.0	141.0	-312.0	-366.0	-355.0	-250.0	-159.0	-82.0 7.21x10 ⁵
GWR	3	1/ σ^2	(-27.3)	(-29.5)	(33.6)	(-7.2)	-110.3	(12.2)	(1.9)	(-2.5)	-7.8	(5.5) 1.51x10 ⁴
GWR	4	1/ σ^2	(-10.7)	(-37.4)	(26.4)	(-8.0)	-101.0	15.0	(2.6)	(-2.6)	-8.4	(6.8) 1.28x10 ⁴

Key to data treatment: G Geometry correction factor considered

W Weight correction factor considered

R Higher resonance absorption by indium foil correction factor considered

() Residual lies within experimental standard deviation

Table 5. Study of amplitudes and ranges of resonance fits.

Data treatment	No. of terms	Weight function	Values of ranges, amplitudes and fractions												
			1st term			2nd term			3rd term			4th term			
			r ₁	B ₁	f ₁	r ₂	B ₂	f ₂	r ₃	B ₃	f ₃	r ₄	B ₄	f ₄	$\sum_{i=1}^4 f_i^2/4$
Raw	3	1	16.70	4,711	0.015	33.25	28,223	0.686	50.85	3,442	0.299				384.2
G	3	1	16.85	4,787	0.015	33.25	28,238	0.685	50.56	3,516	0.300				332.1
W	3	1	16.21	4,583	0.013	33.42	28,183	0.698	50.44	3,395	0.289				379.6
R	3	1	26.39	10,546	0.128	36.95	22,455	0.750	63.88	703	0.122				402.4
GW	3	1	16.07	4,488	0.012	33.31	28,280	0.692	50.06	3,566	0.296				378.1
GR	3	1	26.48	10,713	0.131	36.96	22,448	0.749	63.76	700	0.120				400.6
RW	3	1	26.50	10,328	0.128	37.05	22,446	0.758	63.13	684	0.114				396.5
GWR	3	1	26.61	10,495	0.131	37.05	22,445	0.755	63.48	673	0.114				397.2
GWR	4	1	24.38	5,335	0.050	34.00	22,914	0.579	44.65	5,269	0.302	97.09	101	0.069	488.6
GWR	2	1	31.56	22,574	0.572	47.79	5,937	0.428							386.7
GWR	1	1	34.30	33,217	1.000										294.1
GWR	3	1/ σ^2	27.31	11,112	0.149	36.94	21,756	0.722	65.44	695	0.129				411.9
GWR	4	1/ σ^2	24.79	5,250	0.048	33.90	23,108	0.545	44.69	5,128	0.277	113.08	100	0.129	708.0

Key to data treatment: G Geometry correction factor considered
W Weight correction factor considered
R Higher resonance absorption by indium foil correction factor considered.

A fit of the data with one term was considered poor since the residual was much greater than the standard deviation at all experimental points. A fit with two terms was clearly an improvement since the sum of the weighted squares of the residuals decreased by over a factor of ten. The weighted three-term fit of the data corrected for geometry, higher resonance absorption and foil weights, was considered to be the best fit. The residuals of this fit were within or near the standard deviation of the experimental data for all points but one. The fit at 46.31 cm was consistently poor no matter what manner of fit was used. It may be seen from either the individual residuals or the sum of the weighted residuals squared that a fit with four terms did not give an improvement over a fit using three terms. Inspection of the fourth term in the fit reveals the effort of the machine to suppress the fourth term by giving it a small amplitude and a slope tending towards zero, the slope being equal to the reciprocal of the square of the Gaussian range associated with this term.

Consideration of the difference in foil weights had a noticeable improving effect upon the empirical fit. Little improvement was gained from using the correction factors for finite detector and source. The use of the correction factor for absorption of neutrons by the higher resonances of indium markedly changed the various amplitudes, B_i , the Gaussian ranges, r_i , and the fractional contributions, f_i .

Using the parameters of the appointed best fit, the expression for the indium resonance data distribution was

$$A_{res} = 11,112 e^{-\left(\frac{z}{27.31}\right)^2} + 21,756 e^{-\left(\frac{z}{36.94}\right)^2} + 695 e^{-\left(\frac{z}{65.44}\right)^2} \quad (35)$$

From Eq. 14, the absolute slowing down density to indium resonance energy was

$$\frac{q_{res}}{Q_0} 10^6 = 1.314 e^{-\left(\frac{z}{27.31}\right)^2} + 2.572 e^{-\left(\frac{z}{36.94}\right)^2} + 0.824 e^{-\left(\frac{z}{65.44}\right)^2} \quad (36)$$

The IBM-650 program required initial estimates of the fitting parameters which were found from a "stripping-off" procedure. Shown in Fig. 14 are the three "stripped-off" curves which have been superimposed to give the empirical fit of the experimental points.

DISCUSSION AND RESULTS

Standardization Constants

Table 6 lists the values of absolute flux and slowing down density in the Kansas State University Standard Pile, using a source with an emission rate of 1.58×10^6 neutrons per second. The absolute slowing density was determined from Eq. 36. The absolute thermal flux was obtained from the computer code described in Appendix D which numerically evaluated the absolute flux defined by Eq. 20. This code used the empirically determined parameters f_i and r_i after r_i had been extended to thermal energy by Eq. 18. Figures 15 and 16 show the absolute flux and the absolute slowing down density to indium resonance energy. Superimposed upon these calculated curves are

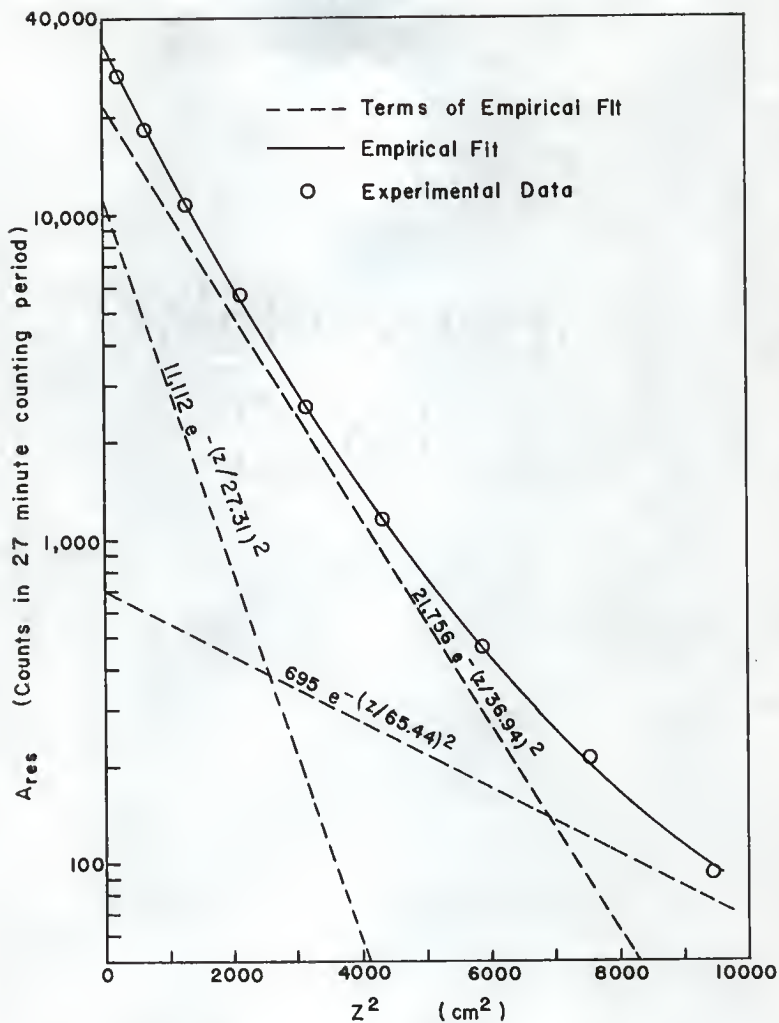


Fig. 14. Indium resonance distribution as empirically fit by three terms of Gaussian form.

Table 6. Summary of standardization constants and standard pile flux.
 $Q_0 = 1.58 \times 10^6 \text{ n/sec.}$

Distance from source	q_{res}	$(nv)_{th}$	$K_{res}(foil) = \frac{q_{res}}{A_{res}}$	$K_{th}(foil) = \frac{(nv)_{th}}{A_{th} C}$	$K_{th}(BF_3) = \frac{(nv)_{th}}{A_{BF_3} C}$	$K_{th}(Sc) = \frac{(nv)_{th}}{A C}$
cm	$n/cm^3\text{-sec}$	$n/cm^2\text{-sec}$	Density per count in 27 minute counting period	Flux per count in 27 minute counting period	Flux per count per minute	Flux per count per minute
5.63	6.090	2,233.	0.00016903	0.01355	1.2031	0.7910
15.82	4.990	2,058.	0.00016088	0.01337	1.1667	0.8229
25.96	3.432	1,768.	0.00016136	0.01337	1.1571	0.7975
36.11	2.021	1,430.	0.00016106	0.01318	1.1645	0.8333
46.31	1.040	1,101.	0.00015803	0.01368	1.1307	0.8210
56.45	0.4842	822.1	0.00016205	0.01361	1.1744	0.8664
66.15	0.2173	609.4	0.00016168	0.01335	1.1812	0.8806
76.78	0.08768	434.02	0.00016058	0.01323	1.1685	0.8520
86.94	0.03836	312.7	0.00015662	0.01376	1.1458	0.8356
97.12	0.01841	225.0	0.00017078	0.01346	1.1421	0.8738
117.44		117.2			1.1547	0.8753
137.76		61.32			1.1494	0.8861
158.08		32.15			1.1281	0.8861
178.40		16.89			1.1428	0.8684
Average Standardization Constant :						
			0.00016130	0.01346	1.1578	0.8465
			± 0.00000122	± 0.00070	± 0.0055	± 0.0088

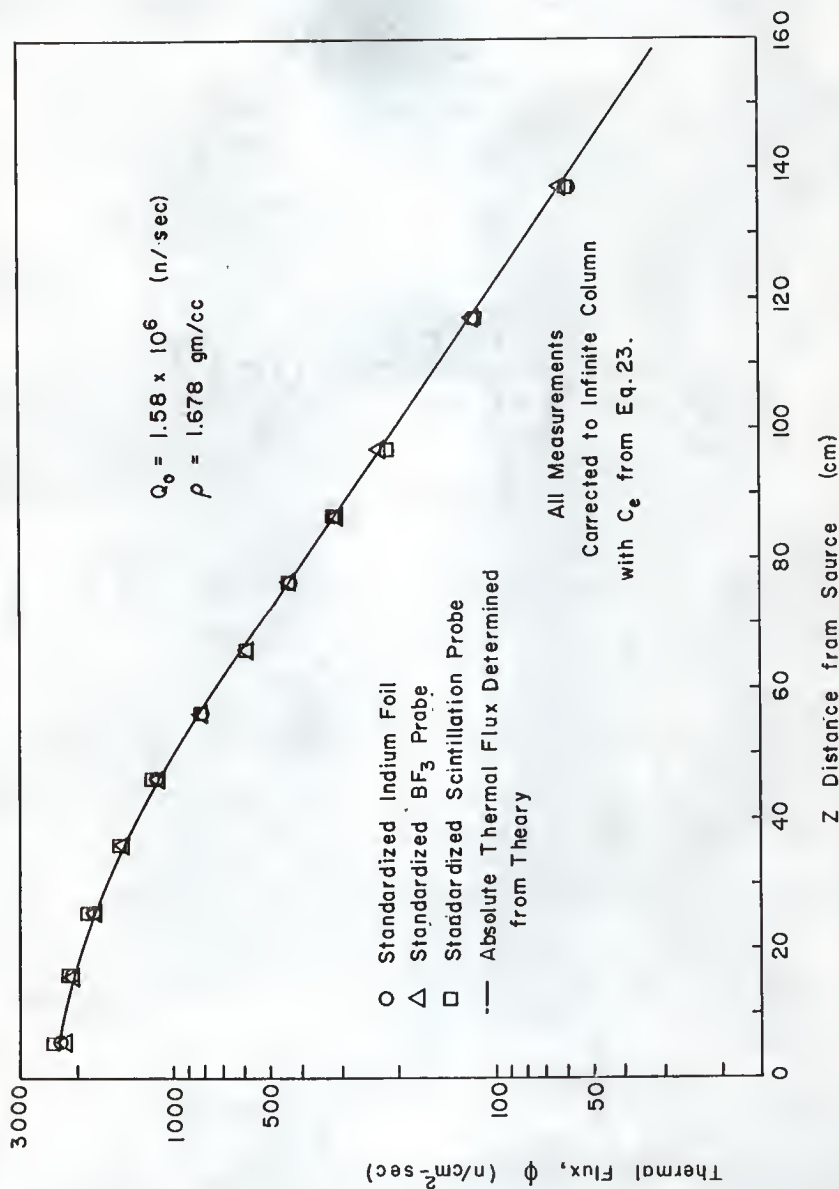


Fig. 15. Thermal flux in KSU Standard Pile.

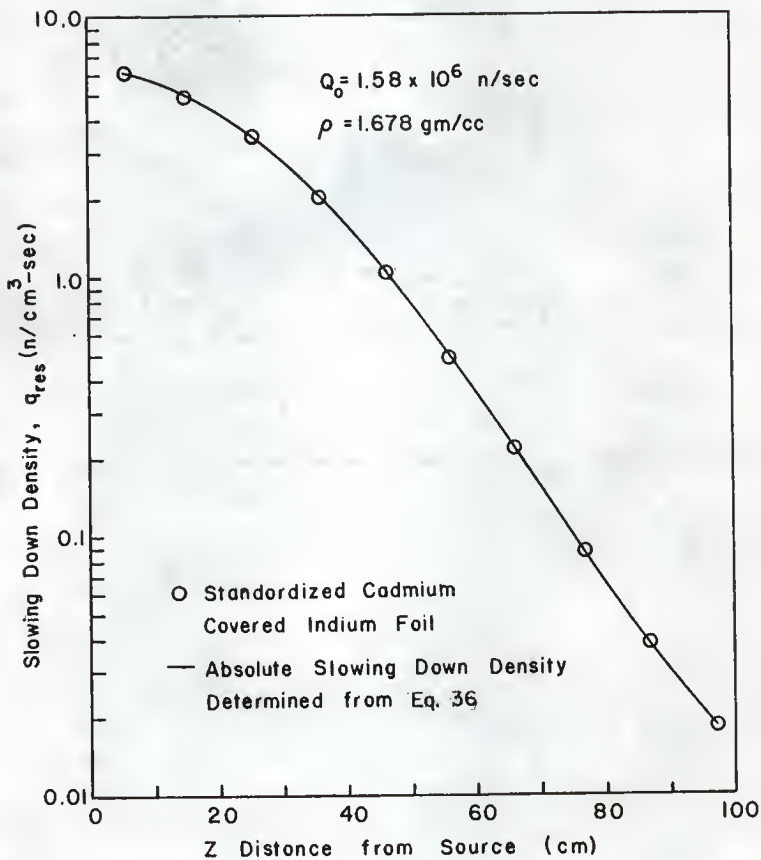


Fig. 16. Slowing down density to indium resonance energy in KSU Standard Pile.

points showing absolute quantities as determined by detectors which have been standardized according to this thesis.

Columns 4 through 7 of Table 6 list the standardization constants of the various detectors as they were determined in the standard pile analysis. The average standardization constant is listed at the bottom of each column.

Figures 17 show the variation of the measured standardization constants for each detector as a function of the distance from the source. Since the spectrum is harder near the source, a non-random distribution of these constants would indicate a possible energy dependence in the assumed thermal neutron detectors. It can be seen from Figs. 17 that the distributions appear to be random with respect to the average for all detectors except the scintillation probe. The standardization constant distribution of the scintillation probe suggests that the scintillation probe has an appreciable sensitivity for neutrons of epithermal energies. In order to determine a more reliable standardization constant for the scintillation probe, it would be necessary to use a cadmium difference technique such as that used with the indium foils.

Subsequent use of these standardization constants has been made with the average standardization constant.

The absolute flux or slowing down density in a graphite medium may be found from a particular standardized detector by merely multiplying its standardization constant by a properly measured quantity. In the case of the Kansas State University BF_3 probe or scintillation probe, this quantity is counts per minute, corrected for background. In the

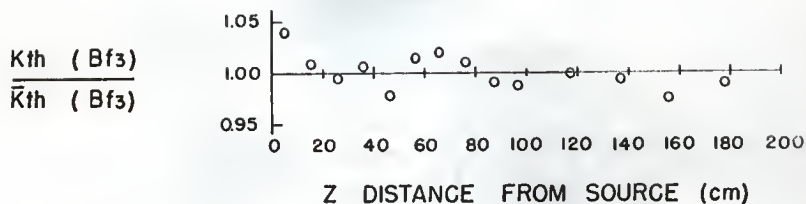


Fig. 17a. Distribution of BF_3 thermal standardization constants about average.

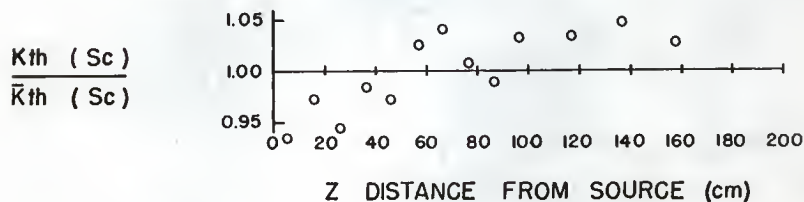


Fig. 17b. Distribution of scintillation probe thermal standardization constants' about overage.

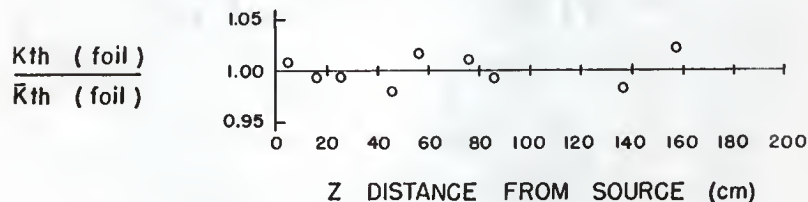


Fig. 17c. Distribution of foil thermal standardization constants about overage.

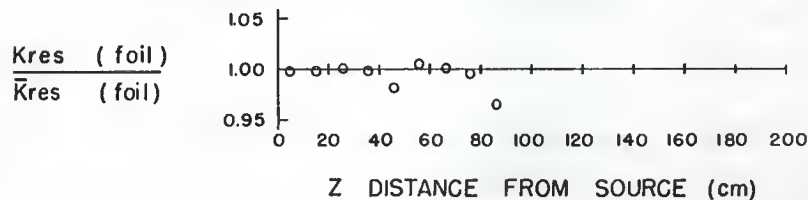


Fig. 17d. Distribution of foil resonance standardization constants about overage.

case of KSU standard indium foils, the quantity is expressed in terms of total counts over the 27 minute counting period as explained in the experimental outline.

From Eq. 28, it was shown that for foil measurements this properly determined quantity could be the saturation activity at the time of foil removal from the pile if the standardization constant is used as $K(\text{foil})/0.0422$.

Before a standardization constant may be used, it must be verified that the counting system reproducibility has not changed. This can be done by reproducing the counter stability check points described in the discussion of the experimental methods.

Confidence Limits on Flux Assignment

The deviation reported on each standardization constant is the standard deviation of the mean standardization constant. This deviation is a measure of the accuracy to which the detector was standardized. It is not a measure of the accuracy of the flux assignment, since as previously pointed out, the accuracy of the flux assignment depends upon the accuracy in the knowledge of the source strength and particular diffusion parameters.

Neutron Sources. The neutron sources, listed in Table 1, were prepared and calibrated by the Mound Laboratory. Their catalog (8) states that the sources were calibrated by comparison with standards calibrated at the Los Alamos Scientific Laboratory. Since the Los Alamos source has a relative absolute calibration ratio of 1.016, (7), compared with the National Bureau of Standards source, a KSU source strength

should be divided by 1.016. Table 1 explains the assignment of the confidence limit of ± 7 per cent to KSU sources.

The Ra-Be (α, n) source number 38 at Argonne National Laboratories has a relative absolute calibration ratio of 1.049 compared with the Bureau of Standards source (7). To compare the KSU source with the Argonne source, the KSU source should be divided by 1.016/1.049. The Hanford source is not compared with NBS-I in Reference (7).

Diffusion Coefficient. A diffusion parameter of particular importance to an absolute determination of flux is the diffusion coefficient D ; for as can be seen in Eqs. 20, 24, and 25, it serves to scale the value of the absolute flux. A dilemma arises when considering the best value to use for the diffusion coefficient of graphite as calculated values and experimental values may differ as much as 10 per cent (see Table 7).

D can be calculated, in principle, from expressions such as Eqs. 37, 38, 40 and 41 below (15).

$$D = \frac{1}{3\Sigma(1-\bar{\mu}_0) \left(1 - \frac{4}{5} \cdot \frac{\Sigma_a}{\Sigma} + \frac{\Sigma_a}{\Sigma} \cdot \frac{\bar{\mu}_0}{1 - \bar{\mu}_0} + \dots\right)} \quad (37)$$

In this expression, $\bar{\mu}_0$ is the average cosine of the scattering angle in the laboratory system, given by $Z/3A$ where A is the atomic weight.

For weak absorbers where $\Sigma_a/\Sigma_s \ll 1$, this equation reduces to

$$D = \frac{1}{3\Sigma_s(1 - \bar{\mu}_0)} \quad (38)$$

Table 7. Summary of graphite diffusion parameters.

Density	σ_a	σ_s	λ_{tr}	D	References
gm/cm ³	millibarns, mb	barns	cm	cm	
1.60	3.73	4.8		0.886	(5, 21, 44)
1.60	3	4.8		0.778	(12)
1.60			$2.58 \pm .02$	0.860	(6)
1.60			$2.55 \pm .09$	0.850	(29)
	4.5	4.8			(30)
1.62				0.903	(15)
				0.90	(43)
1.60	4.65		2.74	0.913	(20)
1.60	4.8	4.8	2.75	0.917	(14)
1.60	4.8			1.040	(24)
	2.80 ± 0.04 mb including impurities 3.51 ± 0.06 mb without impurities				(26)

Defining the transport mean free path as

$$\lambda_{tr} = \frac{1}{\Sigma_s(1-\bar{\mu}_0)} \quad , \quad (39)$$

the diffusion coefficient becomes

$$D = \frac{\lambda_{tr}}{3} \quad (40)$$

From a development of the significance of the diffusion length for monoenergetic neutrons in a weak absorber (15)

$$D = \Sigma_a L^2 \quad , \quad (41)$$

where Σ_a is evaluated at the mean energy of the thermal spectrum (43).

An often quoted value of D is calculated from Eq. 40 where λ_{tr} is calculated from Eq. 39. Σ_s appears to be known with some certainty as 0.385 cm^{-1} (21); and $(1 - \bar{\mu}_0)$ is calculated as 0.944 (12). This results in a λ_{tr} in the range from 2.71 cm to 2.75 cm and corresponding diffusion coefficients in the range from 0.903 cm to 0.917 cm, respectively. This has been the range of D values used in previous pile standardizations (11, 35).

It has not been feasible to calculate adequately D from Eq. 41; for until recently, accurate direct measurements of Σ_a were difficult to make.

Direct measurements of D thus λ_{tr} made since 1955, (6, 29), by pulsed source techniques disagree somewhat with the calculated values outlined above. These two independent measurements of λ_{tr}

have been reported as 2.55 ± 0.09 and 2.58 ± 0.02 , both disagreeing considerably with the values for λ_{tr} calculated above.

Amaldi (2) claims that one cannot rely on the values of the diffusion parameters computed from scattering and absorption cross sections of the atoms of the medium. He points out that these various relationships for the diffusion parameters are useful however, since they provide the possibilities of checking in detail the fulfillment of the assumptions underlying their derivation.

From transmission experiments, one measures Σ_s not λ_{tr} . λ_{tr} is found from Σ_s by involvement of $\bar{\mu}_0$, the calculation of which depends upon the angular distribution of the scattered neutrons and this depends in a rather complicated way upon the molecular structure of the medium.

Singwi and Kothari (36), in pointing out this discrepancy between the calculated λ_{tr} and the measured λ_{tr} , offer no conclusion as to the best value to use. They say that the theory in the case of graphite is still in an unsatisfactory state and that a better theoretical calculation must await a better model for the vibrational spectrum of graphite. They suggest that a direct measurement of the angular distribution of the scattered neutrons in the thermal energy group would be valuable.

On the basis of this review and from communication with the Critical Mass Physics Section of Hanford Laboratories (9), it was felt that the most reasonable value of the diffusion coefficient would be found from the directly measured values of λ_{tr} . Thus D was taken as $2.58/3 = 0.860$ cm at a graphite density of 1.60 gm/cm³.

A paper by P. F. Nichols (26) gives a direct measurement of the graphite absorption cross section in the Physical Constants Testing Reactor. The reactor grade graphite (GAF) tested had a 2200 m/sec cross section of $\sigma_a = 3.80 \pm 0.04$ mb including all impurities. Using this and the diffusion length measured in the KSU pile of 55.3 ± 0.3 cm, a diffusion coefficient of 0.828 cm is obtained from Eq. 41, thus further indicating that the diffusion coefficient obtained from Eq. 38 may be an overestimate.

Table 7 lists a summary of the diffusion parameters of graphite.

Age. In the finite pile flux calculations, the Fermi age measured by Steichen (39) has been used, whereas in the standard pile absolute flux calculations, a combination of Gaussian ranges has been used instead of a Fermi age. In either case, to evaluate the source for the thermal diffusion equation, the Fermi age or a Gaussian range to indium resonance must be extended to represent the age or range at thermal energy by Eq. 17 which resulted from Fermi's slowing down theory

$$\tau(E_{oi}, E_{th}) = \tau(E_{oi}, E_{In}) + \int_{E_{th}}^{E_{In}} \frac{D}{\xi \Sigma_s} \frac{dE}{E} \quad (42)$$

where

$$r_{th-i}^2 = 4\tau(E_{oi}, E_{th}). \quad (43)$$

Using the following diffusion parameters appropriate to this work,

$$\begin{aligned}
 D &= 0.860 \text{ cm} & E_{\text{In}} &= 1.44 \text{ ev} \\
 \Sigma_s &= 0.385 \text{ cm}^{-1} & E_{\text{th}} &= 0.025 \text{ ev} \\
 \xi &= 0.158
 \end{aligned}$$

the age integral above has a value of 57.3 cm^2 .

The Reactor Handbook (30) gives an estimated age from indium resonance energy to thermal energy of 53 cm^2 . Weinberg and Wigner (43) estimate the age from resonance to thermal as 39 cm^2 by means of

$$\tau(E_{\text{th}}) = \tau(E_{\text{In}}) + \int_{E_{\text{th}}}^{E_{\text{In}}} \frac{dE}{3E \sum_j (\xi_j \Sigma_j) \sum_j [\Sigma_j (1 - \bar{\mu}_{0j})]} \quad (44)$$

A study of the slowing down of neutrons in graphite by Duggal and Martelly (13) of France states that the most probable value of the effective slowing down age between indium resonance and thermal equilibrium is 49 cm^2 . This value of 49 cm^2 was used for this work since it seemed to lie in between the extreme values and it agreed quite well with that given by the Reactor Handbook (30).

Thermalization theory (43) was not applicable in this case since there were no heavy absorbers such as uranium to harden the spectrum.

The age of neutrons from a Pu-Be neutron source to indium resonance energy as measured by Steichen (39) was taken as 419 cm^2 at a graphite density of 1.6 gm/cm^3 . This number was the result of an experimental determination of 422 and a theoretical calculation of 416. Extrapolating this age to thermal energy with the estimated age difference of 49 cm^2 gave the age of neutrons from a Pu-Be source to

thermal energy as 468 cm^2 . At the effective density of the KSU pile of 1.678 gm/cm^3 , the age was 381 cm^2 to indium resonance and 426 cm^2 to thermal.

To extend any indium resonance Gaussian range to the thermal Gaussian range, the expression

$$\frac{r_{\text{th-i}}^2}{4} = \frac{r_{\text{In-i}}^2}{4} + (49)^2 \quad (45)$$

was used.

Diffusion Length. The diffusion length was experimentally determined to be $52.76 \pm 0.30 \text{ cm}$ by Kaiser (22) at the effective density of the KSU pile. At a density of 1.6 gm/cm^3 this would be $55.33 \pm 0.30 \text{ cm}$. This number is the result of the average of ten determinations of diffusion length, each determination getting 1,000 counts with the BF_3 probe in each of 13 selected pile positions. The model from which the diffusion length was determined assumed a thermal point source.

It would be a difficult task to propagate the errors of each individual parameter to give the confidence limits in the standard pile flux as determined by Eq. 20. Considering the uncertainty in the diffusion coefficient to be ± 5 per cent, (estimated from the difference between 0.860 and 0.910), the uncertainty in the thermal flux, considering only the effect of the source strength and the diffusion coefficient, amounts to ± 12 per cent. Error in the diffusion length (55.33 ± 0.30), or estimated error in the age (39) or a Gaussian range should have a small effect on the flux compared with the effect of the error in the source strength or the diffusion coefficient. A study of the variation of standard

flux with variation of diffusion length is presented in Fig. 18.

Intercalibration with Argonne Standard Pile and Hanford Standard Pile

Table 8 presents standardization constants of KSU gold foils as determined from the irradiation of the bare foils in known flux positions of the Argonne Standard Pile and the Hanford Standard Pile. The foils were irradiated for approximately two half-lives and then sent to Kansas State University where the saturation activity of the foils was determined by use of the KSU standard foil counting system described in the section on experimental facilities. On the basis of the saturation activity of the foil and the knowledge of the flux to which the bare foil was exposed, a standardization constant was determined for the foil according to

$$K_{th} (gf) = \frac{(nv)_{th}}{A_{sat}} \quad (46)$$

The results of the subsequent use of these foils in the KSU Standard Pile may be seen in Table 9.

It must be pointed out that the pile at Hanford was standardized with a diffusion coefficient of 0.910 cm (11) and the pile at Argonne was standardized with a diffusion coefficient of 0.903, (32, 35). The KSU pile was standardized on the basis of a diffusion coefficient of 0.860 cm since, as previously pointed out, this was thought to be a better estimate of the diffusion coefficient for graphite. To intercalibrate the fluxes of the various standard piles on the basis of a consistent diffusion coefficient, the Argonne flux was multiplied by

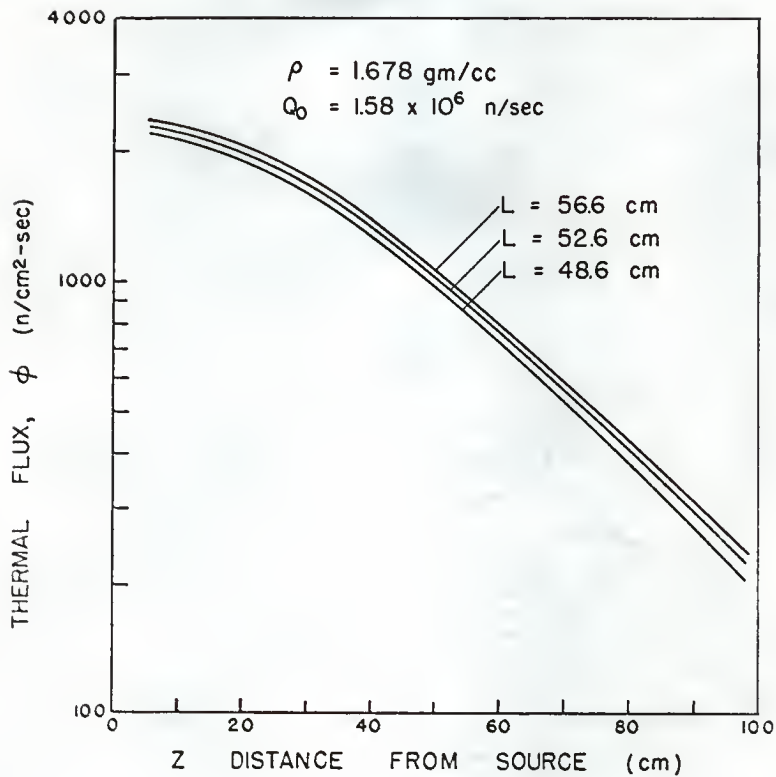


Fig. 18. Effect of diffusion length variation on KSU Standard Pile flux.

Table 8. Summary of Gold foil standardization constants found from bare foil irradiation in standard piles at Argonne and Hanford.

Foil identification	Standardizing conditions			Saturation activity determined from KSU standard counter (counts/sec)	Standardization constant (flux/counts/sec)
	Laboratory	Distance from source (cm)	Absolute flux ($n/cm^2\text{-sec}$)		
KSU-1	Argonne	15.75	6,611	50.247 ± 0.199	164.3 ± 0.8
KSU-2	Argonne	36.75	4,497	26.251 ± 0.142	171.3 ± 0.9
KSU-1 HAN	Hanford	10.64	8,565	62.116 ± 0.313	137.9 ± 0.7
KSU-2 HAN	Hanford	31.91	6,149	36.835 ± 0.183	166.9 ± 0.8

Table 9. Intercalibration of KSU Standard Pile flux with standard pile flux at Hanford and Argonne by use of standardized gold foils.

Foil identification	Exposure condition in KSU Standard Pile		Flux determined from standardized foil (n/cm ² -sec)	Flux from standardized foil using consistent diffusion coefficients (n/cm ² -sec)	Discrepancy with KSU standard flux
	Distance from source (cm)	KSU standard flux (n/cm ² -sec)			
Top					
Bottom					
KSU-1	25.96	1,768	1,520	1,596	-9.7 %
KSU-2	46.11	1,101	1,049	1,101	0.0 %
KSU-1 HAN	25.96	1,768	1,471	1,557	-11.9 %
KSU-2 HAN	46.11	1,101	978.7	1,036	-5.9 %
KSU-1	15.82	2,058	1,866	1,960	-4.8 %
KSU-2	36.11	1,430	1,326	1,392	-2.7 %

0.903/0.860 and the Hanford flux was multiplied by 0.910/0.860. Such an adjustment led to the flux listed in Column 6 of Table 9 which was the flux to be compared with the KSU assigned value of the absolute flux.

One cause of the unsatisfying intercomparison was the assumption expressed in Eq. 46 that the thermal flux is proportional to the saturation activity of a bare gold foil. Since gold has its peak cross section at an epithermal energy, a considerable portion of the activation of the foil near the source was due to epithermal neutrons. The epithermal content of the fluxes in the intercalibrated cases was not necessarily the same since a KSU neutron source has a different energy spectrum and since the irradiations took place at different distances from the source. The correct procedure for the intercalibration of standard pile fluxes would be the exchange of both bare and cadmium covered gold foils since the thermal flux is more correctly proportional to the cadmium difference saturation activity.

The most reliable intercomparisons made with this bare foil exchange are those made at the positions farthest from the source, even though at these points there is still an epithermal flux contribution.

Theoretical Standardization of BF_3 Neutron Probe

A theoretical standardization constant for the BF_3 neutron detector was determined according to a development by Price (28). Based on the manufacturer's specifications for the BF_3 probe described in the

section on experimental facilities, the theoretical standardization constant of the probe was calculated to be 0.872 neutron flux per count per minute. The standardization constant determined from this thesis was 1.1578. Considering the average of 1.1578 and 0.872 to be correct, this amounts to a discrepancy between the two of 28 per cent with the theoretical standardization constant giving the lower flux.

All assumptions made in the theoretical calculation appear to be reasonably correct. However, experience at Kansas State University with the construction of BF_3 neutron detectors (25) indicates that such important specifications as the gas pressure and the active volume are difficult to determine accurately. Perhaps the specifications given by the manufacturer were meant to be nominal.

Scintillation Probe Standardization

The standard pile analysis gave a standardization constant of 0.8465 neutron flux per count per minute for the scintillation probe. The instrument manufacturer assigned a sensitivity of 0.014 counts per second per unit neutron flux to the probe. Expressing the standardization constant of 0.8465 in terms of counts per second per unit neutron flux results in a sensitivity of 0.0197. Considering the average of 0.0197 and 0.014 to be correct, a 34 per cent discrepancy appears to be involved with the manufacturer's assigned sensitivity giving the higher flux.

It must be pointed out that the manufacturer's assignment of the sensitivity was based on a calibration with the Argonne Standard Pile. In order to compare the KSU standard flux with the flux indication from an Argonne standardized detector, the detector indication must be ad-

justed in order to base the comparison on consistent diffusion coefficients. Such a consideration would decrease the manufacturer's assigned value of the sensitivity from 0.014 to 0.0133, giving a larger 39 per cent discrepancy with the KSU assigned sensitivity value of 0.0197.

Inspection of Table 6 or Fig. 17 reveals that the scintillation probe gave the least reliable standardization constant of the various detectors. The lower standardization constants near the source suggest that a standardization using a cadmium difference technique would give more reliable results for the scintillation probe.

The Use of Gaussian Ranges and the Fermi Age to Describe Slowing Down

Steichen (39) has shown that the age from a polyenergetic neutron source may be theoretically represented by

$$\tau = \sum_{i=1}^N f_i \tau_i \quad (47)$$

where f_i represents the fractional contribution of τ_i , the age from the i^{th} energy group of the source to an energy such as indium resonance energy. Writing τ_i in terms of r_i according to the defining equation of r_i , Eq. 47 may be written as

$$\tau = \sum_{i=1}^N f_i \frac{r_i^2}{4} \quad (48)$$

This value of the age, hereafter referred to as the equivalent age, has been calculated for each of the empirical fits and tabulated in Column 16 of Table 5. Inspection of this column reveals that even though the equivalent ages are near 381 cm^2 , Steichen's (39) value of the age to indium resonance, they could not be used to determine accurately the age. Steichen shows that the value of the Fermi age is determined to a great degree by the extrapolation to infinity of the measured resonance distribution beyond the last measured point at 97.12 cm . This variation of the equivalent ages with choice of empirical fit may be a result of the different extrapolations beyond 97.12 cm given by various empirical fits.

It was of interest to study the variation of the calculated standard pile flux that resulted from different choices of the indium resonance data fit given in Table 5. Two different fits were used to calculate the standard pile flux. One was the appointed best fit which had an equivalent age of 411.9 cm^2 . The other was a three term fit of the indium resonance data corrected for geometry and foil weights, but not corrected for neutron absorption by higher energy indium resonances. This latter fit had an equivalent age of 378.1 cm^2 . Even though the equivalent ages and the individual terms of the two fits were different, the small difference in the calculated fluxes was difficult to show clearly in a plot of the two fluxes. The maximum difference was a little greater than 2 per cent.

Use of the three Gaussian ranges allows a more accurate description of the slowing down density than does the use of the Fermi age.

As can be seen from the form of Eq. 8, use of the Fermi age to describe the slowing down distribution would yield a straight line on Fig. 14. The use of three Gaussian ranges, however, provides an adequate description of the actual measured slowing down distribution.

Further, it must be stated that the use of the three Gaussian ranges to determine the slowing down to thermal energy will allow a more accurate description of the thermal neutron flux than will the use of the Fermi Age. This conclusion has not been explicitly demonstrated but it follows from the fact that a more accurate description of the slowing down of neutrons to thermal energy will allow a more accurate source boundary condition to the thermal diffusion equation.

Study of Source Boundary Condition in Finite Pile

Table 10 is a summary of flux calculations in the study of the source boundary condition to the thermal diffusion equation in the finite pile geometry. Column 2 lists the flux using fast point source theory as obtained from the computer code described in Appendix E which numerically evaluates Eq. 24. Column 3 lists the flux using thermal point source theory as obtained from the computer code described in Appendix F which numerically evaluates Eq. 25. Column 4 lists the experimental absolute flux determined by the standardized BF₃ probe. All measurements and calculations were made with a source having a strength of 1.71×10^6 neutrons per second.

Figures 20 are isometric plots of the flux values in Table 10. The absolute flux is plotted along the vertical axis as a function of

Table 1C. Study of the flux from two assumed source boundary conditions for the thermal diffusion equation in a finite pile. $Q_0 = 1.71 \times 10^6$ n/sec.

Distance from source			Thermal flux from fast point source	Thermal flux from thermal point source	Thermal flux from standardized BF ₃ probe
X	Y	Z	n/cm ² -sec	n/cm ² -sec	n/cm ² -sec
inches					
0	0	0	2,238.0		
4			2,162.0	13,150.0	2,432.0
8			1,951.0	5,356.0	2,190.0
12			1,647.0	2,879.0	1,794.0
16			1,304.0	1,716.0	1,423.0
20			966.0	1,061.0	1,115.0
24			659.4	650.5	666.9
28			391.6	363.2	389.8
32			154.3	139.1	167.6
0	8	0	1,951.0	5,356.0	2,094.0
4			1,886.0	4,594.0	2,037.0
8			1,706.0	3,177.0	1,820.0
12			1,445.0	2,101.0	1,508.0
16			1,150.0	1,377.0	1,115.0
20			855.4	896.5	842.6
24			586.8	569.6	585.6
28			349.9	320.8	338.7
32			138.2	123.8	136.4
0	16	0	1,304.0	1,716.0	1,335.0
4			1,263.0	1,615.0	1,298.0
8			1,150.0	1,373.0	1,159.0
12			982.7	1,078.0	982.4
16			790.8	799.9	771.7
20			596.7	566.9	578.0
24			414.5	378.3	404.4
28			249.8	222.6	257.0
32			99.29	87.41	100.3
0	24	0	659.4	650.5	621.7
4			640.5	629.5	511.3
8			586.8	565.8	566.5
12			507.7	474.6	482.2
16			414.5	378.5	396.0
20			317.7	283.0	300.7
24			224.2	196.5	219.0
28			136.8	118.2	132.5
32			54.74	47.33	54.74
0	32	0	154.3	126.3	147.1
4			150.1	134.8	142.8
8			138.2	125.9	133.4
12			120.5	106.2	113.4
16			99.29	86.61	94.42
20			76.87	67.36	68.31
24			54.75	47.25	52.33
28			33.64	28.60	32.53
32			13.53	11.58	14.39

Table 10 (cont.)

Distance from source X : Y : Z			Thermal flux from fast point source	Thermal flux from thermal point source	Thermal flux from standardized BF ₃ probe
inches			n/cm ² -sec	n/cm ² -sec	n/cm ² -sec
0	0	8	1,951.0	5,356.0	2,148.0
4			1,886.0	4,594.0	2,062.0
8			1,706.0	3,177.0	1,815.0
12			1,445.0	2,101.0	1,516.0
16			1,150.0	1,377.0	1,188.0
20			855.4	896.5	861.4
24			586.8	564.6	605.5
28			349.9	320.8	339.2
32			138.2	123.8	148.2
0	8	8	1,706.0	3,177.0	1,775.0
4			1,650.0	2,889.0	1,721.0
8			1,495.0	2,258.0	1,536.0
12			1,271.0	1,623.0	1,266.0
16			1,015.0	1,130.0	1,012.0
20			759.3	764.0	747.4
24			523.3	492.5	514.9
28			313.2	283.8	318.7
32			124.0	110.3	126.4
0	16	8	1,149.0	1,373.0	1,162.0
4			1,114.0	1,312.0	1,105.0
8			1,015.0	1,127.0	1,002.0
12			870.7	909.9	896.7
16			703.3	689.3	692.9
20			532.8	496.3	528.0
24			371.8	334.7	371.9
28			224.8	198.5	224.0
32			89.52	78.25	91.62
0	24	8	586.8	565.8	564.4
4			570.2	541.0	542.4
8			523.3	491.3	498.0
12			453.9	417.4	434.2
16			371.8	335.2	362.4
20			285.9	253.3	273.5
24			202.4	176.6	192.6
28			123.8	106.9	122.5
32			49.63	42.69	49.94
0	32	8	138.2	125.9	128.86
4			134.5	121.8	128.32
8			124.0	111.3	119.75
12			108.3	96.36	103.08
16			89.52	78.03	84.44
20			69.50	60.43	66.96
24			49.63	42.84	47.53
28			30.56	26.19	29.99
32			12.30	10.52	13.89

Table 10 (cont.)

Distance from source			Thermal flux from fast point source	Thermal flux from thermal point source	Thermal flux from standardized BF_3 probe
X	Y	Z	n/cm^2 -sec	n/cm^2 -sec	n/cm^2 -sec
inches					
0	0	16	1,304.0	1,716.0	1,330.0
4			1,263.0	1,615.0	1,269.0
8			1,150.0	1,373.0	1,167.0
12			982.7	1,078.0	992.5
16			790.8	799.9	774.3
20			596.5	566.9	594.4
24			419.5	378.3	412.4
28			249.8	222.6	252.4
32			99.29	87.41	103.7
0	8	16	1,149.0	1,373.0	1,118.0
4			1,114.0	1,312.0	1,092.0
8			1,015.0	1,127.0	1,010.0
12			870.7	909.9	870.7
16			703.3	689.3	696.7
20			53.28	496.3	529.3
24			37.18	334.7	365.6
28			224.8	198.5	224.30
32			89.52	78.25	92.43
0	16	16	790.8	799.9	753.4
4			767.9	772.3	767.9
8			703.3	690.2	686.9
12			608.2	576.8	597.4
16			496.2	457.8	482.5
20			480.1	341.2	367.9
24			268.0	235.7	274.1
28			163.4	141.7	166.8
32			65.41	56.37	66.69
0	24	16	414.5	378.5	398.3
4			403.4	355.8	385.9
8			371.8	334.4	359.4
12			324.6	290.7	310.7
16			268.0	234.8	255.3
20			208.0	181.3	198.9
24			148.4	128.6	143.20
28			91.34	78.90	91.85
32			36.77	31.48	39.02
0	32	16	99.26	86.61	94.94
4			96.75	84.95	90.52
8			89.52	74.81	87.22
12			78.64	66.14	77.32
16			65.82	57.40	63.48
20			51.15	43.31	49.32
24			36.77	31.66	36.41
28			22.76	19.82	22.15
32			9.02	7.896	10.74

Table 10 (cont.)

Distance from source X : Y : Z			Thermal flux from fast point source	Thermal flux from thermal point source	Thermal flux from standardized BF ₃ probe
inches			n/cm ² -sec	n/cm ² -sec	n/cm ² -sec
0	0	24	659.4	650.5	650.0
4			640.5	679.5	630.2
8			586.8	565.8	578.4
12			507.7	474.6	502.3
16			414.5	378.5	413.6
20			317.7	283.0	317.7
24			224.2	196.5	227.6
28			136.8	118.2	142.6
32			54.74	47.33	61.80
0	8	24	586.8	565.8	554.1
4			570.2	541.0	553.7
8			523.3	491.3	517.3
12			453.9	417.4	445.5
16			371.8	335.2	363.6
20			285.9	253.3	277.9
24			202.4	176.6	197.1
28			129.3	106.9	120.6
32			49.63	42.69	53.29
0	16	24	414.5	378.5	405.9
4			403.4	365.8	386.4
8			371.8	334.4	349.7
12			324.5	290.7	313.5
16			268.0	234.8	265.4
20			208.0	181.3	205.5
24			148.4	128.6	144.5
28			91.34	78.90	93.53
32			36.77	31.48	38.71
0	24	24	224.2	196.5	215.2
4			218.5	189.3	207.7
8			202.4	175.3	196.7
12			178.1	154.6	168.3
16			148.3	128.0	144.3
20			116.3	100.2	110.2
24			83.75	71.77	82.53
28			51.92	44.84	54.10
32			20.99	18.18	24.02
0	32	24	54.75	47.25	52.60
4			53.42	45.21	51.27
8			49.63	41.95	47.04
12			43.86	37.11	44.00
16			36.77	32.30	37.11
20			28.98	24.25	29.23
24			20.99	17.65	21.40
28			13.07	11.53	14.33
32			5.30	4.67	7.56

Table 10 (concl.)

Distance from source X : Y : Z			Thermal flux from fast point source	Thermal flux from thermal point source	Thermal flux from standardized BF ₃ probe
inches			n/cm ² -sec	n/cm ² -sec	n/cm ² -sec
0	0	32	154.3	139.1	149.4
4			150.1	134.8	149.1
8			138.2	125.9	138.1
12			120.5	106.2	121.9
16			99.29	86.61	95.63
20			76.87	67.36	74.66
24			54.75	47.25	54.42
28			33.64	28.60	34.13
32			13.53	11.58	14.47
0	8	32	134.9	125.9	126.06
4			134.5	121.8	128.28
8			124.0	111.3	122.73
12			108.3	96.36	100.8
16			89.52	78.03	83.99
20			69.50	60.43	68.66
24			49.63	42.84	51.52
28			30.56	26.19	28.13
32			12.30	10.52	13.69
0	16	32	99.29	86.61	99.10
4			96.75	84.95	88.90
8			89.52	74.81	84.50
12			78.64	66.14	76.80
16			65.42	57.40	65.57
20			51.15	43.31	50.51
24			36.77	31.66	35.95
28			22.76	19.82	23.62
32			9.195	7.90	10.08
0	24	32	54.75	47.25	52.74
4			53.42	45.21	47.91
8			49.63	41.95	47.27
12			43.86	37.11	40.81
16			36.77	32.30	35.31
20			28.98	24.25	27.73
24			20.99	17.65	20.64
28			13.07	11.53	12.09
32			5.297	4.67	5.89
0	32	32	13.53	11.58	12.39
4			13.21		12.64
8			12.31	10.53	13.35
12			10.92		11.61
16			9.195	7.90	8.949
20			7.279		8.660
24			5.297	4.67	5.708
28			3.304		4.006
32			1.343	1.22	1.424

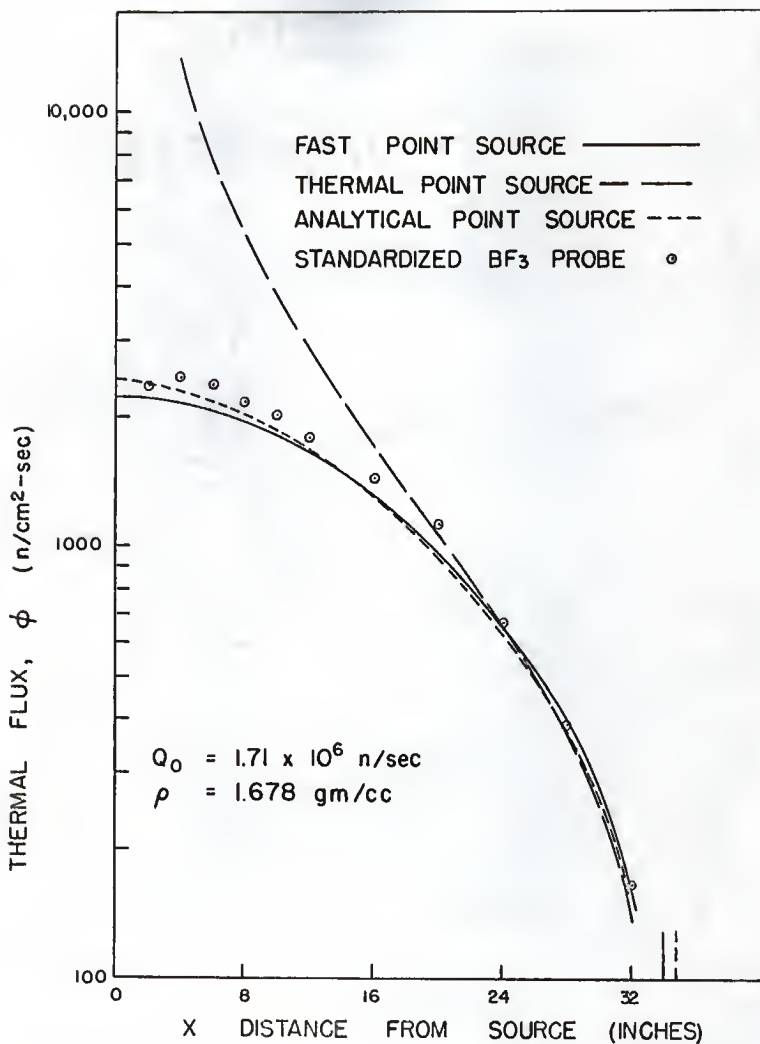


Fig. 19. Thermal flux study in finite pile.

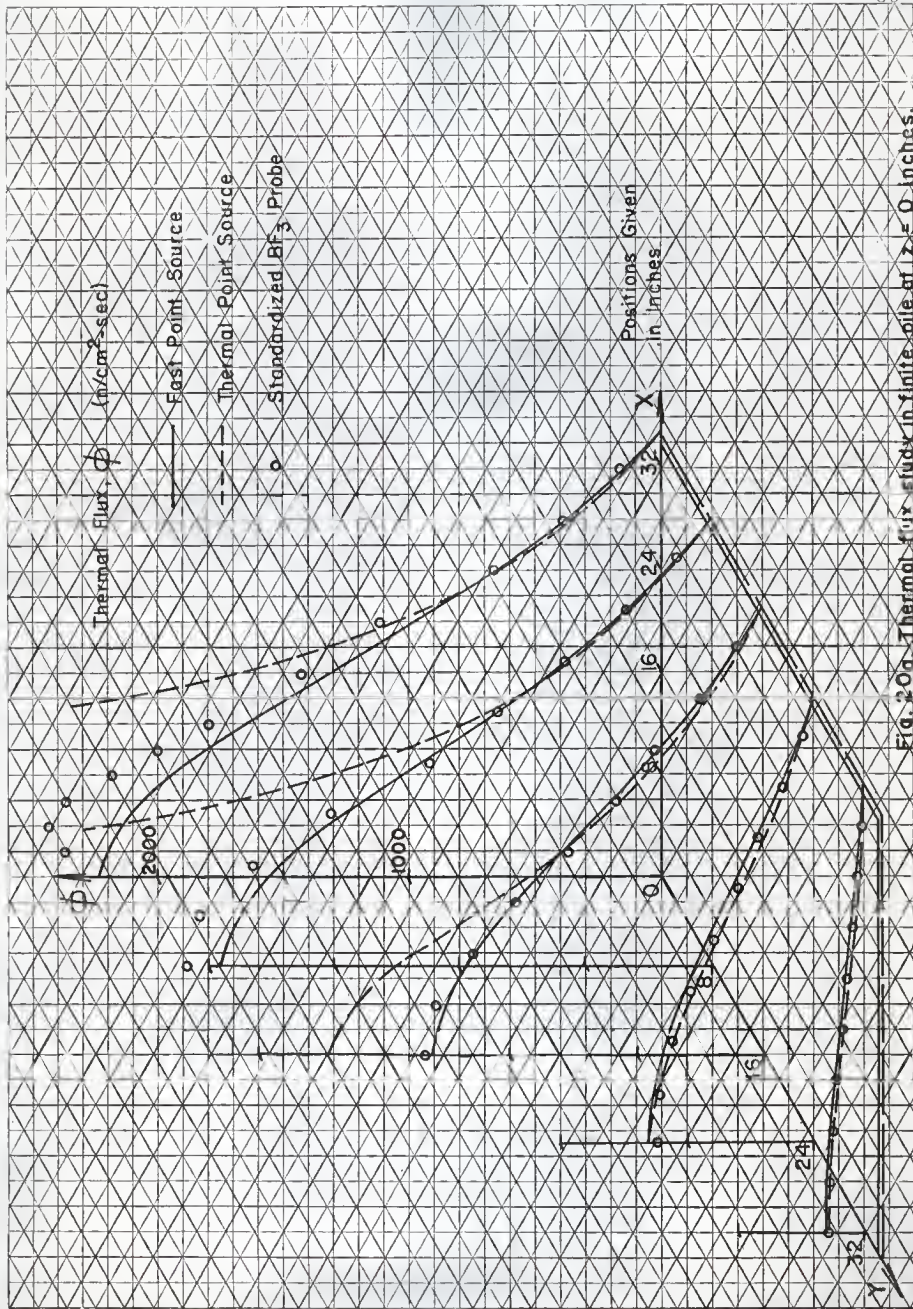
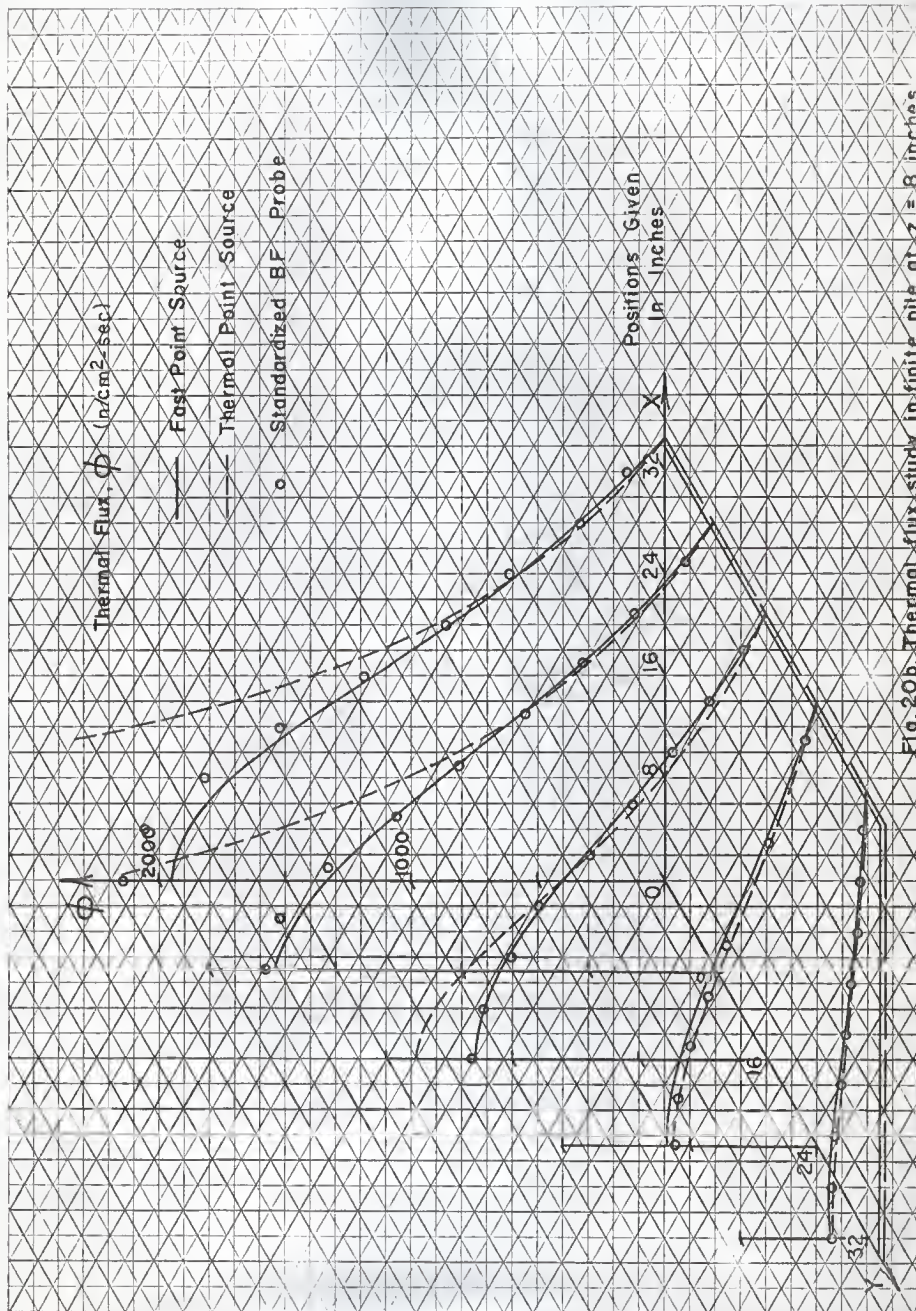


Fig. 2.0a. Thermal flux study in finite pile at $z = 0$ inches.

Fig. 20b. Thermal flux study in infinite plate at $z = 8$ inches.

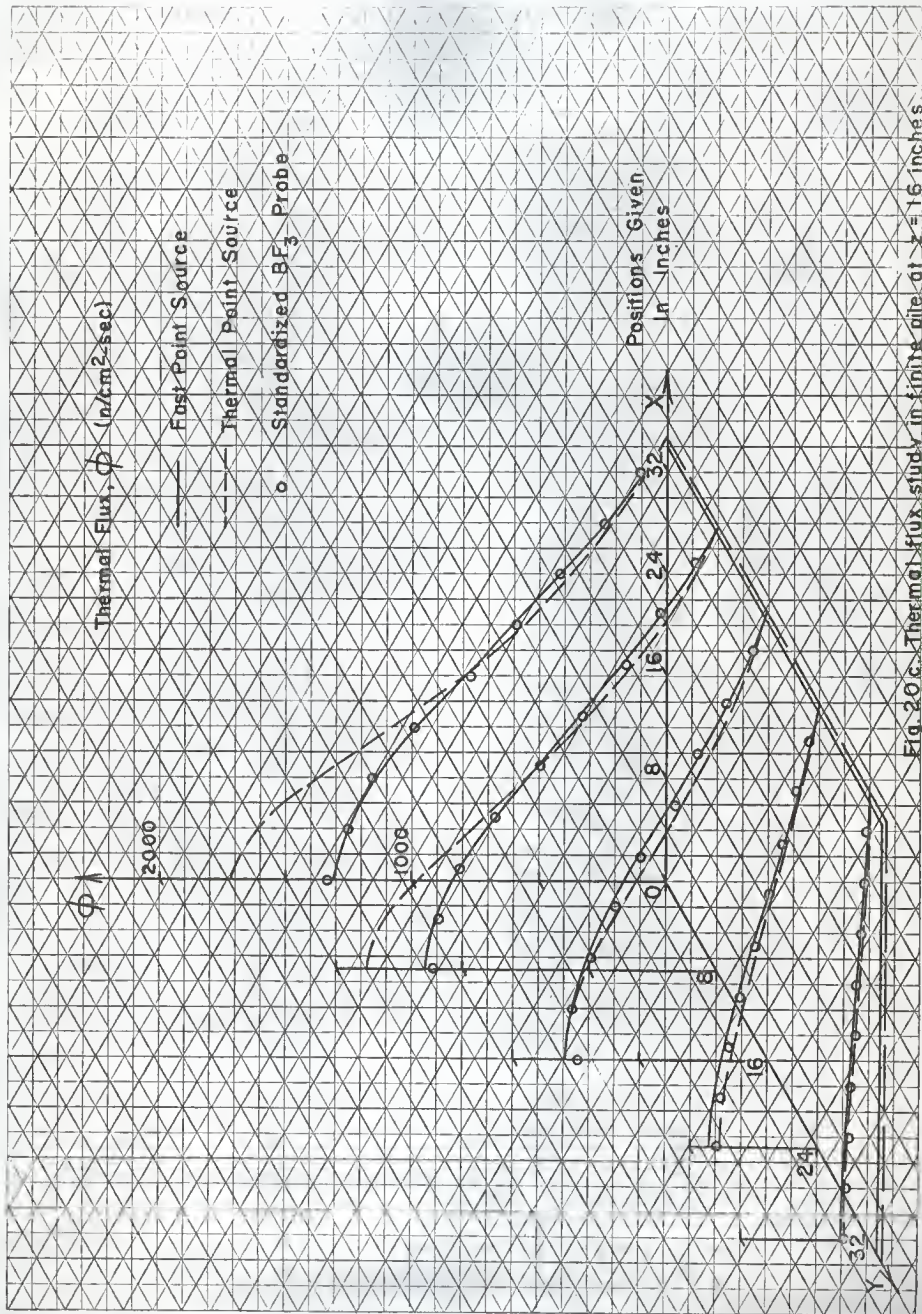


Fig. 20c. Thermal flux study in finite pile at $x = 16$ inches.

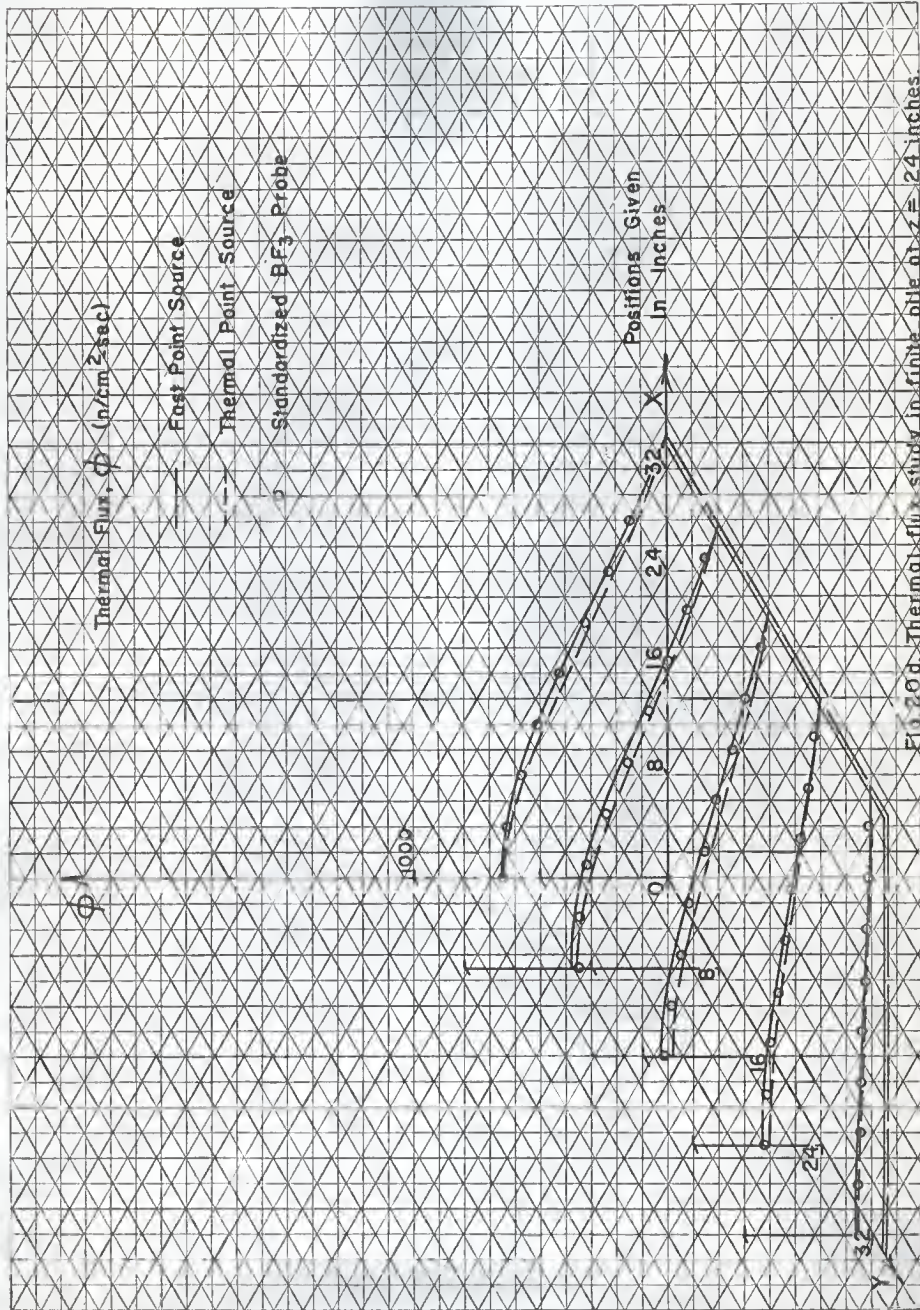
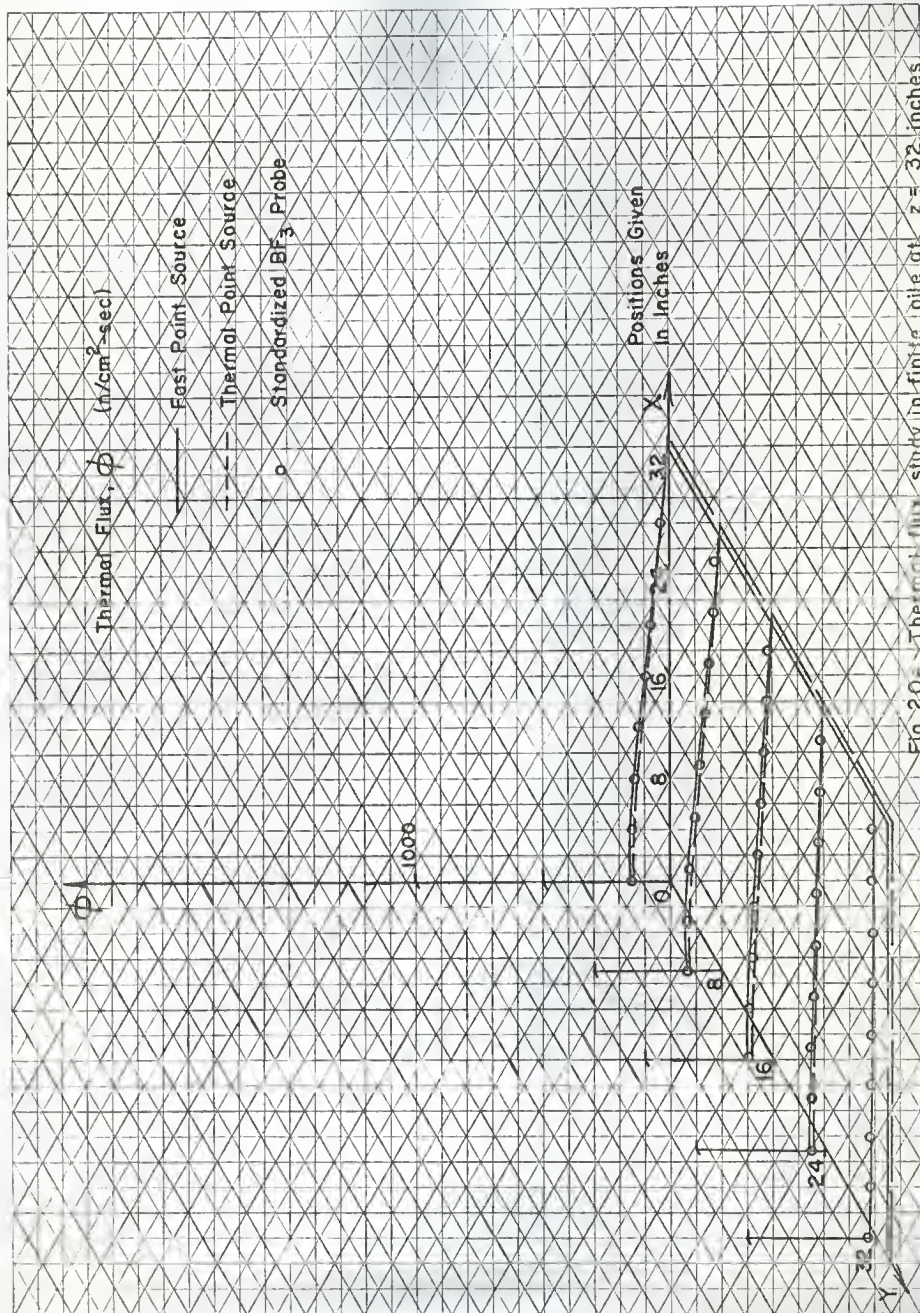


Fig. 20d. Thermal flux study in finite pile at $z = 24$ inches.

Fig. 20a. Thermal flux study in finite pile at $z = 32$ inches

x, y and z with each figure representing a different z level in the finite pile. Figure 19 is a semi-logarithmic plot of the flux as a function of x alone, z and y being zero. Figure 19 clearly shows the difference between the flux from fast source theory and the flux from thermal source theory. The fast source calculations used the single value of the age of neutrons from a Pu-Be source to thermal energy. Figure 19 shows the effect of using the three range groups, or an analytical source expression, determined from the standard pile analysis instead of the single value of the age. This curve, calculated by Eq. 24, resulted from the superposition of the flux contributions from three different monoenergetic sources, each source having its respective Gaussian range and fractional contribution determined empirically from Eq. 36 and extended to thermal energy by Eq. 45. It can be seen that the breaking up of the source into three energy groups by the use of Gaussian ranges does give an improved effect.

Studies of the variation of the flux in fast source theory and thermal source theory with the variation of various parameters are given in Figs. 21 through 23. Graphs showing the variation of flux with variation of source strength or diffusion coefficient are not given, since both of these parameters are merely scaling coefficients to the flux.

The values of the source strength and the diffusion coefficient do not affect the various plots in Figs. 19 and 20 with respect to each other since they were all based on consistent values.

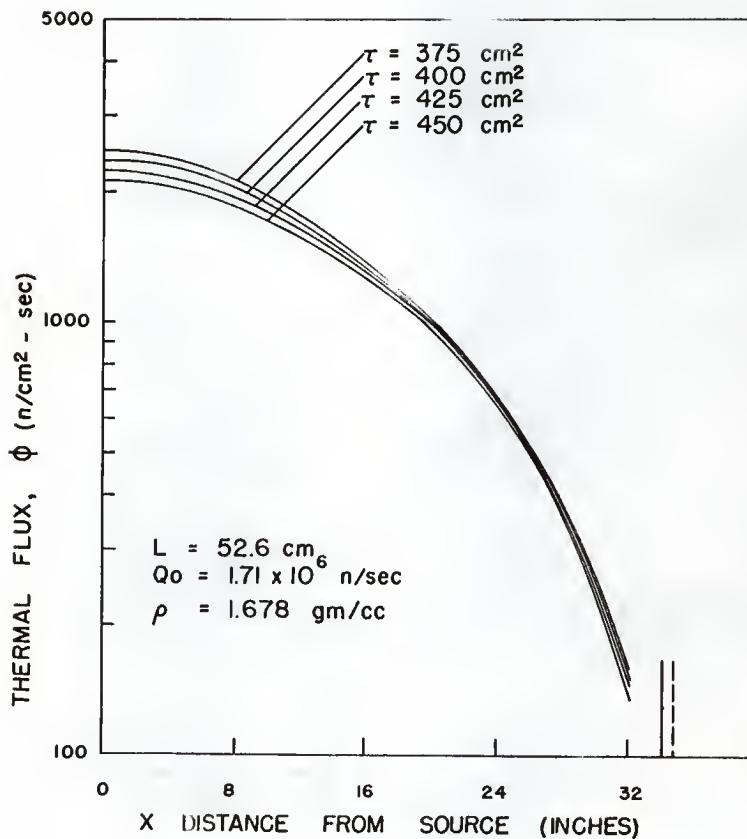


Fig. 21. Effect of variation of Fermi age on thermal flux from fast point source in finite pile.

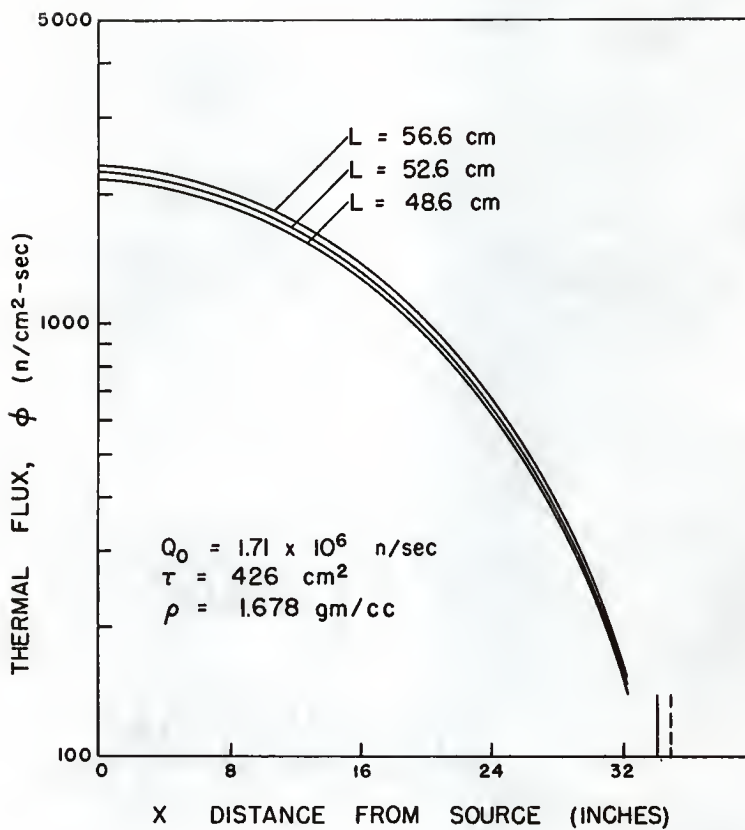


Fig. 22. Effect of variation of diffusion length on thermal flux from fast point source in finite pile.

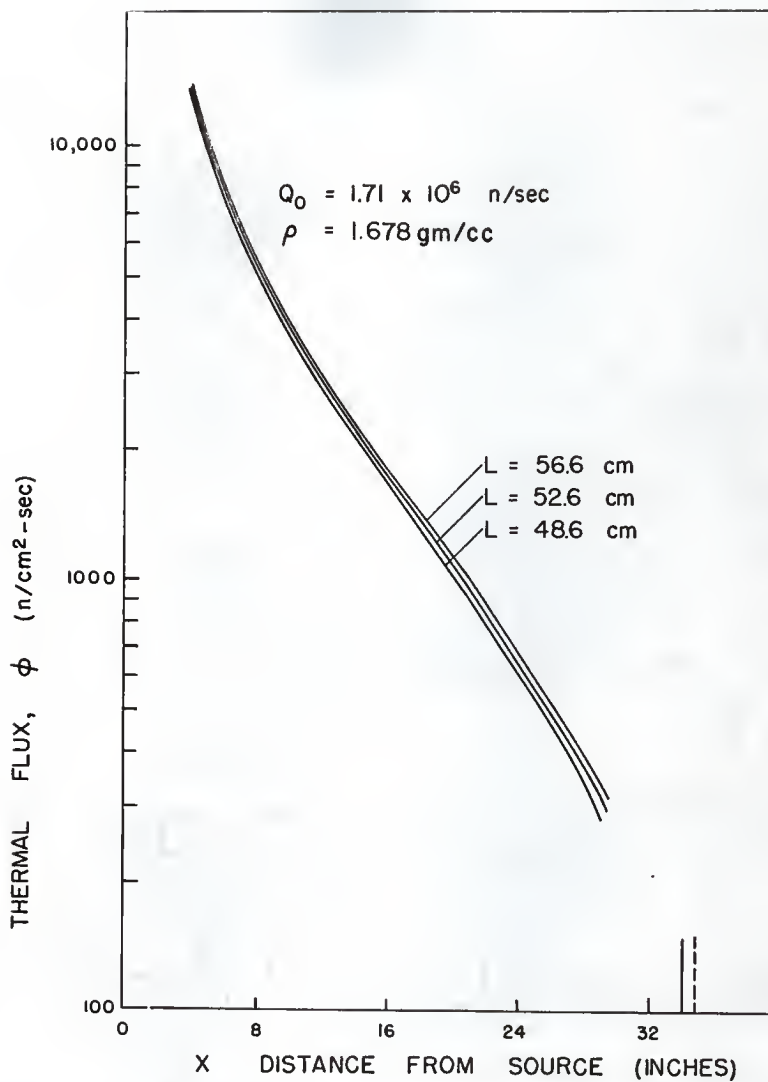


Fig.23. Effect of variation of diffusion length on thermal flux from thermal point source in finite pile.

Suggestions for Further Work

The IBM-650 program which calculates the thermal flux from fast point source theory in finite geometry offers interesting possibilities for research with superposition of fluxes. Sources may be placed at various positions in the pile and the absolute flux may be determined experimentally with the standardized detectors. This experimental absolute flux may be compared with the superimposed fluxes determined from machine calculations of the flux from individual sources.

It is evident that there is still uncertainty in defining the absolute flux. An independent calculation of absolute flux could be made with the absolute counting of beta particles from indium foils. A recent outline for such work is References (17) and (23).

An approximate method for an absolute flux determination using a water medium has been outlined by Reference 1. The method assumes:

- (a) The count rate of a thermal neutron detector such as the BF_3 probe, is directly proportional to the thermal flux at all points in the water medium.
- (b) The water medium is infinite and spherical geometry can be used. Reference (30) considers the water volume necessary to approximate infinity.
- (c) Neutron capture occurs only at thermal energies.
- (d) Σ_a for water is accurately known.
- (e) Q_0 is accurately known.

Since leakage from the "infinite medium" is negligible, the only loss of neutrons is due to capture at thermal energies. It can then be written in spherical coordinates that

$$Q_0 = \int_{\text{all space}} \Sigma_a \phi(r) 4\pi r^2 dr \quad (49)$$

From the assumption that $\phi = KR(r)$ where r is the count rate, K may be written as

$$K = \frac{Q_0}{\int_0^{\infty} 4\pi \Sigma_a R(r) r^2 dr} \quad (50)$$

R may be experimentally determined and the integral may be evaluated numerically.

Some work may be done in attempting to tie up the foil standardizations in graphite with the absolute flux in other media such as water or paraffin. A first approximation, ignoring any difference in the energy of the thermal neutron spectrum in graphite and water for example, would require the determination of K_{th}^0 , the standardization constant independent of perturbing effects introduced in the section on data analysis. This is necessary since many of the perturbations depend upon the moderating properties of the medium.

It is felt by this author that a complete systematic study of the foil correction factors would be desirable. In addition to the contribution of helping to make possible the use of the standardized foils in media other than graphite, this study would be necessary in determining the absolute value of an unperturbed flux from absolute beta counting of foils.

An interesting addition to this work might be the comparison of the standard pile flux with the flux obtained from the finite pile solu-

tions which would use the standard pile in its finite dimensions. It may be recalled that in the standard pile analysis, the pile was assumed to have an infinite height. A difficulty of interest that would arise would be the definition of the boundary condition at the lower face of the pile, which rests on concrete.

In the discussion of the results it was stated that the use of Gaussian ranges to determine the slowing down to thermal would allow a more accurate description of the thermal neutron flux than would the use of the Fermi age. A standard pile flux calculation using Steichen's value of the age instead of the three Gaussian ranges would show this difference in thermal flux.

ACKNOWLEDGMENT

The author wishes to express his sincere appreciation to the Kansas State University Engineering Experiment Station for their financial support and to the Atomic Energy Commission, who through their fellowship program have made the opportunity for this study possible. Sincere gratitude is given to Dr. William R. Kimel, Head of the Department of Nuclear Engineering, for his guidance, encouragement and help throughout the course of this study. I also wish to extend thanks to Professor R. W. Clack, Dr. J. O. Mingle, and Professor R. C. Bailie of the Kansas State University Nuclear Engineering Staff; to Dr. F. G. Prohammer of Argonne National Laboratory, and to Dr. E. D. Clayton of Hanford Laboratories for their particular contributions.

LITERATURE CITED

- (1) Absolute Calibration of a Thermal Neutron Detector.
Engineering and Sciences Extension, University of
California, Berkeley, California.
- (2) Amaldi, E.
in Handbuch der Physik, Vol. 38, Part II. Berlin:
Springer, 1959.
- (3) Anderson, H. L., and E. Fermi.
Production of Neutrons by Uranium. CPA-6, 1941
- (4) Anselone, P. M.
Distribution of Thermal Neutrons from Fast Sources in
Exponential Piles. HW-31925, 1954.
- (5) Baucom, H. H.
Nuclear Data for Reactor Studies. Nucleonics. 18(11):
198-200. 1960.
- (6) Beckurts, K. H.
Measurements with a Pulsed Neutron Source. Nuc. Sci. and
Eng., 2(4): 516-522. 1957.
- (7) Caswell, R. S., E. R. Mosburg and J. Chin.
Standards for Neutron Flux Measurement and Neutron Dosimetry.
A/CONF. 15/21/P/752. Geneva: United Nations, 1958.
- (8) Catalog for Polonium and Plutonium Sources. Mound Laboratory.
Miamisburg, Ohio.
- (9) Clayton, E. D.
Private Communication. Hanford Laboratory. Richland,
Washington. December 5, 1960.
- (10) Davenport, D. E., G. L. Lynn and D. C. Pound.
Hanford Standard Pile. HW-21793, 1951.
- (11) Davenport, D. E., G. L. Lynn and C. R. Richey.
The Standardization (nv/q) of Gold and Indium Foils and the
Absolute Neutron Flux Determination in the Hanford Standard
Pile. HW-26207, 1954.
- (12) Davis, M. V., and D. T. Hauser.
Thermal-Neutron Data for the Elements. Nucleonics.
16(3): 87. 1958.

- (13) Duggal, V. P., and J. Martelly.
A Study of the Slowing Down of Neutrons in Graphite.
A/CONF. 8/5/P/358. New York: United Nations, 1956.
- (14) Etherington, H.
Nuclear Engineering Handbook. New York: McGraw-Hill,
1958.
- (15) Glasstone, W., and E. C. Edlund.
The Elements of Nuclear Reactor Theory. Princeton:
Van Nostrand. 1952.
- (16) Graves, A. C., and D. K. Froman.
Miscellaneous Physical and Chemical Techniques of the
Los Alamos Project. New York: McGraw-Hill, 1952.
- (17) Greenfield, M. A., R. L. Koontz, A. A. Jarrett, and J. K. Taylor.
Measuring Flux Absolutely with Indium Foils. Nucleonics.
15(3):57. 1957.
- (18) Hess, W. N.
Neutrons from (α , n) Sources, UCRL-3839, 1957.
- (19) Hill, J. E., L. D. Roberts, and G. McCammon.
A Study of the Slowing Down Distribution of Sb^{124} - Be
photoneutrons in Graphite and the Use of Indium Foils.
Phys. Rev. 80:6. 1950.
- (20) Hughes, D. J.
Pile Neutron Research. Cambridge: Addison-Wesley, 1953.
- (21) Hughes, D. J., and R. B. Schwartz.
Neutron Cross Sections. Suppl. 1, BNL-325, 2nd ed., 1960.
- (22) Kaiser, R. E.
Unpublished work and private communication. Kansas State
University. 1961.
- (23) Koontz, R. L., H. A. Greenfield, and A. A. Jarrett.
Absolute Thermal Neutron Determination. Parts I, II and III.
NAA-SR-1137, 1957.
- (24) Meghreblian, R. V., and D. K. Holmes.
Reactor Analysis. New York: McGraw-Hill. 1960.
- (25) Nasim, Mohammed.
Unpublished work and private communication. Kansas State
University, 1961.

- (26) Nichols, P. F.
Absorption Cross Section of Graphite. *Nuc. Sci. and Eng.*,
7(5):395-399, 1960.
- (27) Prohammer, F.
Private communication. Argonne National Laboratory,
Lemont, Illinois. Nov. 9, 1960.
- (28) Price, W. J.
Nuclear Radiation Detection. New York: McGraw-Hill, 1958.
- (29) Raievski, V., and J. Horowitz.
Determination of the Mean Transfer Free Path of Thermal
Neutrons by Measurement of the Complex Diffusion Length.
A/CONF. 8/5/P/360. New York: United Nations, 1956.
- (30) Reactor Handbook. AECD-3645, 1955.
- (31) Reactor Physics Constants. ANL-5800, 1958.
- (32) Redman, C.
Calibration of the New Argonne Standard Pile. AECD-3383,
1946.
- (33) Scarborough, J. B.
Numerical Mathematical Analysis. Baltimore: Johns
Hopkins, 1950.
- (34) Segre, E.
Experimental Nuclear Physics. Vol. 2. New York:
John Wiley, 1953.
- (35) Seren, L.
Report on Argonne Standard Pile. CP-704, 1943.
- (36) Singwi, K. S., and L. S. Kothari.
Transport Cross Section of Thermal Neutrons in Solid
Moderators. A/CONF 15/16/P/1638. Geneva: United
Nations, 1958
- (37) Sneddon, I. N.
Fourier Transforms. New York: McGraw-Hill, 1951.
- (38) Stewart, L.
The Energy Spectrum of Neutrons from a Pu-Be Source.
Phys. Rev. 98:740, 1955.
- (39) Steichen, C. U.
The Experimental Determination and Analytical Verification
of the Age of Pu-Be Source Neutrons in Graphite. M. S.
Thesis. Kansas State University, 1960.

- (40) Tittle, C. W.
Slow Neutron Detection by Foils. *Nucleonics*. 9(1):60-67,
1951.
- (41) Wade, J. W.
Neutron Age in Mixtures of D_2O and H_2O . *Nuc. Sci. and
Eng.*, 4(1):12-24. 1958.
- (42) Wallace, P. R., and J. LeCaine.
Elementary Approximations in the Theory of Neutron
Diffusion. AECL-336, 1943.
- (43) Weinberg, A. M., and E. P. Wigner.
The Physical Theory of Neutron Chain Reactors. Chicago:
University of Chicago, 1958.
- (44) Wright, W. B., and R. T. Frost
KAPL-M-WBW, 1956.

APPENDICES

APPENDIX A

Solutions to the Fermi Age Equation and
the Thermal Diffusion Equation for the
Standard Pile Analysis

The geometry for the standard pile solution is shown in Fig. 24.

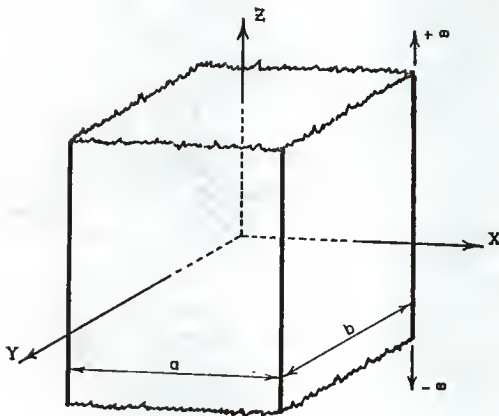


Fig. 24. Geometry for the standard pile solution.

The equations solved were the Fermi age equation

$$\nabla^2 q = \frac{\partial q}{\partial \tau} \quad (\text{A-1})$$

and the thermal diffusion equation

$$D\nabla^2 \phi - \Sigma_a \phi + S = 0 \quad (\text{A-2})$$

The Fermi age equation was subjected to the boundary conditions that $q = 0$ at $x = \pm a/2$, $y = \pm b/2$, and $q \rightarrow 0$ as $|z| \rightarrow \infty$.

The source condition was that all source neutrons entered the system at $x = y = z = 0$, at an age $\tau = 0$.

This condition was written into the Fermi age equation in the form

$$\nabla^2 q = \frac{\partial q}{\partial \tau} - Q_0 \delta(\tau) \delta(x) \delta(y) \delta(z). \quad (\text{A-3})$$

The boundary conditions to the thermal diffusion equation were that $\phi = 0$ at $x = \pm a/2$, $y = \pm b/2$, and $\phi \rightarrow 0$ as $|z| \rightarrow \infty$. The source condition was that $S = q(x, y, z, \tau_{th})$.

Q_0 , q and ϕ were expressed as double Fourier series satisfying the boundary conditions

$$\phi = \sum_{m=1}^{\infty} \sum_{n=1}^{\infty} \phi_{mn}(z) \cos \frac{m\pi x}{a} \cos \frac{n\pi y}{b} \quad (\text{A-4})$$

$$q = \sum_{m=1}^{\infty} \sum_{n=1}^{\infty} q_{mn}(z) \cos \frac{m\pi x}{a} \cos \frac{n\pi y}{b} \quad (\text{A-5})$$

and

$$Q_0 \delta(\tau) \delta(x) \delta(y) \delta(z) = \sum_{m=1}^{\infty} \sum_{n=1}^{\infty} Q_{mn}(z) \cos \frac{m\pi x}{a} \cos \frac{n\pi y}{b} \quad (\text{A-6})$$

where m and n are summed over odd integers. Each side of Eq. A-6 was multiplied by orthogonal functions and then was integrated over the range of orthogonality which resulted in

$$Q_0 \delta(\tau) \delta(x) \delta(y) \delta(z) = \frac{4Q_0}{ab} \delta(\tau) \delta(z) \cos \frac{m\pi x}{a} \cos \frac{n\pi y}{b} \quad (\text{A-7})$$

Substitution of Eqs. A-5 and A-7 into the age equation, Eq. A-3 gave

$$\sum_{m=1}^{\infty} \sum_{n=1}^{\infty} \left[-\frac{\partial q_{mn}}{\partial \tau} + \frac{\partial^2 q_{mn}}{\partial z^2} - \left(\frac{m^2 \pi^2}{a^2} + \frac{n^2 \pi^2}{b^2} \right) q_{mn} + \frac{4Q_0}{ab} \delta(\tau) \delta(z) \right] = 0. \quad (\text{A-8})$$

Taking the Fourier transform of the equation for a particular m and n and letting

$$\alpha_m = \frac{m \pi}{a} \quad (\text{A-9})$$

and

$$\beta_n = \frac{n \pi}{b} \quad (\text{A-10})$$

led to

$$\frac{\partial \bar{q}(\omega)}{\partial \tau} + (\alpha_m^2 + \beta_n^2 + \omega^2) \bar{q}(\omega) = \frac{4Q_0}{ab} \delta(\tau) \quad (\text{A-11})$$

where $\bar{q}(\omega)$ represents the Fourier transform of $q_{mn}(z)$.

The solution to this differential equation was

$$\bar{q}(\omega) = \frac{4Q_0}{ab} e^{-(\alpha_m^2 + \beta_n^2 + \omega^2)\tau} \quad (\text{A-12})$$

Taking the inverse transform of Eq. A-12 and substituting it into Eq. A-5 gave the slowing down density along the z axis as

$$q(z) = \sum_{m=1}^{\infty} \sum_{n=1}^{\infty} \frac{4Q_0 e^{-(\alpha_m^2 + \beta_n^2)\tau}}{ab \sqrt{4\pi\tau}} e^{-z^2/4\tau} \quad (\text{A-13})$$

Substitution of Eqs. A-4 and A-5 into the thermal diffusion equation, Eq. A-2, and designating $\frac{\Sigma_a}{D}$ as κ^2 gave

$$\sum_{m=1}^{\infty} \sum_{n=1}^{\infty} \left[\frac{\partial^2 \phi_{mn}}{\partial z^2} - (\alpha_m^2 + \beta_n^2 + \kappa^2) \phi_{mn} + \frac{q_{mn}}{D} \right] = 0. \quad (\text{A-14})$$

Taking the Fourier transform of Eq. A-14 for a particular m and n and designating the Fourier transforms of ϕ_{mn} and q_{mn} by $\bar{\phi}(\omega)$ and $\bar{q}(\omega)$, respectively, gave

$$\bar{\phi}(\omega) = \frac{\bar{q}(\omega)}{D(\alpha_m^2 + \beta_n^2 + \omega^2)}. \quad (\text{A-15})$$

Taking the inverse transform of Eq. A-15 by means of the convolution theorem (42), after Eq. A-12 had been used to express $\bar{q}(\omega)$ gave

$$\phi_{mn} = \frac{2Q_0 b_{mn} e^{-(\alpha_m^2 + \beta_m^2)\tau}}{D a b \sqrt{4\pi\tau}} \int_{-\infty}^{\infty} e^{-z^2/4\tau} e^{-|z-z'|/b_{mn}} dz' \quad (\text{A-16})$$

where

$$b_{mn} = \frac{1}{\sqrt{\alpha_m^2 + \beta_n^2 + \kappa^2}}. \quad (\text{A-17})$$

Glasstone and Edlund (15), on pages 185 to 187, give the development showing how the integral in Eq. A-16 may be expressed in terms of the error function

$$\text{erf}(t) = \frac{2}{\sqrt{\pi}} \int_0^t e^{-u^2} du. \quad (\text{A-18})$$

Writing Eq. A-16 in terms of the error function and substituting it into Eq. A-4 gave the thermal flux along the z axis as

$$\phi(z) = \sum_{m=1}^{\infty} \sum_{n=1}^{\infty} \frac{Q_0 b_{mn}}{D a b} e^{\kappa^2 \tau} \left[e^{-z/b_{mn}} \left\{ 1 + \operatorname{erf} \left(\frac{z}{2\sqrt{\tau}} - \frac{\sqrt{\tau}}{2b_{mn}} \right) \right\} \right. \\ \left. + e^{z/b_{mn}} \left\{ 1 - \operatorname{erf} \left(\frac{z}{2\sqrt{\tau}} + \frac{\sqrt{\tau}}{2b_{mn}} \right) \right\} \right] \quad (\text{A-19})$$

If difficulty has been encountered in following this solution, it may be helpful to study References (37) and (42).

APPENDIX B

Finite Pile Solution to the Thermal Diffusion
Equation Using the Distributed Thermal
Source Found from the Solution to
the Fermi Age Equation.

The geometry for this finite pile solution is shown in Fig. 25.

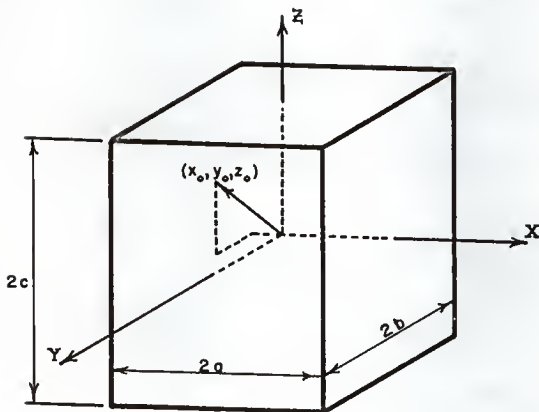


Fig. 25. Pile geometry for fast point source in finite pile.

The equations solved were the Fermi age equation

$$\nabla^2 q = \frac{\partial q}{\partial \tau} \quad (\text{B-1})$$

and the thermal diffusion equation

$$D\nabla^2 \phi - \Sigma_a \phi + S = 0. \quad (\text{B-2})$$

The Fermi age equation was subjected to the boundary conditions that $q = 0$ at $x = \pm a$, $y = \pm b$, and $z = \pm c$. The source condition was that all source neutrons entered the system at $x = x_0$, $y = y_0$,

and $z = z_0$; and at $\tau = 0$.

The boundary conditions to the thermal diffusion equation were that $\phi = 0$ at $x = \pm a$, $y = \pm b$, and $z = \pm c$. The source condition was that $S = q(x, y, z, \tau_{th})$.

By assuming that the variables of q were separable,

$$q(x, y, z, \tau) = M(x, y, z) N(\tau) \quad (B-3)$$

the age equation could be written

$$\frac{1}{M} \nabla^2 M = \frac{1}{N} \frac{dN}{d\tau} = -B^2 \quad (B-4)$$

Solutions satisfying the boundary conditions and the two independent differential equations were

$$M(x, y, z) = \sum_{m=1}^{\infty} \sum_{n=1}^{\infty} \sum_{o=1}^{\infty} A'_{mno} F_m(x) G_n(y) H_o(z) \quad (B-5)$$

where

$$F_m(x) = \frac{1}{\sqrt{a}} \cos \alpha_m x$$

$$F_m(x) = \frac{1}{\sqrt{a}} \sin \alpha_m x \quad (B-6)$$

$$\alpha_m = \frac{m\pi}{2a}$$

and

$$N(\tau) = \sum_{m=1}^{\infty} \sum_{n=1}^{\infty} \sum_{o=1}^{\infty} A''_{mno} e^{-B^2_{mno} \tau} \quad (B-7)$$

where

$$B^2_{mno} = \alpha_m^2 + \beta_n^2 + \gamma_o^2. \quad (B-8)$$

$G_n(y)$, and $H_o(z)$ are similar to $F_m(x)$ except that b and β replace a and α , respectively, for the y direction; and c and γ are used for the z direction.

To evaluate A_{mno} in the resulting expression for q ,

$$q = \sum_{m=1}^{\infty} \sum_{n=1}^{\infty} \sum_{o=1}^{\infty} A_{mno} F_m(x) G_n(y) H_o(z) e^{-B_{mno}^2 \tau} \quad (B-9)$$

the source condition that

$$q(x, y, z, 0) = Q_0 \delta(x - x_0) \delta(y - y_0) \delta(z - z_0) \quad (B-10)$$

was used. Expressing Eq. B-10 with the use of Eq. B-9, multiplying both sides of the result by orthonormal functions, and integrating over the range of orthonormality led to the expression for A_{mno} ,

$$A_{mno} = Q_0 F_m(x_0) G_n(y_0) H_o(z_0). \quad (B-11)$$

The expression for the slowing down density evaluated at thermal energy was then

$$q(x, y, z, \tau_{th}) = \sum_{m=1}^{\infty} \sum_{n=1}^{\infty} \sum_{o=1}^{\infty} Q_0 F_m(x) F_m(x_0) G_n(y) G_n(y_0) H_o(z) H_o(z_0) e^{-B_{mno}^2 \tau_{th}} \quad (B-12)$$

Assuming that ϕ could be represented by the same orthonormal set used for q , a solution for the thermal diffusion was

$$\phi(x, y, z) = \sum_{m=1}^{\infty} \sum_{n=1}^{\infty} \sum_{o=1}^{\infty} C_{mno} F_m(x) G_n(y) H_o(z). \quad (B-13)$$

Substitution of this expression and the expression for slowing down density evaluated at thermal energy, Eq. B-12, into the thermal diffusion equation yielded

$$C_{mno} = \frac{Q_0 F_m(x_0) G_n(y_0) H_o(z_0)}{D(\alpha_m^2 + \beta_n^2 + \gamma_o^2 + \kappa^2)} e^{-B_{mno}^2 \tau_{th}} \quad (\text{B-14})$$

where

$$\kappa^2 \equiv \Sigma_a / D. \quad (\text{B-15})$$

The thermal flux was then

$$\phi(x, y, z) = \sum_{m=1}^{\infty} \sum_{n=1}^{\infty} \sum_{o=1}^{\infty} \frac{Q_0 F_m(x) F_m(x_0) G_n(y) G_n(y_0) H_o(z) H_o(z_0)}{D(\alpha_m^2 + \beta_n^2 + \gamma_o^2 + \kappa^2)} e^{-B_{mno}^2 \tau_{th}} \quad (\text{B-16})$$

APPENDIX C

Finite Pile Solution to the Thermal Diffusion Equation
using a Point Source of Thermal Neutrons.

The solution using a point source emitting only thermal neutrons, could have been determined by merely using τ_{th} as zero in Eq. B-15. However, it was found that such an expression converged quite slowly. The thermal diffusion equation was re-solved using the geometry shown in Fig. 26.

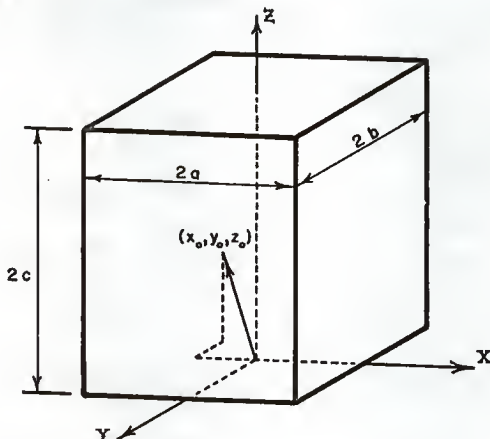


Fig. 26. Pile geometry for thermal point source in finite pile.

The boundary conditions to the thermal diffusion equation were that $\phi = 0$ at $x \pm a$, $y \pm b$, and $z = 0, 2c$. The point thermal neutron source was considered to be in the $z = z_0$ plane at $x = x_0$, and $y = y_0$. The source was introduced through the boundary

conditions that

$$\phi_1(z_0) = \phi_2(z_0) \quad (\text{C-1})$$

and

$$-D \left[\frac{d\phi_1}{dz} - \frac{d\phi_2}{dz} \right]_{z_0} = Q_0 \quad (\text{C-2})$$

where ϕ_1 was considered to be the flux of the region below the $z = z_0$ plane and ϕ_2 was the flux of the region above the z_0 plane.

Assuming that the variables of ϕ were separable,

$$\phi(x, y, z) = F(x) G(y) H(z) \quad (\text{C-3})$$

the thermal diffusion equation written without a source term,

$$\nabla^2 \phi - \kappa^2 \phi = 0 \quad (\text{C-4})$$

could be written as

$$\frac{1}{F} \frac{d^2 F}{dx^2} + \frac{1}{G} \frac{d^2 G}{dy^2} + \frac{1}{H} \frac{d^2 H}{dz^2} - \kappa^2 = 0. \quad (\text{C-4})$$

A solution for the region above the z_0 plane that satisfied the boundary conditions and the diffusion equation was

$$\phi(x, y, z) = \sum_{m=1}^{\infty} \sum_{n=1}^{\infty} A_{mn} F_m(x) G_n(y) H_{mn}(z) \quad (\text{C-6})$$

where

$$\begin{aligned} F_m(x) &= \frac{1}{\sqrt{a}} \cos \alpha_m x && \text{for } m \text{ odd} \\ &= \frac{1}{\sqrt{a}} \sin \alpha_m x && \text{for } m \text{ even} \end{aligned} \quad (\text{C-7})$$

$$\alpha_m = \frac{m\pi}{2a}$$

and

$$H_{mn}(z) = \sinh \gamma_{mn} (2c - z) \quad (C-8)$$

where

$$\gamma_{mn}^2 = \alpha_m^2 + \beta_n^2 + \kappa^2 \quad (C-9)$$

$G_n(y)$ is similar to $F_m(x)$ except that b , n , and β replace a , m , and α , respectively.

Expanding the source term in a similar two-dimensional set in x and y ,

$$Q_0 \delta(x - x_0) \delta(y - y_0) = \sum_{m=1}^{\infty} \sum_{n=1}^{\infty} Q_{mn} F_m(x) G_n(y), \quad (C-10)$$

multiplying both sides by the orthonormal functions and integrating over the range of orthonormality gave

$$Q_0 \delta(x - x_0) \delta(y - y_0) = \sum_{m=1}^{\infty} \sum_{n=1}^{\infty} Q_{mn} F_m(x_0) G_n(y_0) \quad (C-11)$$

Using the boundary conditions, Eq. C-1 and Eq. C-2 with Eq. C-11 led to the evaluation of A_{mn} for the region above the z_0 plane,

$$A_{mn} = \frac{Q_0 F_m(x_0) G_n(y_0) \sinh \gamma_{mn}(z_0)}{D \gamma_{mn} \sinh 2\gamma_{mn} C} \quad (C-12)$$

The expression for the thermal flux in the region above the plane of the source was then

$$\phi(x, y, z) = \sum_{m=1}^{\infty} \sum_{n=1}^{\infty} \frac{Q_0}{D \gamma_{mn}} F_m(x) F_m(x_0) G_n(y) G_n(y_0) \frac{\sinh \gamma_{mn} z_0 \sinh \gamma_{mn}(2c-z)}{\sinh 2\gamma_{mn} C} \quad (C-13)$$

APPENDIX D

Description and Explanation of the IBM-650
Computer Program used to Calculate the
Flux in the Standard Pile

This computer program was written to calculate the thermal neutron flux along the central axis of the KSU Standard Pile. The program was written in SOAP II and floating point. The object program and the logic diagram are given in this section.

$$\phi(z) = \sum_{i=1}^N \sum_{j,k=1}^{\infty} \frac{3f_i Q_0 b_{jk}}{\lambda_{r,ab}} e^{-(\alpha_j^2 + \beta_k^2) \frac{r_{th-i}^2}{4}} e^{\frac{r_{th-i}^2}{4b_{jk}}} \left\{ e^{-\frac{z}{b_{jk}}} \left[1 + \operatorname{erf} \left(\frac{z}{r_{th-i}} - \frac{r_{th-i}}{2b_{jk}} \right) \right] \right. \\ \left. + e^{\frac{z}{b_{jk}}} \left[1 - \operatorname{erf} \left(\frac{z}{r_{th-i}} + \frac{r_{th-i}}{2b_{jk}} \right) \right] \right\} \quad (D-1)$$

$$\text{where } \left(\frac{1}{b_{jk}} \right)^2 = \frac{1}{L^2} + \frac{\pi^2 j^2}{a^2} + \frac{\pi^2 k^2}{b^2} = \kappa^2 + \alpha_j^2 + \beta_k^2 \quad (D-2)$$

$$\text{and } \operatorname{erf}(t) = \frac{2}{\sqrt{\pi}} \int_0^t e^{-u^2} du. \quad (D-3)$$

The program was set up to sum the infinite series j and k by summing over odd integers j , holding k constant, until the contribution of a term of the series became less than a specified precision. Index k was then increased by two and the summation on index j repeated until the precision specification was met.

This summation process was repeated in such a manner that contributions from all possible combinations of odd j and k that were greater than a specified precision were included in the summation.

Input data consisted of diffusion parameters, numerical constants and geometrical specifications. The positions along the central z axis at which the flux was to be calculated were read into drum storage locations starting with 1001. The program had a capacity for 100 flux positions. The Gaussian ranges were read into drum storage locations 0101, 0102, and 0103. The corresponding fractional contributions of each Gaussian term were read into drum locations 0104, 0105, and 0106, respectively. Table 11 lists other input data required for program use.

Table 11. Input data required for use of the IBM-650 program which calculates the flux in the standard pile.

Symbol	Explanation	Drum storage location
1	Identification number 1	0041
3	Identification number 3	0969
4	Identification number 4	0389
ZERO	0.00	0226
ONE	1.00	0250
TWO	2.00	0212
THREE	3.00	0340
FOUR	4.00	0407
A	Width of pile in x direction (cm)	0369
B	Width of pile in y direction (cm)	0469
PI	π	0259
SQPI	$\sqrt{\pi}$	0350
Q	Source strength (n/sec)	0572
KAPP2	Reciprocal of diffusion length squared (cm^{-2})	0158
LMBDA	Transport mean free path (cm)	0025
INDXA	Number of Gaussian range groups	0114
INDXC	Number of flux points	0202
PREC	Specified precision of last term in summation	0047

Other symbols corresponding to terms in the program print out and the logic diagram are given as follows:

FRAC = f_i , the fractional contribution of the i^{th} Gaussian range

TURM = The part of the solution which depends on a particular j and k

SUM 1 = Summation of TURMS

$E = f_i e^{r_{\text{th}-i}^2 \kappa^2}$ (SUM 1)

$F = \sum_{i=1}^N E_i$

The machine yielded an answer card having a capacity of eight words, a word being a ten digit number and a sign. Provision was made for printing out partial answers for checking purposes, thus making it necessary to identify partial answer cards by the use of an identification number which was always printed in the word 1 location of the answer card. Table 12 lists the identification number and the answer card content of the various print outs. If the partial answer print outs are not needed, they may be eliminated by use of the one word load cards listed in Table 13.

Table 12. Answer identification table for various answer print outs for the standard pile flux.

Word 1	Word 2	Word 3	Word 4	Word 5	Word 6	Word 7	Word 8
1	J	K	R	Z	TURM	SUM 1	
3	FRAC	SUM 1	SUM 2	E			
4	Z					F	FLUX

Table 13. One word load cards used for eliminating unnecessary answer print outs for standard pile flux program.

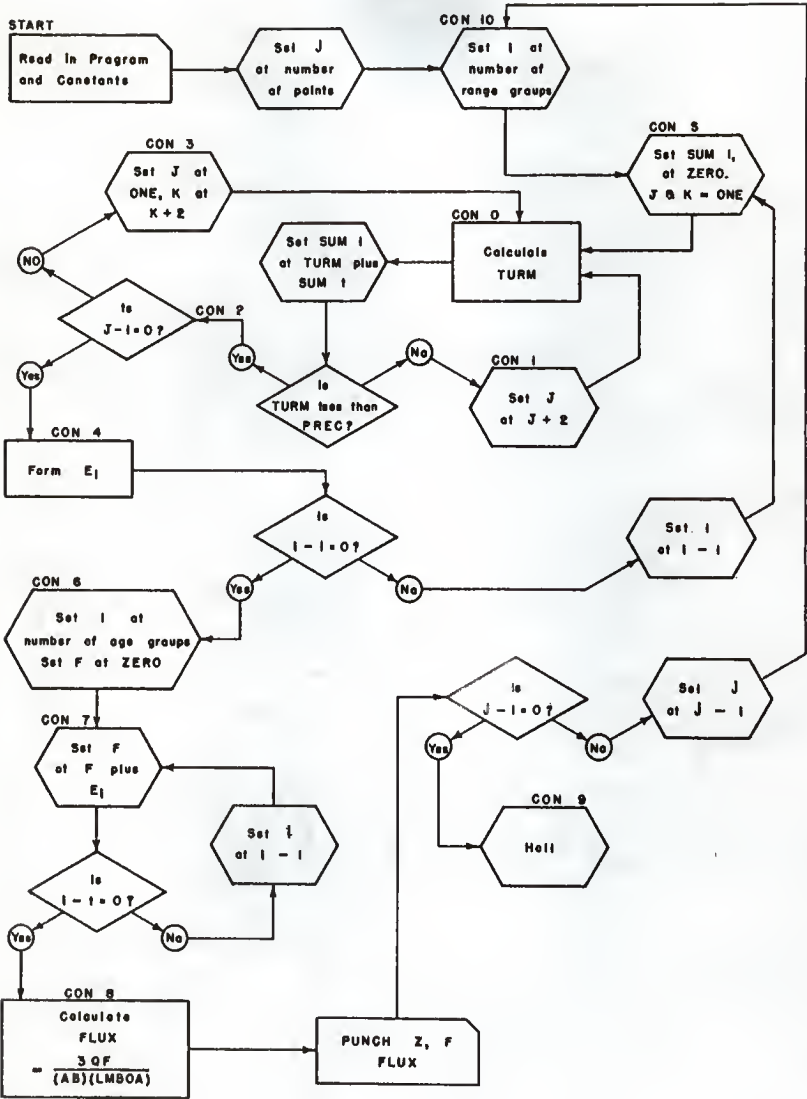
Print out identification :	Instruction address :	Instruction
1	0435	60 0152 0357
3	0263	50 0001 0183

Table 14. Computer precision study for standard pile flux.

PREC :	Flux at $z = 5.63$ cm	Convergence time	Flux at $z = 158.08$ cm	Convergence time
10^0	2259.4 n/cm ² -sec		32.361 n/cm ² -sec	
10^{-1}	2273.9	49 sec	32.758	17 sec
10^{-2}	2275.1	62	32.758	17
10^{-3}	2275.3	89	32.768	29
10^{-4}	2275.3	114	32.768	35

Table 14 presents a study showing the flux values as a function of the specified accuracy of the last term in the finite series.

LOGIC DIAGRAM - APPENDIX D



STANDARD				BILL				
FLUX				FLUX				
BLR	0100	0110		1	0000	00	0000	0000
BLR	1000	1100		2	0000	00	0000	0000
BLR	1951	1960		3	0000	00	0000	0000
BLR	1977	1985		4	0000	00	0000	0000
SVN	FRAC	0104		5	0000	00	0000	0000
SVN	FRAC	0107		6	0000	00	0000	0000
SVN	START	0110		7	0000	00	0000	0000
SVN	Z	1909		8	0000	00	0000	0000
SVN	Z	1000		9	0000	00	0000	0000
EDDEA	STO AAA1		E TO X	10	0000	24	0003	0005
	RID AAA2		SUBROUTINE	11	0005	24	0005	0199
	BITL AAA3		X FOR CALC	12	0014	67	0011	0015
	RID AAA3			13	0035	20	0019	0023
	FMP AAA3			14	0038	30	0038	0038
	FAD AAA16			15	0023	39	0026	0076
	FAD AAA15			16	0076	32	0039	0076
	FAD AAA15			17	0005	35	0019	0049
	FAD AAA14			18	0069	32	0072	0049
	FAD AAA13			19	0049	39	0049	0039
	FAD AAA13			20	0119	32	0122	0099
	FAD AAA3			21	0099	32	0019	0168
	FAD AAA12			22	0169	32	0172	0149
	FAD AAA3			23	0149	32	0019	0219
	FAD AAA11			24	0219	32	0222	0199
	FMP AAA3			25	0199	39	0019	0269
	FAD AAA10			26	0269	32	0272	0249
	STU AAA4			27	0249	21	0004	0007
	FMP AAA4			28	0007	39	0004	0054
	FMP AAA4			29	0054	21	0004	0057
	FMP AAA4			30	0057	39	0004	0154
	STU AAA4			31	0154	21	0004	0157
	RID AAA4			32	0157	24	1998	0033
	BMI AAA5	AAA5		33	0065	46	0018	0319
	STU AAA4			34	0018	40	0018	0027
AAA5	RAU AAA10			35	0027	34	0004	0204
	STU AAA4	AAA5		36	0204	21	0004	0319
	RAU AAA4	AAA5		37	0319	45	0000	0000
AAA6	10	0000	0051	38	0272	10	0000	0051
AAA10	24	9928	6850	39	0272	24	9928	6850
AAA12	31	2575	8349	40	0172	31	2575	8349
AAA13	25	9137	1248	41	0122	25	9137	1248
AAA14	37	9137	0047	42	0072	17	0000	0047
AAA15	54	3020	0045	43	0029	54	3020	0045
AAA16	69	0000	0044	44	0086	69	0000	0044
EDDCL	STO ZZZ1		CLEAR	45	0000	40	0051	0056
	LOD ZZZ10		PUNCH	46	0056	69	0009	0012
	STO 1977		ROUTINE	47	0012	64	0012	0030
	STO 1978			48	0030	24	1978	0031
	STO 1979			49	0031	24	1978	0032
	STO 1980			50	0032	24	1980	0033
	STO 1981			51	0033	24	1981	0034
	STO 1982			52	0034	24	1982	0035
	STO 1983			53	0035	24	1983	0036
	STO 1984	ZZZ1		54	0036	24	1984	0037
	00	0000	0000	55	0000	00	0000	0000
EDDAU	STO SEXT		SQUARE	1	0500	24	0153	0156
	BMI BERR		8BIT	2	0000	45	0066	0160
	WZ	SEXT	SUB	3	0010	45	0064	0153
	STU SA		ROUTINE	4	0064	31	0068	0081
	FAD B10			5	0081	30	0081	0081
	FMP SHAF	SB		6	0001	39	0084	0304
	STU SHAF	SAB		7	0024	21	0008	0065
SB	RID SBA		8 CAPT A	8	0064	30	0068	0073
	FVD SBAV			9	0073	34	0008	0058
	FMP SBAV			10	0068	34	0008	0062
	FMP SHAF			11	0085	39	0085	0354
	FMB SBAV			12	0073	21	0008	0335
	WZ	SR		13	0035	44	0019	0040
	BMI	SR		14	0039	46	0042	0040
	FAD SBAV	SAB		15	0042	32	0008	0185
	STU SBAV	SAB		16	0185	21	0008	0061
	SR	SBAV	SEXT	17	0040	60	0008	0153
	BERR	HIT	0000	18	0000	60	0000	0000
	SHAF	BD	0000	19	0254	50	0000	0050
	S10	BD	0000	20	0254	10	0000	0051
	ERF	STO EXIT	ERROR	75	0200	24	0803	0205
	RAU A1		SUBROUTINE	77	0026	60	0159	0013
	FMP A1			78	0013	39	0016	0066
	STU A1X1			79	0066	21	0020	0123
	FVD A1			80	0123	34	0159	0209
	FMP A2			81	0209	38	0062	0112
	FMP X			82	0112	39	0016	0116
	FVD A2X2			83	0116	21	0016	0116
	FVD A2			84	0173	34	0062	0162
	FMP X			85	0162	39	0116	0165
	STU A3			86	0165	39	0016	0166
	FMP A3X3			87	0166	21	0120	0223
	FVD A3			88	0223	14	0116	0215
	FMP A4			89	0215	30	0118	0268
	FMP X			90	0168	39	0016	0216
	STU A4X4			91	0216	21	0016	0273
	FVD A4			92	0273	34	0118	0218
	FMP A5			93	0218	39	0016	0321
	FMP X			94	0211	39	0016	0265
	STU A5X5			95	0266	21	0220	0321
	FVD A5			96	0321	34	0071	0171
	FMP A6			97	0171	39	0074	0124
	FMP X			98	0124	39	0016	0316
	FAD A5X5			99	0316	33	0220	0047
	FAD A4X4			100	0047	32	0170	0097
	FAD A3X3			101	0097	32	0080	0147
	FAD A2X2			102	0147	32	0078	0197
	FAD A1X1			103	0197	32	0078	0247
	FAD ONE			104	0247	32	0250	0077
	STU TERM1			105	0077	21	0082	0235
	FMP TERM1			106	0235	39	0235	0235
	STU TERM2			107	0132	21	0086	0282
	FMP TERM2			108	0282	39	0086	0282
	STU TERM3			109	0089	39	0086	0143
	FMP TERM3			110	0143	21	0090	0040
	STU TERM4			111	0040	21	0090	0140
	FMP TERM4			112	0297	39	0044	0094
	RAU ONE			113	0094	21	0084	0111
	FVD ONE			114	0051	60	0250	0055
	STU TERM			115	0055	34	0048	0098
	FMP TERM			116	0098	21	0002	0135
	RAU ONE			117	0155	60	0250	0205
	FBS TERM			118	0205	33	0002	0203
	A1	70	5230	119	0159	70	5330	7849
			EXIT					
			7849					

A2	42	2820	1249		120	0052	42	2820	1249
A3	92	7052	7248		122	0112	43	2821	7248
A4	15	2014	3047		128	0118	15	2014	3047
A5	27	6567	8047		123	0071	27	6567	8047
A6	43	0618	0046		124	0074	43	0618	0046
REPET	STO	EXET		SUBROUTINE	125	0300	24	0253	0286
	RAU	P1		TO FIND	126	0056	60	0256	60
	FMP	J		TURN FOR	127	0063	39	0366	0416
	FOV	A		PARTICULAR	128	0416	34	0369	0419
	FMP	ALPH		J AND K	129	0127	39	0174	0224
	STU	ALPH2			131	0081	60	0259	0113
	FMP	K			133	0513	39	0466	0556
	FOV	P1			134	0516	34	0469	0558
	STU	BETA			135	0519	21	0274	0177
	FMP	BETA			136	0177	39	0274	0324
	FAD	KAPP2			137	0034	60	0034	0034
	STU	TEMP1			138	0255	32	0158	0285
	RAU	ONE			139	0093	60	0250	0305
	FOV	TEMP1			141	0305	34	0198	0240
	LOO		EOOAU		142	0405	34	0143	0180
	STU	BJK		FORM BJK	143	0143	21	0148	0151
	RAU	R	A		144	0151	60	2104	0309
	FOV	TRO			145	0309	34	0212	0262
	FOV	BJK			146	0568	34	0148	0198
	STU	ROVER			147	0198	21	0032	0358
	RAU	Z	C		148	0358	60	7000	0405
	FOV	R			149	0405	34	0128	0404
	STU	ZOVER			150	0404	21	0208	0111
	FAO	ROVER			151	0111	32	0052	0079
	LDD	X	ERF		152	0179	21	0016	0349
	LDD	X			153	0569	69	0322	0200
	STU	ERFK			154	0322	21	0126	0154
	RAU	ONE			155	0129	60	0250	0455
	FBS	ERFK			156	0455	33	0126	0303
	STU	PAR1			157	0126	21	0214	0111
	RAU	ZOVER			158	0161	60	0208	0163
	FBS	ROVER			159	0163	21	0052	0129
	STU	X			160	0179	21	0016	0619
	RAU	B003	SUB2		161	0619	46	0372	0373
	RAU	B002			162	0372	60	8003	0269
	STU	X			163	0229	60	8002	0032
	LDD	X	ERF		164	0032	21	0016	0669
	RAL	B003			165	0669	65	8003	0279
	FOV	ONE	SUB3		166	0279	60	0032	0287
	LDD	ONE	ERF		168	0087	32	0250	0227
	FAD	ONE	SUB3		169	0275	68	0176	0200
	STU	PAR2	SUB3		171	0176	32	0016	0227
	FOV	BJK	C		172	0227	21	0122	0338
	STU	TEMP1			173	0338	60	1036	0115
	LDD	TEMP1			174	0508	34	0148	0248
	RAL	B003			175	0248	21	0100	0393
	LDD	B002	EOOEA		176	0201	69	0454	0000
	FMP	PAR1			177	0454	60	0250	0253
	STU	PAR1			178	0213	39	0258	0308
	RAL	TEMP1			179	0308	21	0322	0265
	LDD	B002	EOOEA		180	0265	60	0198	0349
	FMP	PAR2			181	0045	68	0238	0000
	RAU	PAR2			182	0238	60	8002	0207
	FAD	RAP1		TURN FOR	183	0207	39	0122	0232
	FMP	BJK		J AND K	184	0232	32	0312	0139
	STU	TURN	EXET		185	0139	21	0348	0148
	LDD	INDX0		SET -TRG AT	186	0348	21	0152	0253
	RAL	B001	CON10	NUMR OF Z	187	0253	69	0803	0096
	LDD	INDXA		SET -TRA AT	189	0911	69	0114	0017
	RSA	B001	CON5	NUMR OF R	190	0017	61	0017	0123
	LDD	ZERO		SET -SUM1	191	0423	65	0006	0309
	STU	SUM1		AT ZERO	192	0309	24	0293	0385
	LDD	ONE		SET J AT 1	193	0385	60	0293	0385
	STU	K	CON0	SET K AT 1	194	0353	24	0366	0719
	LDD	ONE	REPET	FIND TURN	195	0719	24	0466	0769
	RAU	SUM1		A00 TURN	196	0466	60	0252	0287
	STU	SUM1		TO SUM1	198	0257	35	0282	0359
	LDD	1	EOOCL	PRINT	199	0359	21	0282	0435
	STO	1977		PARTIAL	201	0038	65	0041	0144
	LDD	J		ARGUMENTS	202	0144	24	1977	0000
	STO	1978		FOR	203	0280	33	0366	0436
	LDD	J	A	CHECKING	204	0819	24	1976	0131
	STO	1979			205	0405	60	0466	0868
	LDD	R	C		206	0869	24	1979	0332
	STO	1980			207	0332	69	2104	0307
	LDD	Z	A		208	0307	60	1980	0011
	STO	1981			209	0083	69	7000	0403
	LDD	TURN			210	0403	60	1981	0004
	STO	1982			211	0084	60	1981	0005
	LDD	SUM1			212	0605	24	1982	0485
	STO	1983			213	0485	69	0282	0377
	PCN=1977				214	0538	24	1983	0186
	RAU	TURN		TEST	216	0277	60	0152	0357
	FBS	PREC		PRECISION	217	0357	33	0060	0137
	RAU	J	CON1	OF TURN	218	0137	32	0232	0211
	STU	J		SET J AT	219	0091	60	0366	0221
	FAD	TRO	CON0	J PLUS 2	220	0221	32	0212	0189
	STU	J			221	0189	60	0250	0228
	RAU	J		TEST	222	0290	60	0366	0271
	FBS	ONE		PRECISION	223	0271	33	0232	0211
	NZE	CON3	CON4	OF TURN	224	0327	45	0130	0181
	STU	J		SET J AT 1	225	0215	60	0130	0255
	RAU	J			226	0655	21	0366	0919
	FAD	TRO		SET K AT	227	0919	60	0466	0321
	STU	K	CON0	K PLUS 2	228	0321	32	0366	0221
	RAU	R	A		229	0339	21	0466	0769
	FMP	R	A		230	0769	60	0250	0230
	FMP	R	A		231	0409	39	0104	0504
	FOV	FOUR			232	0504	34	0407	0457
	FMP	KAPP2			233	0457	39	0158	0274
	RAL	B003			234	0358	65	8003	0315
	LDD	B002	EOOEA		235	0315	69	0268	0000
	RAU	B002		STORE FLUX	236	0268	60	8002	0377
	FMP	SUM1		CONTRIBU	237	0377	39	0228	0382
	STU	SUM2		CONTRIBU	238	0382	39	0282	0219
	FMP	FRAC	A	PARTICULAR	239	0289	39	2107	0527
	STU	E	A		240	0507	21	0110	0263
	LDD	B003	EOOCL		240	0263	69	0266	0050

LDD 3			242	0566	69	0969	0522
STO 1977		PRINT	243	0522	69	1977	0210
LDD FRAC A		PARTIAL	244	0180	69	2107	0160
STO 1978		ANSWERS	245	0160	24	1978	0251
LDD RW1		FOR	246	0231	69	0292	0385
STO 1979		CHECKING	247	0585	24	1979	0432
LDD BU1			248	0432	69	0432	0359
STO 1980			249	0339	24	1980	0133
LDD E	A		250	0133	69	2110	0313
STO 1981			251	0113	24	1981	0134
PCH 1977			252	0134	71	1977	0427
AXA 0001		SET R AT	253	0427	30	0001	0183
NZC 005	CON6	NEW R	254	0183	40	0403	0368
LDD INDXA			255	0187	59	0114	0067
R A 0001			256	0067	69	0067	0473
LDD ZER0			257	0473	66	0224	0339
STO F	CON7	SUM	258	0379	24	0428	0535
RAU F	A	CONTRIBU	259	0635	40	2110	0368
FAO F		FROM EACH	260	0365	32	0428	0459
ST F		R	261	0459	69	0459	0285
AXA 0001			262	0685	50	0001	0141
NZC 007	CON8		263	0341	40	0628	0058
FMP THREE			265	0237	39	0340	0390
LDD 2			266	0390	34	0340	0119
FDV 8			267	1119	34	0429	1149
FMP 8			268	1169	39	0572	0622
FDV LMBDA		DETERMINE	269	0222	14	0023	0072
STU FLUX		FLUX	270	0075	21	0230	0233
LDD			271	0233	69	0286	0030
LDD 4	E00CL		272	0286	69	0389	0092
STO 1977		PRINT Z	273	0092	24	1977	0280
LDD 2		F AND FLUX	274	0280	69	7000	0453
STO 1978	C		275	0453	24	1978	0281
STO 1983			277	0735	24	1983	0336
LDD FLUX			278	0336	69	0230	0203
STO 1984			279	0283	24	1984	0287
PCH 1977		SET Z AT	280	0287	71	1977	0477
STC 0011		NEW Z	281	0477	53	0011	0333
NZC CON10	CON9		282	0333	48	0211	0337
HLT			283	0337	01	0387	0387
1	00 1000	0000	284	0041	00	1000	0000
3	00 3000	0000	285	0969	00	3000	0000
4	00 4000	0000	286	0389	00	4000	0000
7ER0	01 0000	0000	287	0286	00	0000	0000
ONE	10 0000	0051	288	0250	10	0000	0051
TWO	20 0000	0051	289	0222	20	0000	0051
THREE	30 0000	0051	290	0340	30	0000	0051
FOUR	40 0000	0051	291	0407	40	0000	0051
PI	51 4159	0051	292	0259	51	4159	0051
A	17 6230	0051	293	0369	17	6230	0051
B	17 6230	0053	294	0469	17	6230	0053
BOPI	17 7245	3951	295	0350	17	7245	3951
0	18 1000	0057	297	0578	18	1000	0057
KAPP2	33 2820	0047	298	0338	33	2820	0047
LMBDA	24 6000	0051	300	0025	24	6000	0051
INDXA	00 0000	0003	311	0114	00	0000	0003
INXC	00 0000	0014	308	0202	00	0000	0014
RO1	30 8400	0052	310	0101	30	8400	0052
RO2	39 3900	0052	310	0102	39	3900	0052
RO3	66 8500	0052	310	0103	66	8500	0052
FRACT1	12 8000	0050	310	0104	12	8000	0050
FRACT2	63 1000	0050	310	0105	63	1000	0050
FRACT3	24 1000	0050	310	0106	24	1000	0050
PREC	10 0000	0047	310	0060	10	0000	0047
Z1	56 3000	0051	1001	56	3000	0051	
Z2	18 8200	0052	1002	18	8200	0052	
Z3	25 9500	0052	1003	25	9500	0052	
Z4	36 1100	0052	1004	36	1100	0052	
Z5	46 3100	0052	1005	46	3100	0052	
Z6	56 4500	0052	1006	56	4500	0052	
Z7	66 1500	0052	1007	66	1500	0052	
Z8	76 7800	0052	1008	76	7800	0052	
Z9	86 9400	0052	1009	86	9400	0052	
Z10	97 1200	0052	1010	97	1200	0052	
Z11	11 7440	0053	1011	11	7440	0053	
Z12	11 7260	0053	1012	11	7260	0053	
Z13	15 8090	0053	1013	15	8090	0053	
Z14	17 8400	0053	1014	17	8400	0053	

APPENDIX E

Description and Explanation of the IBM-650
Computer Program Used to Calculate the Fast
Point Neutron Source in a Finite Pile.

This computer code was written to calculate from theoretical considerations, the thermal flux in a finite pile due to a point source of epithermal neutrons. The program was written in SOAP II and floating point. The object program and a logic diagram are given in this section.

The solution to be programmed was

$$\phi(x, y, z) = \sum_{m=1}^{\infty} \sum_{n=1}^{\infty} \sum_{o=1}^{\infty} \frac{Q_0 F_m(x) F_m(x_0) G_n(y) G_n(y_0) H_o(z) H_o(z_0) e^{-(\alpha_m^2 + \beta_n^2 + \gamma_o^2)\tau_{th}}}{D(\alpha_m^2 + \beta_n^2 + \gamma_o^2 + 1/L^2)} \quad (E-1)$$

where

$$F_m(x) = \frac{1}{\sqrt{a}} \cos \alpha_m x \quad \text{for } m \text{ odd} \quad (E-2)$$

$$F_m(x_0) = \frac{1}{\sqrt{a}} \sin \alpha_m x \quad \text{for } m \text{ even}$$

and
$$\alpha_m = \frac{m\pi}{2a}$$

$F_m(x_0)$, $G_n(y)$, $G_n(y_0)$, $H_o(z_0)$, and $H_o(z)$ are written in a similar manner. The geometry for this solution is shown in Fig. 25.

The program was set up to sum the infinite series by the process of summing over index o , holding m and n constant, until the contribution of a term became less than a specified precision. Index n

was then increased by unity and the summation on index o repeated until the precision specification was met. This summation process was repeated in such a manner that contributions from all possible combinations of m , n and o that were greater than a specified precision were included in the summation.

Input data consisted of various diffusion parameters, numerical constants, and geometrical specifications. Data were read into the machine with the program deck on one-word load cards. Each one-word load card contained the numerical value of a particular constant and its specified machine storage location. Table 15 lists the input data required for program use.

Table 15. Input data required for use of the IBM-650 program which calculates the thermal flux from a fast point source in a finite pile.

Symbol	Explanation	Drum Storage location
2	Identification number 2	0450
4	Identification number 4	0500
6	Identification number 6	0550
7	Identification number 7	0173
TWO	2.00	0151
ONE	1.00	0350
ZERO	0.00	0080
PI	π	0098
A	Half width of pile in x-direction (cm)	0254
B	Half width of pile in y-direction (cm)	0354
C	Half width of pile in z-direction (cm)	0454
D	Diffusion coefficient (cm)	0457
Q	Source strength (n/sec)	0160
XINIT	Initial value of x (cm)	0102
YINIT	Initial value of y (cm)	0256
ZINIT	Initial value of z (cm)	0168
XO	Source location in x-direction (cm)	0397
YO	Source location in y-direction (cm)	0447
ZO	Source location in z-direction (cm)	0547

Table 15. (concl.)

Symbol	Explanation	Drum storage location
DELX	Increment in x (cm)	0958
DELY	Increment in y (cm)	0170
DELZ	Increment in z (cm)	0282
XMAX	Maximum value of x (cm)	0456
YMAX	Maximum value of y (cm)	0968
ZMAX	Maximum value of z (cm)	0330
TAU	Fermi age (cm ²)	0126
K2	Reciprocal of diffusion length squared (cm ⁻²)	0226
BETSQ	Lateral buckling in y-direction (cm ⁻²)	0202
GAMSQ	Lateral buckling in z-direction (cm ⁻²)	0242
PREC	Specified precision of term in summation	0064

Other symbols corresponding to terms in the program print out and the logic diagram are given as follows.

$$FX = a F_m(x) F_m(x_0)$$

$$FY = b G_n(y) G_n(y_0)$$

$$FZ = c H_o(z) H_o(z_0)$$

$$\text{CONSTANT or CONST} = \frac{e^{-(\alpha_m^2 + \beta_n^2 + \gamma_o^2)}}{(\alpha_m^2 + \beta_n^2 + \gamma_o^2 + \kappa^2)}$$

M, N, and O = Summation indices in the x, y, and z directions.

INDXM, INDXN, and INDXO = Summation indices for testing the oddness or evenness of M, N, and O.

The program calculated the flux at the initial values of x, y, and z. The coordinates were then varied according to specified increments in a particular manner in order to give a three-dimensional mapping of the flux in the region.

The machine yielded an answer card having a capacity for eight words, a word being a ten digit number and a sign. Provision was made for printing out partial answers for checking purposes, thus making it necessary to identify partial answer cards by use of an identification number which was always printed in the word 1 location. Table 16 lists the identification number and the answer card content of the various print outs. If the partial answer print outs are not needed they may be eliminated by use of the one word load cards listed in Table 17.

Table 16. Answer identification table for various answer print outs for thermal flux from fast point source in finite pile.

Word 1	Word 2	Word 3	Word 4	Word 5	Word 6	Word 7	Word 8
2	M	N	O	SUM 1	SUM 2	SUM 3	
4	M	N	O	SUM 1	SUM 2	SUM 3	
6	M	N	O	SUM 1	SUM 2	SUM 3	
7	XO	YO	ZO	X	Y	Z	FLUX

Table 17. One-word load cards used for eliminating unnecessary answer print outs for fast point source flux in finite pile.

Print out identification	Instruction address	Instruction
2	0441	46 1077 0651
4	0541	46 1127 0401
6	0591	46 1177 0101

Table 18. Computer precision study for fast point source flux in finite pile.

PREC	Flux at $x = 10.16$ cm $y = 0.00$ $z = 0.00$	Flux at $x = 80.00$ cm $y = 80.00$ $z = 80.00$	Convergence time
10^0	2151.4 n/cm ² -sec	2.033 n/cm ² -sec	
10^{-1}	2153.0	2.214	
10^{-2}	2153.1	2.207	3 min 21 sec

Table 18 presents a study showing the flux value as a function of the specified accuracy of the last term in the infinite series.

				THERMAL FLUX FROM FAST POINT SOURCE IN PILE				
	BLR 1951	1960		1	0000	00	0000	0000
	BLR 1977	1985		2	0000	00	0000	0000
	BYN START	1999		3	0000	00	0000	0000
	BYN X	1000		4	0000	00	0000	0000
EODEA	STD AAA1		E TO THE X	5	0000	24	0003	0006
	STL AAA2		SUB	6	0006	20	0011	0014
	RAM AAA2		ROUTINE	7	0014	67	0014	0015
	STL AAA3		ROUTINE	8	0018	20	0019	0022
	RAM AAA3		X FOR CALC	9	0028	60	0019	0033
	FAD AAA16			10	0023	30	0019	0036
	FAD AAA15			11	0076	33	0019	0005
	FMP AAA3			12	0003	39	0019	0069
	FAD AAA14			13	0069	32	0072	0049
	FMP AAA3			14	0049	39	0019	0119
	FAD AAA13			15	0119	32	0128	0098
	FMP AAA3			16	0059	39	0019	0159
	FAD AAA12			17	0159	32	0172	0149
	FMP AAA3			18	0149	39	0019	0219
	FAD AAA11			19	0219	32	0222	0159
	FMP AAA3			20	0199	39	0019	0269
	FAD AAA10			21	0269	32	0272	0249
	STU AAA4			22	0249	21	0004	0007
	FMP AAA4			23	0007	39	0004	0054
	STU AAA4			24	0054	21	0004	0057
	FMP AAA4			25	0057	39	0004	0104
	STU AAA4			26	0104	21	0004	0107
	RAM AAA2			27	0107	60	0011	0065
	BMI AAA5			28	0065	46	0018	0319
AAAS	RAM AAA10	AAA6		29	0018	60	0272	0027
	FOV AAA4			30	0027	34	0004	0154
	STU AAA4	AAA6		31	0154	21	0004	0319
AAA6	RAM AAA4	AAA1		32	0319	65	0003	0033
AAA10	10 0000	0051		33	0072	10	0000	0051
AAA11	84 9998	6850		34	0222	24	9998	6850
AAA12	34 1 8375	8342		35	0172	31	0004	0342
AAA13	25 9137	1248		36	0122	25	9137	1248
AAA14	14 1 5520	0042		37	0172	17	0004	0342
AAA15	54 3020	0045		38	0029	54	3020	0045
AAA16	69 0600	0044		39	0026	53	0600	0044
EDDSR	STD EXIT		COSINE	40	0030	34	0033	0056
	RAM 8002		SUB	41	0056	60	8002	0115
	BMI 8002		ROUTINE	42	0115	46	0168	0059
	FAD TNDP1	REQUO		43	0068	15	0002	0047
NEGAT	BMI NEGAT			44	0047	46	0068	0001
	F8B ONEPI	CO310		45	0001	33	0004	0031
REDUC	F8B TWOP1		REDUC	46	0369	33	0021	0097
	FAD ONEPI	REDUC	CO310	47	0097	46	0100	0359
COB10	STU THETA		COB10	48	0100	39	0264	0031
	STU TERM			49	0031	21	0036	0039
	STU TERM			50	0039	61	0002	0058
	STU FUNKT	NEGBT		51	0147	21	0002	0058
	STU FUNKT			52	0058	21	0010	0033
EDDSR	STD EXIT		SINE	53	0013	38	0013	0050
	RAM 8002		SUB	54	0150	24	0053	0106
	BMI 8002		ROUTINE	55	0210	60	0003	0166
NEGAV	FAD TNDP1	REQUO		56	0166	46	0118	0439
	BMI NEGAV			57	0118	32	0021	0197
	F8B ONEPI	SINET		58	0197	46	0118	0439
REGUD	F8B TNDP1		SINET	59	0042	33	0204	0024
	BMI	REDUD	SINET	60	0419	33	0419	0024
	FAD ONEPI			61	0247	46	0200	0419
	STU THETA			62	0200	32	0204	0081
BINET	STU TERM			63	0081	21	0003	0081
	RAM 8003			64	0089	61	8003	0297
	STU TERM			65	0297	21	0002	0155
	STU FUNKT			66	0105	21	0010	0063
	LDU FPONE	NEGBT		67	0063	69	0042	0048
	STU ENN			68	0048	24	0017	0020
NEGBT	RAM ENN			69	0020	60	0017	0071
	FAD FPONE			70	0071	32	0042	0469
	STU FPONE			71	0469	21	0054	0077
	FAD FPONE			72	0077	32	0042	0519
	STU ENN			73	0519	21	0017	0070
	RAM TERM			74	0070	61	0002	0157
	FMP THETA			75	0157	39	0036	0086
	FMP THETA			76	0086	39	0036	0136
	FOV ENN			77	0136	34	0024	0074
	STU TERM			78	0074	34	0017	0067
	RAM FUNKT			79	0067	21	0002	0155
	STL FMAC			80	0155	67	0010	0215
	RAM TERM			81	0215	80	0268	0322
	RAM TERM			82	0322	67	0002	0207
	RAM 8002			83	0207	60	0007	0268
	FOV FMAC			84	0268	34	0069	0619
	BMI 8002			85	0619	33	0372	0289
	RAM ENUFF			86	0289	46	0002	0133
	RAM TERM			87	0103	60	0010	0335
	STU TERM			88	0335	32	0002	0079
	STU FUNKT	NEGBT		89	0079	21	0010	0020
	RAM FUNKT			90	0020	65	0010	0053
ENUFF	STD 0000	0043		91	0072	10	0000	0043
SIZB	TNDP1	68 8318	5351	92	0021	62	8318	5351
ONEPI	STL 4359	8751		93	0044	21	0004	0751
FPONE	STD 10 0000	0051		94	0042	10	0000	0051
EDDCL	LDU 2222		CLEAR	95	0250	24	0153	0126
	STD 2220		PUNCH	96	0156	69	0036	0032
	STD 1977		ROUTINE	97	0012	24	1977	0030
	STD 1978			98	0030	24	1978	0032
	STD 1979			99	0131	24	1979	0032
	STD 1980			100	0032	24	1980	0033
	STD 1981			101	0031	24	1981	0034
	STD 1982			102	0034	24	1982	0035
	STD 1983			103	0035	24	1983	0036
	STD 1984	ZZZ1		104	0186	24	1984	0113
ZZZ10	DD 0000	0000		105	0009	60	0000	0000
NEW	STD INRS		SUBROUTINE	106	0030	24	0203	0016
	RAM ALPH2		FOR	107	0206	60	0055	0113
	FAD T12		CONSTANT	108	0113	32	0016	0043
	FAD GAM2			109	0043	39	0126	0176
	FMP TAU			110	0073	39	0126	0176
	ISL 8003			111	0176	66	8003	0033
	LDU	EODEA		112	0083	69	0236	0000
	ST TEMP1			113	0236	60	0041	0044
	RAM ALPH2			114	0044	60	0039	0033
	FAD BETA2			115	0163	32	0016	0023

	FAD GAM2		116	0093	32	0046	0123
	FAD K2		117	0123	32	0226	0253
	STU TEMP2		118	0253	31	0008	0061
	RAU TEMP1		119	0061	60	0041	0098
	FOV TEMP2		120	0095	34	0008	0203
START	LD X INIT	EXINS	121	1999	21	0000	0000
	STO X		122	0205	24	1000	0303
	LD Y INIT		123	0303	69	0556	0109
	STO Y		124	0109	69	0062	0305
	LD Z INIT		125	0358	69	0169	0121
	STO Z		126	0121	24	0000	0000
CON37	LOO ZERO	CON37	127	0127	69	0080	0133
	STO SUM3		128	0133	24	0286	0139
	STO M		129	0139	69	0000	0000
	STO INDXM	CON13	130	0145	24	0048	0101
CON13	RAU M		131	0101	69	0000	0000
	FAD ONE		132	0347	32	0350	0177
	STU M	TO M	133	0177	21	0092	0196
	FMP PI		134	0098	69	0000	0000
	FMP TWO		135	0148	34	0151	0201
	FOV A		136	0201	34	0000	0104
	STU ALPHA	FORM ALPHA	137	0304	21	0058	0144
	FMP ALPHA	ANO ALPHA	138	0111	39	0058	0108
	STU ALPHA2	SQUARED	139	0108	69	0000	0000
	RAU INDXM		140	0112	60	0048	0353
	NZE CONTS	CON11	141	0112	45	0300	0259
CON11	RAU X	TEST M FOR	142	0257	60	1000	0255
	FMP ALPHA	EVEN OR OD	143	0255	32	0058	0158
	RAL BOO3	FORM GRS	144	0158	65	8003	0415
	LOO	ALPHA X	145	0415	69	0218	0050
	STL TEMP1	EODCR	146	0228	20	0041	0094
	RAU XO		147	0094	60	0397	0251
	FMP ALPHA	FORM COS	148	0251	39	0058	0208
	RAL BOO3	ALPHA XO	149	0208	65	8003	0415
	LOO		150	0465	69	0268	0050
	RAU BOO2	EODCR	151	0268	60	8002	0227
	FMP TEMP1		152	0041	39	0000	0000
	STU FX	FORM FX	153	0091	21	0096	0349
	RAU INDXM	ADD ONE TO	154	0349	60	0000	0000
	FAD ONE	INDXM	155	0403	32	0350	0277
	STU INDXM	CON12	156	0277	21	0048	0301
CON19	RAU XO	TEST BORCE	157	0306	60	0397	0213
	NZU CON10	X POSITION	158	0213	44	0117	0318
CON18	RAU INDXM		159	0318	60	0000	0000
	FBS ONE	RESET	160	0453	33	0350	0327
	STU INDXM	CON13	161	0327	21	0048	0101
CON10	RAU X	FORM BINE	162	0117	60	1000	0310
	FMP ALPHA	ALPHA X	163	0305	39	0058	0258
	RAL BOO3		164	0258	65	8003	0415
	LOO		165	0515	69	0368	0150
	STL TEMP1	EODCR	166	0368	20	0041	0144
	RAU BOO2		167	0144	60	0000	0000
	FMP ALPHA	FORM BINE	168	0351	39	0058	0308
	RAL BOO3	ALPHA XO	169	0308	65	8003	0415
	LOO	EODCR	170	0545	69	0418	0150
	RAU BOO2		171	0418	60	8002	0377
	FMP TEMP1		172	0377	39	0041	0094
	STU FX	FORM FX	173	0141	21	0026	0359
	RAU INDXM		174	0359	60	0048	0503
	FBS ONE	SUBT ONE	175	0303	33	0300	0300
CON12	STU INDXM	CON12	176	0427	21	0048	0301
	LD ZERO	FROM INDXM	177	0301	67	0198	0101
	STO N		178	0183	24	0336	0189
	STO SUM2	INDXM ANO	179	0189	24	0142	0245
	STO INDXM	N AT ZERO	180	0245	60	0000	0000
CON19	RAU N		181	0401	60	0336	0191
	FAD ONE	ADD ONE	182	0191	32	0000	0000
	STU N	TO N	183	0477	21	0336	0359
	FMP PI		184	0239	39	0098	0248
	FOV TWO		185	0448	69	0000	0000
	FOV BETA	FORM BETA	186	0451	34	0354	0404
	FMP BETA	ANO BETA	187	0404	21	0358	0141
	STU BETA2	SQUARED	188	0141	39	0358	0408
	RAU INDXM		189	0408	21	0016	0269
	NZE CONTS	CON14	190	0669	60	0198	0583
CON14	RAU Y	TEST N FOR	191	0583	48	0356	0307
	FMP BETA	EVEN OR OD	192	0307	60	0068	0167
	RAL BOO3	FORM COS	193	0147	39	0358	0458
	RAU YO	BETA Y	194	0458	65	8003	0615
	STL TEMP1	EODCR	195	0615	69	0468	0050
	RAU BOO2		196	0468	20	0041	0194
	FMP BETA	FORM COS	197	0194	60	0447	0308
	RAL BOO3	BETA YO	198	0501	39	0358	0508
	LOO		199	0508	65	8003	0665
	RAU BOO2	EODCR	200	0665	69	0518	0050
	FMP TEMP1		201	0518	60	8002	0527
	STU FY	FORM FY	202	0541	39	0041	0241
	RAU INDXM	ADD ONE TO	203	0449	60	0198	0603
CON15	FAD ONE	INXS	204	0603	33	0500	0300
	STU INDXM	CON15	205	0577	21	0198	0551
	RAU YO	TEST BORCE	206	0356	40	0447	0363
CON16	NZU CON13	Y POSITION	207	0603	60	0198	0603
	RAU INDXM		208	0566	60	0198	0453
	FBS ONE	RESET	209	0613	33	0300	0300
CON13	STU INDXM	CON12	210	0627	21	0198	0401
	RAU Y	INDXM	211	0217	60	0062	0267
	FMP BETA	FORM SINE	212	0267	39	0358	0408
	RAL BOO3	BETA Y	213	0558	65	8003	0715
	STL TEMP1	EODCR	214	0715	69	0668	0141
	RAU YO		215	0618	20	0041	0244
	FMP BETA	FORM SINE	216	0244	60	0447	0501
	RAL BOO3	BETA YO	217	0601	39	0358	0508
	LOO		218	0608	65	8003	0765
	RAU BOO2	EODCR	219	0765	69	0668	0141
	FMP TEMP1		220	0668	60	8002	0527
	STU FY	FORM FY	221	0577	39	0041	0291
	RAU INDXM		222	0591	60	0198	0703
	FBS ONE	SUBT ONE	223	0503	33	0500	0300
CON15	STU INDXM	CON15	224	0499	60	0198	0703
	STO SUM1	SET ALPHA	225	0703	21	0198	0551
	STO O	FROM INDXM	226	0727	21	0198	0551
	STO INDXM	ANO INDXM	227	0551	69	0080	0233
	STO O	INOXO ANO	228	0533	24	0398	0189
	STO INDXO	O AT ZERO	229	0809	24	0192	0295
CON1	RAU O		230	0295	60	0000	0000
	FAD ONE	ADD ONE	231	0651	60	0192	0497
	STU O	TO O	232	0497	32	0350	0777
	FMP PI		233	0777	21	0257	0300
	FOV TWO		234	0345	39	0028	0348
	FOV C		235	0348	34	0454	0701
	STU GAMMA	FORM GAMMA	236	0701	34	0454	0701
			237	0504	21	0658	0211

	FMP GAMMA	ANO GAMMA	238	0211	39	0658	0708
	STU AW2	QUARED	239	0702	21	0046	0549
	RAU INOXO	TEST O FOR	240	0549	60	0298	0753
	NZU DNT4	EVEN DR DD	241	0753	41	0763	1293
CON16	RAU Z		242	0357	60	0124	0129
	FMP GAMMA	FORM COS	243	0129	39	0658	0758
	RAL B003	GAMMA Z	244	0758	63	0044	0050
	LDD	EODCR	245	0815	69	0718	0050
	BTL TEMP1		246	0718	20	0044	0175
	RAU Z		247	0294	60	0547	0751
	FMP GAMMA	FORM COS	248	0751	39	0658	0808
	RAL B003	GAMMA Z	249	0808	63	0044	0050
	LDD	EODCR	250	0865	69	0768	0050
	RAU B002		251	0768	60	0547	0808
	FMP TEMP1		252	0827	39	0041	0341
	STU FZ	FORM FZ	253	0341	21	0196	0599
	RAU INOXO	ADD ONE TO	254	0599	60	0298	0753
	FAD ONE	INOXO	255	0403	32	0350	0877
	STU INOXO	TEST SOURCE	256	0877	21	0298	0901
CON14	NZU CON17	CON18	257	0404	60	0547	0808
	STU CON17	Z POSITION	258	0313	44	0317	0818
CON17	RAU INOXO		259	0818	63	0044	0050
	FAD ONE	RESET	260	0853	33	0350	0927
	STU INOXO	INOXO	261	0927	21	0298	0875
CON17	RAU Z		262	0377	60	0124	0175
	FMP GAMMA	FORM SINE	263	0179	39	0658	0858
	RAL B003	GAMMA Z	264	0858	65	0003	0915
	LDD	EODCR	265	0915	69	0868	0150
	BTL TEMP1		266	0658	20	0041	0344
	RAU Z		267	0344	60	0547	0831
	FMP GAMMA	FORM SINE	268	0851	39	0658	0908
	RAL B003	GAMMA Z	269	0908	65	0003	0915
	LDD	EODCR	270	0965	69	0918	0150
	RAU B002		271	0918	60	8002	0977
	FMP TEMP1		272	0977	29	0554	0300
	STU FZ	FORM FZ	273	0391	21	0196	0648
	RAU INOXO	FORM TAU	274	0649	60	0599	0977
	FAD ONE	SUBT ONE	275	0903	33	0350	1027
CON18	STU INOXO	CON18	276	1027	21	0298	0901
	LDD	NEW	277	0901	69	0554	0300
	STU CON21	TERM FOR	278	0554	21	0407	0261
	FMP FZ	M N D	279	0261	39	0658	0808
	RAU SUM1	ADD TO	280	0246	32	0386	0363
	STU SUM1	SUM1	281	0363	21	0386	0332
	RAU CONST		282	0339	60	0192	0475
	FBR PREC	TEST	283	0311	33	0064	0441
CON22	SWI CON22	CON11	284	0441	46	0394	0652
	LDD	EODCL	285	0394	69	0377	0250
	STO 1977		286	0597	69	0450	0932
	RAU 1977	PRINT 2	287	0553	69	0450	0932
	LOO M 1978	PARTIAL	288	0130	69	0092	0395
	STO 1978	ANSWERS	289	0395	24	138	0283
	LDD N 1979	FOR	290	0319	39	0316	0349
	STO 1979	CHECKING	291	0389	24	1979	0082
	LDD O 1980		292	0082	69	0192	0475
	RAU 1980		293	0445	24	1380	0283
	LOD SUM1		294	0283	69	0386	0439
	STO 1981		295	0439	24	1381	0384
	LDD SUM2		296	0084	69	0142	0495
	STO 1982		297	0495	24	1382	0525
	LOD SUM3		298	0085	69	0286	0489
	STO 1983		299	0482	24	1383	0426
	PCM 1977		300	0436	60	0197	0477
	LOD ONE	SET D AT 1	301	1077	69	0350	1003
	STO O		302	1003	29	0554	0300
	LDD GAM50		303	0545	69	0243	0333
	STO GAM2		304	0333	24	0046	0699
	LDD GAM2	NEW	305	0699	69	0333	0300
	STU CON21	FORM TAU	306	0152	21	0407	0060
	RAU SUM1	TERM FOR	307	0060	60	0599	0977
	FMP FY	M N D	308	0491	39	0146	0296
	RAD SUM2	ADD TO	309	0296	32	0142	0719
	STU SUM2	SUM2	310	0719	21	0142	0295
	RAU CONST	TEST PREC	311	0595	60	0407	0361
	FBR PREC	SIGN	312	0361	33	0064	0541
	SWI CON27		313	0541	46	0444	0403
CON27	LDD	EODCL	314	0444	69	0647	0250
	RAU 4		315	0647	69	0500	1053
	STO 1977	PARTIAL	316	1053	24	1977	0180
	LOO M 1978	ANSWERS	317	0180	69	0092	0645
	STO 1978	FOR	318	0645	24	1978	0231
	LDD N 1979	CHECKING	319	0231	69	0336	0639
	STO 1979		320	0639	24	1979	0182
	LDD O 1980		321	0132	69	0192	0698
	STO 1980		322	0698	24	1980	0383
	LDD SUM1		323	0384	69	0386	0489
	STO 1981		324	0589	24	1981	0134
	LDD SUM2		325	0134	69	0142	0719
	STO 1982		326	0745	24	1982	0135
	LDD SUM3		327	0135	69	0286	0639
	STO 1983		328	0639	24	1983	0135
	PCM 1977		329	0486	71	1977	1127
	LOD ONE	SET D AND	330	1127	69	0350	1143
	STO O	N AT 1	331	1103	64	0192	0798
	STO N		332	0798	24	0336	0689
	LDD GAM50		333	0689	69	0242	0443
	STO GAM2		334	0845	24	0046	0749
	RAU SET38		335	0749	69	0378	0458
	STO SET48		336	0355	24	0016	0769
	LDD	NEW	337	0769	69	0422	0300
	STU CON21	FORM TAU	338	0422	60	0599	0977
	RAU SUM2	TERM FOR	339	0110	60	0142	0697
	FAP FX	M N D	340	0697	39	0096	0346
	RAD SUM3	ADD TO	341	0339	32	0346	0296
	STU SUM3	SUM3	342	0433	21	0286	0739
	RAU CON21	TEST	343	0739	60	0407	0361
	FBR PREC	PRECISION	344	0411	33	0064	0591
	SWI CON32		345	0591	46	0494	0141
CON32	LDD	CON13	346	0494	69	0747	0950
	RAU 6	EODCL	347	0950	68	0559	1153
	STO 1977	PRINT 6	348	1153	24	1977	0130
	LOO M 1978	PARTIAL	349	0230	69	0092	0895
	STO 1978	ANSWERS	350	0895	24	1978	0283
	LDD N 1979	FOR	351	0291	69	0336	0789
	STO 1979	CHECKING	352	0789	24	1979	0182
	LDD O 1980		353	0182	69	0192	0698
	RAU 1980		354	0945	24	1980	0433
	LDD SUM1		355	0433	69	0386	0439
	STO 1981		356	0439	24	1981	0134
	LDD SUM2		357	0184	69	0142	0995
	STO 1982		358	0995	24	1982	0135
	LDD SUM3		359	0185	69	0286	0639

STO	1983			360	0889	24	1983	0536
PCM	1977			361	0536	71	1977	1177
RAU	BUM3			362	1177	60	0286	0641
FOV	A			363	0641	34	0254	0204
FOV	B			364	0604	34	0354	0654
FDV	C			365	0654	34	0454	0354
FOV	D			366	0704	34	0437	0507
FWP	B			367	0507	39	0160	0220
STU	FLUX		FORM FLUX	368	0210	21	0114	0347
LDD		EODCL		369	0367	69	0120	0250
LOO	7		PRINT 7	370	0120	69	0173	0276
STB	1977			371	0276	24	1977	0280
LOO	X0		ANSWERS	372	0280	69	0397	0600
STC	1978			373	0600	24	1978	0280
LOO	Y0		Y0	374	0331	69	0447	0650
STB	1979		Z0	375	0650	24	1979	0280
LOO	Z0		Y	376	0238	69	0547	0700
OTO	1980		Y	377	0700	24	1980	0483
LOO	X		Z	378	0483	69	0483	0503
STD	1981		FLUX	379	1203	24	1981	0234
LOO	Y			380	0934	69	0062	1015
STO	1982			381	1015	24	1982	0234
LOO	Z			382	0235	69	0124	1227
STC	1983			383	1227	24	1983	0234
LOO	FLUX			384	0586	69	0114	0417
STB	1984			385	0417	24	1984	0037
PCM	1977			386	0037	71	1977	1277
RAU	X		CHANGE X	387	1277	60	1000	0405
FAO	DELX		UNTIL PAST	388	0405	32	0958	0285
STU	Z		MAXIMUM Y	389	0285	24	1000	0285
FSB	XMAX			390	1253	33	0456	0533
CON34		CON34		391	0533	46	0127	0087
RAU	XINIT		DET XINIT	392	0087	60	0102	0557
FAO	DELX		AT XINIT	393	0557	32	0958	0358
STU	Y		PLUS DELX	394	0358	21	0102	0455
FAO	DELY		CHANGE Y	395	0455	21	1000	1303
OTU	Y		UNTIL PAST	397	0467	32	0170	0767
FSB	ZMAX		MAXIMUM Y	398	0797	21	0062	1065
CON35		CON35		399	1065	33	0948	0245
STU	Y		REF Y	400	1045	46	0127	0759
LOO	ZERO		AT YINIT	402	0461	21	0062	1115
OTO	XINIT		SET XINIT	403	1115	69	0080	0583
STO	X		AND Y	404	0583	24	0102	0505
RAU	Z		AT SOURCE	405	0505	24	1000	1353
FAO	DELZ		CHANGE Z	406	1353	60	0124	0229
STU	Z		UNTIL PAST	408	0309	21	0124	1397
FSB	ZMAX		MAXIMUM Z	409	1327	33	0330	0607
CON36		CON36		410	0607	46	0127	0511
STU	Y		REF Y	411	0511	46	0127	0507
2	00	2000	0000	412	0450	00	2000	0000
4	00	4000	0000	415	0450	00	4000	0000
6	00	6000	0000	417	0550	00	6000	0000
7	00	7000	0000	418	0173	00	7000	0000
TBO	20	0000	0051	419	0151	20	0000	0051
JNE	10	0000	0051	420	0350	10	0000	0051
ZERO	00	0000	0000	421	0080	00	0000	0000
PI	31	4161	0051	422	0080	31	4161	0051
A	88	1100	0052		0254	88	1100	0052
B	88	1100	0052		0254	88	1100	0052
C	88	1100	0052		0454	88	1100	0052
D	82	0000	0050		0457	82	0000	0050
O	17	1000	0057		0160	17	1000	0057
XINIT	00	0000	0000		0102	00	0000	0000
YINIT	00	0000	0000		0256	00	0000	0000
ZINIT	00	0000	0000		0168	00	0000	0000
X0	00	0000	0000		0397	00	0000	0000
Y0	00	0000	0000		0447	00	0000	0000
Z0	00	0000	0000		0547	00	0000	0000
DELX	10	1600	0053		0256	10	1600	0052
DELY	20	1200	0052		0170	20	1200	0052
DELZ	20	1200	0052		0282	20	1200	0052
XMAX	88	1100	0052		0456	88	1100	0052
YMAX	88	1100	0052		0268	88	1100	0052
ZMAX	88	1100	0052		0330	88	1100	0052
TAB	42	0000	0053		0324	42	0000	0053
K2	35	9250	0047		0226	35	9250	0047
BETSB	31	7840	0047		0202	31	7840	0047
QWISO	31	7840	0047		0242	31	7840	0047
PREC	10	0000	0049		0064	10	0000	0049

APPENDIX F

Description and Explanation of the IBM-650 Computer Program
Used to Calculate the Thermal Flux from a Thermal
Point Neutron Source in a Finite Pile

This computer code was written to calculate from theoretical considerations, the thermal flux in a finite pile due to a point source of thermal neutrons. The program was written in SOAP II and floating point. The object program and a logic diagram are given in this section.

The solution programmed was

$$\phi(x, y, z) = \sum \sum \frac{Q_0}{D\gamma_{mn}} F_m(x) F_m(x_0) G_n(y) G_n(y_0) \frac{\sinh \gamma_{mn} z_0 \sinh \gamma_{mn} (2c-z)}{\sinh 2\gamma_{mn} c} \quad (F-1)$$

where

$$\begin{aligned} F_m(x) &= \frac{1}{\sqrt{a}} \cos \alpha_m x && \text{for } m \text{ odd} \\ &= \frac{1}{\sqrt{a}} \sin \alpha_m x && \text{for } m \text{ even} \end{aligned} \quad (F-2)$$

and

$$\alpha_m = \frac{m\pi}{2a} .$$

$F_m(x_0)$, $G_n(y)$, and $G_n(y_0)$ are written in a similar manner.

The geometry for this solution is shown in Fig. 26.

The program was set up to sum the infinite series in the same manner as the infinite series was summed in the computer program described in Appendix E. Input data required for use of this program are listed in Table 19.

Other symbols corresponding to terms in the program print out and the logic diagram are given as follows:

$$FX = aF_m(x) F_m(x_0)$$

$$FY = bG_n(y) G_n(y_0)$$

$$FZ = \frac{\sinh \gamma_{mn}(2c-z) \sinh \gamma_{mn} z_0}{\gamma_{mn} \sinh 2\gamma_{mn} c}$$

M and N = Summation indices in the x and y directions

INDXM and INDXN = Summation indices for testing the evenness or oddness of M and N.

Table 19. Input data required for use of the IBM-650 program which calculates the thermal flux from a thermal point source in a finite pile.

Symbol	Explanation	Drum Storage location
1	Identification number 1	0415
2	Identification number 2	0314
3	Identification number 3	0515
4	Identification number 4	0364
7	Identification number 7	0705
TWO	2.00	0182
ONE	1.00	0184
ZERO	0.00	0264
PI	π	0332
A	Half width of pile in x-direction (cm)	0785
B	Half width of pile in y-direction (cm)	1135
C	Half width of pile in z-direction (cm)	0900
D	Diffusion coefficient (cm)	0088
Q	Source strength (n/sec)	0291
XINIT	Initial value of x (cm)	0102
YINIT	Initial value of y (cm)	0356
ZINIT	Initial value of z (cm)	0268
XO	Source location in x-direction (cm)	0950
YO	Source location in y-direction (cm)	1050
ZO	Source location in z-direction (cm)	0016

Table 19. (concl.)

Symbol	Explanation	Drum Storage location
XMAX	Maximum value of x (cm)	0406
YMAX	Maximum value of y (cm)	0418
ZMAX	Maximum value of z (cm)	0414
DELX	Increment in x (cm)	0408
DELY	Increment in y (cm)	0370
DELZ	Increment in z (cm)	0226
K2	Reciprocal of diffusion length squared (cm^{-2})	0374
TOCEE	Height of pile in z-direction (cm)	0151
BETSQ	Lateral buckling in y-direction (cm^{-2})	0376
PREC	Specified precision of last term in summation	0178

This program had provision for printing out partial answers for checking purposes. Table 20 lists the identification number and the answer card content of the various print outs. If the partial answer print outs are not needed they may be eliminated by use of the one word load cards listed in Table 21. Table 22 presents a study showing the flux value as a function of the specified accuracy of the last term in the finite series.

Table 20. Answer identification table for various answer print outs for thermal flux from a thermal point source in a finite pile.

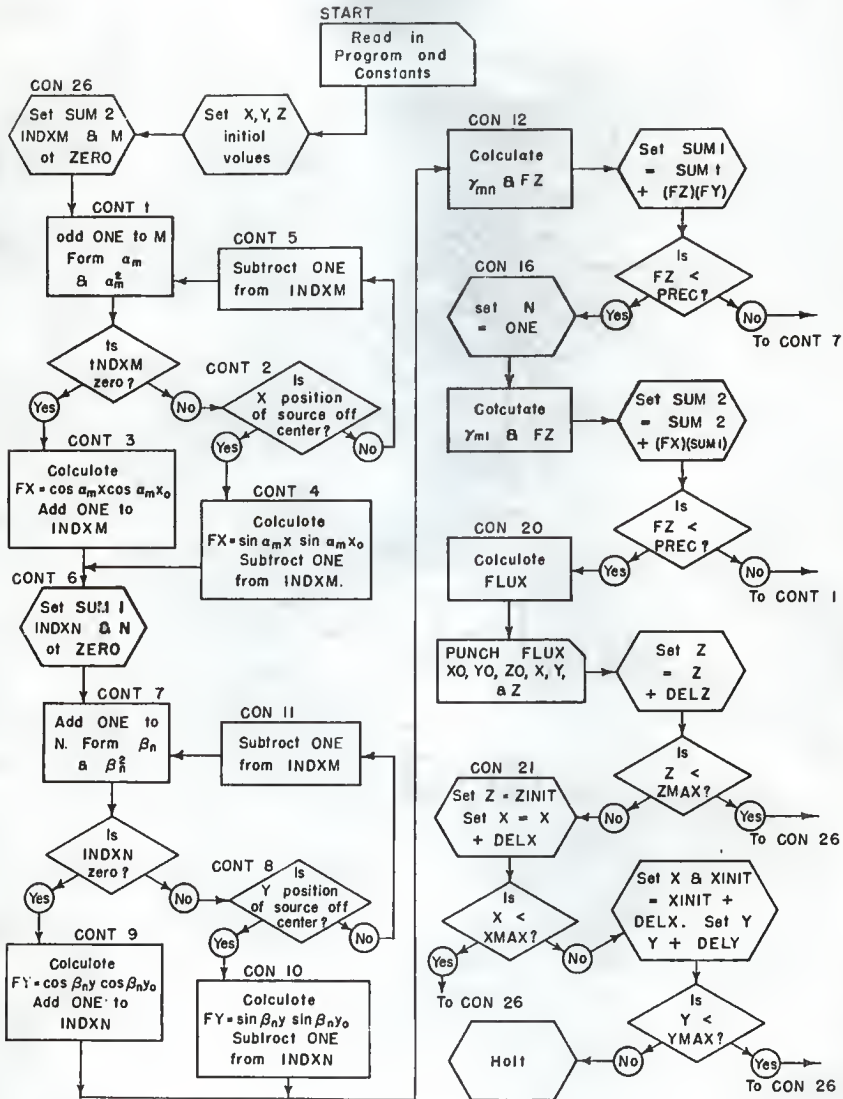
Word 1	Word 2	Word 3	Word 4	Word 5	Word 6	Word 7	Word 8
1	M	N	FY	FZ	SUM 1	SUM 2	
2	M	N	FY	FZ	SUM 1	SUM 2	
3	M	N	FX	FZ	SUM 1	SUM 2	
4	M	N	FX	FZ	SUM 1	SUM 2	
7	XO	YO	ZO	X	Y	Z	FLUX

Table 21. One word load cards used for eliminating unnecessary answer print outs for thermal point source in a finite pile.

Print out identification :	Instruction Address :	Instruction
1	0605	46 0258 1059
2	0258	69 0184 0587
3	0655	46 0308 0735
4	0308	60 0220 0425

Table 22. Computer precision study for thermal point source flux in finite pile.

PREC	Flux at $x = 0$ $y = 0$ and $z = 20.32$ cm	Convergence time	Flux at $x = 0$ $y = 0$ and $z = 81.72$ cm	Convergence time
10^0	4449.1 n/cm ² -sec		107.31 n/cm ² -sec	
10^{-1}	5202.2		126.16	
10^{-2}	5339.7		129.07	
10^{-3}	5363.3	approx. 5 min.	129.47	approx. 30 sec.



LOGIC DIAGRAM—APPENDIX F

				THERMAL FLUX FROM THERMAL RESISTANCE SOURCE IN FINITE FILE					
		READ	PRINT						
BLR	1951	1960	1	0000	00	0000	0000		
BLR	1977	1985	2	0000	00	0000	0000		
BLR	START	1992	3	0000	00	0000	0000		
EO0BZ	SVN X	1000	4	0000	00	0000	0000		
STO	SNH02		5	0000	00	0000	0000		
LOO	EO0LR		6	0006	69	0009	0012		
STU	SNH03		7	0009	21	0009	0025		
RSU	FDONE		8	0017	11	0020	0025		
F0V	SNH03		9	0023	34	0044	0064		
F0V	SNH03		10	0064	34	0044	0064		
FOV	FPTW0	SNH02	11	0041	34	0044	0003		
STO	EXP02		12	0012	26	0032	0018		
STU	EXP03		13	0008	31	0022	0075		
LOO	8007		14	0075	69	8007	0031		
STO	EXP04		15	0031	34	0022	0018		
RAC	0000		16	0037	88	0000	0043		
RAU	EXP03		17	0043	60	0022	0077		
SMI	EXP05		18	0049	46	0030	0081		
FBS	LNTEN		19	0081	33	0084	0021		
SMI	EXP07		20	0011	46	0114	0065		
AXC	0001	EXP06	21	0065	58	0001	0081		
EXP07	FAO	LNTEN	EXP08	018	22	0114	32	0084	0061
EXP05	SXS	0001		019	23	0030	39	0011	0036
	FAO	LNTEN		020	24	0036	32	0084	0111
	SMI	EXP05		021	25	0111	46	0030	0061
EXP08	STU	EXP03		022	26	0061	21	0022	0125
	STU	EXP04		023	27	0025	21	0042	0033
RAL	EXP09		28	0033	65	0034	0039		
LDD	8007		29	0039	69	8007	0045		
STO	EXP04		30	0045	24	0034	0087		
RAC	8002		31	0087	88	8002	0095		
LOO	FPONE		32	0095	69	0020	0023		
STO	EXP10		33	0023	34	0023			
STO	EXP11	EXP12	34	0029	24	0032	0035		
RAL	EXP10		35	0035	60	0032	0137		
FAO	EXP09		36	0131	32	0080	0007		
STU	EXP10		37	0007	21	0026	0079		
RAU	EXP11		38	0079	60	0032	0137		
FAO	FPONE		39	0137	32	0020	0247		
STU	EXP11		40	0047	31	0022	0035		
RAU	EXP09		41	0085	60	0080	0135		
FMP	EXP03		42	0135	39	0022	0072		
FOV	EXP11		43	0072	34	0032	0062		
STU	EXP09		44	0082	21	0080	0083		
F0V	EXP10		45	0083	44	0063	0056		
FBS	SIZE8		46	0076	33	0129	0075		
SMI		EXP12	47	0008	46	0008	0035		
RAU	EXP10		48	0008	60	0008	0035		
AMP	EXP04	EXP02	49	0181	10	0034	0018		
FTW0	20	0000	0051	047	50	0044	20	0000	0051
EXP05	20	0000	0051	048	51	0044	20	0000	0051
EO0AU	STO	SEXT	SQUARE	1	52	0050	24	0053	0056
	FMP	SEXT	ROOT	2	53	0056	04	0054	0060
	NZE	SEXT	SUB	3	54	0164	0053		
	STU	SEXT	ROUTINE	4	55	0164	21	0048	0021
	F0V	810		5	56	0001	39	0004	0054
SS	FMP	SSAV	SS	6	57	0054	31	0008	0054
SAS	RAU	SA	SAS	7	58	0054	31	0008	0054
	FOV	SSAV		8	59	0073	34	0058	0108
	F0V	SSAV		9	60	0108	32	0068	0108
	FMP	SHAF		10	61	0185	39	0004	0104
	FBS	SSAV		11	62	0104	33	0058	0035
	NZU		SR	12	63	0235	44	0089	0040
	SMI		SR	13	64	0089	46	0042	0040
	FAO	SSAV	SAS	14	65	0042	39	0058	0085
	STU	SSAV	SAS	15	66	0149	21	0058	0161
SR	RAU	SSAV	SEXT	16	67	0285	60	0058	0053
SERR	HLT	0000	SEXT	17	68	0040	60	0058	0053
SHAF	50	0000	0050	18	69	0050	41	0000	0053
810	50	0000	0051	19	70	0004	50	0000	0050
EO0EA	STO	AAA1		20	71	0084	10	0000	0051
	ST	AAA2	E TO THE X	72	0100	24	0103	0106	
	RAM	AAA2	SUBROUTINE	73	0106	20	0111	0121	
	STL	AAA3	X FOR CALC	74	0118	20	0049	0122	
	RAU	AAA3		75	0122	60	0119	0123	
	FMP	AAA36		76	0123	39	0126	0176	
	FAO	AAA35		77	0176	32	0179	0053	
	FMP	AAA3		78	0053	39	0119	0069	
	FAO	AAA14		79	0069	32	0178	0049	
	FAO	AAA3		80	0049	39	0019	0069	
	FAO	AAA13		81	0019	32	0222	0099	
	FMP	AAA3		82	0119	39	0019	0169	
	FAO	AAA12		83	0019	32	0072	0149	
	FMP	AAA3		84	0019	39	0019	0219	
	FAO	AAA11		85	0219	32	0119	0199	
	FMP	AAA3		86	0119	39	0019	0269	
	FAO	AAA10		87	0019	32	0019	0249	
	STU	AAA4		88	0269	32	0172	0249	
	FMP	AAA4		89	0249	39	0154	0204	
	STU	AAA4		90	0057	39	0154	0204	
	FMP	AAA4		91	0204	39	0154	0204	
	STU	AAA4		92	0107	39	0154	0254	
	FAO	AAA2		93	0254	21	0154	0157	
	SMI	AAA5	AAA6	94	0157	60	0111	0167	
	RAU	AAA10		95	0165	46	0118	0339	
AAA5	FOV	AAA4		96	0118	40	0118	0079	
	STU	AAA4		97	0077	34	0154	0304	
	RAU	AAA4	AAA6	98	0304	21	0154	0319	
AAA6	RAC	AAA4		99	0154	35	0154	0319	
AAA10	10	0000	0051	100	0372	10	0000	0051	
AAA11	24	9999	8031	101	0372	54	9999	8031	
AAA12	31	2575	8349	102	0272	11	2575	8349	
AAA13	25	9337	1248	103	0248	25	9337	1248	
AAA14	17	1362	0047	104	0172	17	1362	0047	
AAA15	24	3020	0045	105	0172	54	3020	0045	
AAA16	69	0000	0044	106	0172	69	0000	0044	
EO0CL	STO	Z221		107	0150	69	0000	0044	
	LDD	Z220		108	0156	69	0109	0062	
	STO	Z277		109	0062	64	1977	0062	
	STO	Z278		110	0150	24	1978	0031	
	STO	Z279		111	0150	24	1978	0031	
	STO	Z280		112	0150	24	1978	0031	
	STO	Z281		113	0133	24	1981	0134	
	STO	Z282		114	0134	24	1982	0134	
	STO	Z283		115	0335	24	1983	0086	

CLEAR PUNCH ROUTINE

			VALUES	338	0303	69	0356	0809
	LDZ YINIT			339	0809	24	0312	0315
	LDZ ZINIT			240	0315	69	0268	0353
	LDZ Z			242	0315	24	0276	0319
CON26	LDZ ZERO	CON26	SET BUMB	243	0261	69	0264	0217
	STO BUMB		INDXM AND	244	0217	24	0220	0273
	STO M		W AT ZERO	245	0245	69	0276	0319
	STB INDXM	CONT1		246	0379	24	0282	0735
CONT1	RAU M		ADD ONE	247	0735	60	0276	0361
	FAD ONE		TO M	248	0448	69	0284	0341
	STU M			249	0311	21	0276	0429
	FMP F			250	0402	69	0284	0341
	FVY T80			251	0382	34	0182	0432
	FDV A	FORM ALPHA		282	0432	34	0788	0838
	FVY ALPHA	AND ALPHA		253	0382	69	0284	0341
	FMP ALPHA	SQUARED		254	0243	39	0099	0140
	STU ALPHA			255	0140	69	0284	0341
	RAU INDXM		TEST U FOR	256	0547	60	0282	0187
	NZE CONT2	CONT3	EVEN OR OD	257	0187	43	0190	0191
CONT3	FMP ALPHA	FORM COS		259	0505	39	0099	0240
	LDZ 8003	ALPHA Y		260	0240	69	0284	0341
	LDZ	EODCR		261	0597	69	0500	0200
	STL TEMP1			262	0506	20	0074	0327
	RAU X0			263	0327	60	0230	0885
	FMP ALPHA	FORM COS		264	0888	39	0099	0250
	LDZ 8003	ALPHA X0		265	0290	65	0003	0647
	LDZ	EODCR		266	0647	69	0550	0200
	RAU 8002			267	0550	60	8002	0859
	FMP TEMP1			268	0859	39	0074	0374
	STU FX	FORM FX		269	0174	21	0028	0431
	RAU INDXM	ADD ONE TO		270	0431	60	0282	0337
	STU ONE	INDXM		271	0237	39	0184	0361
	RAU INDXM	CONT6		272	0361	21	0282	0935
CONT2	RAU INDXM		TEST SOURCE	273	0190	60	0284	0341
	NZU CONT4	CONT5	X POSITION	274	0328	44	0239	0340
	RAU INDXM			275	0340	60	0284	0341
	FVB ONE		RESET	276	0287	33	0184	0451
	STU INDXM	CONT1	INDXM	277	0411	21	0282	0735
CONT4	RAU X			278	0239	69	0284	0341
	FMP ALPHA	FORM SINE		279	0355	39	0099	0390
	LDZ 8003	ALPHA Y		280	0390	69	0284	0341
	LDZ	EODCR		281	0697	69	0600	0300
	STL TEMP1			282	0600	20	0074	0377
	RAU X0			283	0377	60	0230	1035
	FMP ALPHA	FORM SINE		284	1035	39	0099	0440
	LDZ 8003	ALPHA X0		285	0440	65	0003	0647
	LDZ	EODCR		286	0747	69	0600	0300
	RAU 8002			287	0650	60	8002	0909
	FMP TEMP1	FORM FX		288	0909	39	0074	0374
	STU FX	SUBT ONE		289	0424	21	0028	0481
	RAU INDXM			290	0481	60	0282	0337
	FVB ONE	FORM INDXM		291	0337	33	0184	0461
	STU INDXM	CONT6		292	0461	21	0282	0935
CONT6	STO ZERO		SET BUMB	293	0337	69	0284	0341
	STO M		INDXM AND	294	0267	24	0270	0323
	STO BUMB		N AT ZERO	295	0267	24	0326	0479
	STB INDXM	CONT7		296	0479	24	0282	0735
CONT7	RAU N			297	1085	60	0270	0225
	FAD ONE	ADD ONE		298	0225	35	0226	0551
	STU M	TO N		299	0511	21	0270	0373
	FMP F1			300	0373	35	0318	0532
	FVY T80			301	0338	34	0182	0432
	FDV A			302	0382	34	1135	1185
	STU BETA	FORM BETA		303	1185	21	0490	0240
	FMP BETA	AND BETA		304	0293	33	0420	0540
	STU BETA2	SQUARED		305	0540	21	0144	0797
	FVB ONE	TEST N FOR		306	0297	60	0282	0337
	NZE CONT8	CONT9	EVEN OR OD	307	0387	45	0590	0241
CONT9	RAU Y0			308	0241	69	0284	0341
	FMP BETA	FORM COS		309	0317	39	0490	0640
	LDZ 8003	BETA Y		310	0640	65	8003	0847
	LDZ	EODCR		311	0847	69	0700	0200
	STL TEMP1			312	0700	20	0074	0427
	RAU Y0			313	0427	60	0286	1235
	FMP BETA	FORM COS		314	1235	39	0490	0690
	LDZ 8003	BETA Y0		315	0690	65	8003	0897
	LDZ	EODCR		316	0897	68	0750	0200
	RAU 8002			317	0750	60	8002	0959
	FMP TEMP1			318	0959	39	0074	0274
	STU FY	FORM FY		319	0274	21	0078	0331
	RAU INDXM	ADD ONE TO		320	0531	60	0482	0437
	FAD ONE	INDXM		321	0437	32	0184	0561
	STU INDXM	CON12		322	0561	21	0482	1285
CONT8	RAU Y0		TEST SOURCE	323	0590	60	0280	1335
	FVB ONE	CON10	X POSITION	324	0361	21	0282	0735
CONT11	RAU INDXM			325	0740	60	0482	0997
	FVB ONE		RESET	326	0487	33	0184	0461
	STU INDXM	CONT7	INDXM	327	0611	21	0482	1085
CON10	RAU BETA		FORM SIN	328	0289	60	0312	0367
	LDZ 8003	BETA Y		330	0790	65	8003	0947
	LDZ	EODCR		331	0947	69	0800	0300
	STL TEMP1			332	0800	20	0074	0477
	RAU Y0			333	0477	60	0280	1385
	FMP BETA	FORM SINE		334	0885	39	0490	0640
	LDZ 8003	BETA Y0		335	0640	65	8003	0997
	LDZ	EODCR		336	0997	69	0800	0300
	RAU 8002			337	0850	60	8002	1009
	FMP TEMP1			338	1009	39	0074	0329
	STU FY	FORM FY		339	0324	21	0078	0331
	RAU INDXM			340	0581	60	0482	0537
	FVB ONE	SUBT ONE		341	0537	33	0184	0661
	STU INDXM	CON12	FROM INDXM	342	0461	21	0282	1285
CON12	RAU ALPHA2			343	1285	60	0094	0499
	FAD BETA2			344	0499	32	0144	0797
	FAD K2	FORM		345	0271	32	0374	0201
	STU GAMMA	GAMMA FOR		346	0201	63	0209	0080
	LDZ	M AND N		347	0404	24	0209	0367
	LDZ	DETERMINE		348	0367	69	0365	0450
	STU FZ	FZ		349	0167	21	0370	0331
	RAU FZ			350	0423	60	0320	0275
	FMP FZ	ADD FY		351	0275	35	0278	0128
	FAD SUM1	TIMES FZ		352	0128	32	0278	0128
	STU BUM1	TO BUM1		353	0403	21	0326	0529
	RAU FZ			354	0403	60	0320	0300
	FVB PREC	TEST FZ		355	0289	33	0178	0605
	SMI COM16	PRECISION		356	0605	46	0228	1059
	LDZ			357	1059	69	0412	0150
	LDZ	EODCL		358	0412	69	0415	0318
	STO 1977	PRINT		359	0318	24	1977	0318
	LDZ M	PARTIAL		360	0330	69	0276	0579

8TD 1978	ANSWERS	361	0579	24	1978	0631
LDD M		362	0631	69	0270	0473
8TD 1979	CHECKING	363	0473	24	1979	0632
LDD FZ		364	0632	69	0270	0473
8TD 1980		365	0681	24	1980	0333
LDD FZ		366	0333	69	0326	0629
8TD 1981		367	0629	24	1981	0334
LDD SUM1		368	0234	69	0326	0629
8TD 1982		369	0629	24	1982	0334
LDD SUM2		370	1436	69	0220	0573
8TD 1983		371	0573	24	1983	0286
8TD 1977	CON16	372	0286	71	1027	0827
LDD	EDOCL	373	0258	69	0711	0150
LDD B		374	0111	68	0011	0577
8TD 1977		375	0417	24	1977	0380
LDD M	PRINT	376	0380	69	0276	0679
8TD 1978	ANSWERS	377	0679	24	1978	0381
LDD M	FOR	378	0731	69	0270	0623
8TD 1979	CHECKING	379	0623	24	1979	0682
LDD FZ		380	0682	69	0326	0629
8TD 1980		381	0781	24	1980	0383
LDD FZ		382	0383	69	0326	0629
8TD 1981		383	0673	24	1981	0284
LDD SUM1		384	0284	69	0326	0729
8TD 1982		385	0729	24	1982	1485
LDD SUM2		386	1485	69	0220	0723
8TD 1983		387	0723	24	1983	0336
FCM 1977		388	0336	71	1027	0827
LDD ONE	SET N AT	389	0527	69	0184	0587
8TD M		390	0587	24	0276	0733
RAU SET80		391	0773	60	0376	0831
FAD DELZ	FORM GAMMA	392	0831	32	0226	0503
FAD KB	FOR M	393	0321	32	0374	0251
LDD	AND N	394	0251	68	0464	0450
8TD GAMMN	EQOAU	395	0450	60	0320	0477
LDD		396	0462	69	0465	0450
8TD FZ	OLDHI DETERMINE	397	0465	24	0320	0477
RAU SUM1	FZ	398	0823	60	0326	0881
FMP FX	ADD SUM1	399	0881	39	0028	0228
LDD SUM2	TIMES FX	400	0228	60	0326	0477
8TD SUM2	TD SUM2	401	1047	21	0220	0873
RAU FZ		402	0873	60	0326	0477
F88 PREC	TEST FZ	403	0375	33	0178	0655
RMI CON20	PRECISION	404	0655	46	0308	1109
LDD		405	1109	69	0312	0350
LDD 3	EDOCL	406	0512	69	0535	0368
LDD M		407	0368	24	1977	0380
LDD M	PRINT	408	0430	69	0276	0779
8TD 1978	PARTIAL	409	0779	24	1978	0931
LDD M	ANSWERS	410	0931	69	0276	0779
8TD 1979	FOR	411	0923	24	1979	0732
LDD FZ	CHECKING	412	0732	69	0276	0779
8TD 1980		413	0981	24	1980	0433
LDD FZ		414	0433	69	0326	0629
8TD 1981		415	0973	24	1981	0334
LDD SUM1		416	0334	69	0326	0629
8TD 1982		417	0829	24	1982	1535
LDD SUM2		418	1535	69	0220	0723
8TD 1983		419	1023	24	1983	0386
8TD 1977	CON17	420	0386	71	1027	0827
LDD	EDOCL	421	0309	69	0761	0150
LDD A	Z	422	0761	69	0150	0467
8TD 1977		423	0467	24	1977	0480
LDD	PRINT	424	0480	69	0276	0679
8TD 1978	PARTIAL	425	0679	24	1978	0381
LDD M	ANSWERS	426	1031	69	0276	1073
8TD 1979	FOR	427	1073	24	1979	0732
LDD FZ	CHECKING	428	0732	69	0276	1081
8TD 1980		429	1081	24	1980	0483
LDD FZ		430	0483	69	0220	0723
8TD 1981		431	1123	24	1981	0384
LDD SUM1		432	0384	69	0326	0629
8TD 1982		433	0929	24	1982	1385
LDD SUM2		434	1385	69	0220	1173
8TD 1983		435	1173	24	1983	0336
FCM 1977		436	0436	71	1027	0827
RAU SUM2		437	0577	60	0220	0425
FDV 8		438	0425	34	0785	1635
FDV 8		439	1635	34	1135	1685
FCM 8		440	1685	34	0028	0338
FMP D	DETERMINE	441	0138	39	0291	0341
8TU FLUX	FLUX	442	0341	21	0046	0549
LDD Y	EDOCL	443	0549	69	0150	0150
8TD 1977		444	0152	69	0705	0358
LDD X0	PRINT Y	445	0358	24	1977	0530
8TD 1978	ANSWERS	446	0530	69	0276	0679
LDD X0		447	0533	24	1978	1131
8TD 1979	YO	448	1131	69	0276	0679
8TD 1980	YO	449	0583	24	1979	0832
LDD Z0	Z0	450	0832	69	0016	0619
8TD 1980		451	0619	24	1980	0333
LDD X		452	0633	69	1008	0453
8TD 1981		453	0453	24	1981	0334
LDD Y	FLUX	454	0434	69	0332	0645
8TD 1982		455	0665	24	1982	1735
LDD		456	1735	69	0208	0833
8TD 1983		457	0811	24	1983	0486
FCM 1977		458	0486	69	0220	0723
8TD 1984		459	0599	24	1984	0637
FCM 1977		460	0637	71	1027	0827
RAU Y	CHANGE Z	461	0627	60	0208	0633
FAD DELZ	UNTIL PAST	462	0163	32	0226	0503
RAU XMAX	MAXIMUM X	463	0503	39	0208	0633
F88 ZMAX		464	0261	33	0454	0101
RMI CON26	CON21	465	0391	46	0261	0395
LDD	SET Z AT	466	0385	60	0312	0517
8TU Z	INITIAL Z	467	1223	21	0208	0911
LDD X		468	0911	60	0312	0517
FAD DELX	CHANGE X	469	0755	32	0408	1785
8TU	UNTIL PAST	470	1785	21	1008	0553
RAU XMAX	MAXIMUM X	471	0543	33	0406	0101
RMI CON26	CON22	472	0683	46	0261	0627
8TU XINIT	REBET X	473	0687	60	0312	0517
FAD DELX	AND XINIT	474	0257	32	0408	1835
8TU XINIT		475	1835	21	0102	0805
LDD X		476	0805	21	1008	0553
RAU Y	CHANGE Y	477	0603	60	0312	0517
FAD DELY	UNTIL PAST	478	0517	32	0376	1031
8TU Y	MAXIMUM Y	479	1097	24	0326	0629
F88 YMAX		480	0618	33	0418	0445
RMI CON26	CON25	481	0445	46	0261	0627
CON25	HLT	482	0649	01	0699	0699

1	00	1000	0000	IDENTIFI	483	0415	00	1000	0000
2	00	2000	0000	CATIDN	484	0312	00	2000	0000
3	00	3000	0000	NUMBERS	485	0515	00	3000	0000
4	00	4000	0000		486	0364	00	4000	0000
7	00	7000	0000		487	0705	00	7000	0000
TWB	20	0000	0051		488	0182	20	0000	0051
DWE	10	0000	0051		489	0184	10	0000	0051
ZFRD	00	0000	0000		490	0264	00	0000	0000
PI	31	4161	0051		491	0332	31	4161	0051
A	88	1100	0052	PILE SIZE		0755	88	1100	0052
B	88	1100	0052	PILE SIZE		1135	88	1100	0052
C	88	1100	0052	PILE SIZE		0900	88	1100	0052
D	82	0000	0050	DIFF COEFF		0088	82	0000	0050
R	17	1000	0057	SOURCE STR		0281	17	1000	0057
XINIT	00	0000	0000	INITIAL X		0102	00	0000	0000
YINIT	00	0000	0000	INITIAL Y		0356	00	0000	0000
ZINIT	98	2700	0052	INITIAL Z		0268	98	2700	0052
XD	00	0000	0000	SOURCE POS		0950	00	0000	0000
YD	00	0000	0000	SOURCE POS		1050	00	0000	0000
ZD	88	1100	0052	SOURCE POS		0016	88	1100	0052
TMAX	88	1100	0052	MAXIMUM		0406	88	1100	0052
TMAX	88	1100	0052	VALUER OF		0410	88	1100	0052
ZMAX	17	6220	0053	X Y AND Z		0414	17	6220	0053
DELX	20	3200	0052	CHANGES IN		0408	20	3200	0052
DELY	20	3200	0052	X Y AND Z		0370	20	3200	0052
DELZ	10	1600	0052			0226	10	1600	0052
F2	35	9250	0047	KAPPA 800		0374	35	9250	0047
F0CEE	17	6220	0053	PILE SIZE		0161	17	6220	0053
BETRD	31	7840	0047	Y BUCKLING		0376	31	7840	0047
-PREC	10	0000	0049	PRECISION		0178	10	0000	0049

APPENDIX G

Description and Explanation of the IBM-650
Computer Program Used for Fitting Empir-
ically Experimental Data with the Sum of
Several Terms of Gaussian Form

The computer code was written to fit empirically the experimental indium resonance activity with the sum of several Gaussian terms having adjustable parameters. The program was written in SOAP II and floating point form. The object program is listed and the logic diagram is given in this section.

This method of fit was not exact. There was no guarantee that the result of this fit would be the best; but in a practical approach to the problem of fitting a non-linear function, the result appeared to be adequate.

The criterion that the machine inspected was that the sum of the weighted squares of the residuals between the experimental data and calculated values should be made as small as possible. This was done through a trial and error process. Each of the fitting parameters was varied in turn by a specified increment, holding all other parameters constant, until such time that a specified increment could make no further reduction in the sum of the weighted squares of the residuals. This parameter was then stored as the best available estimate of the particular empirical parameter. When none of the parameters could be varied by the specified increment to give a smaller sum of the weighted squares of the residuals, the increments were refined and the trial and error process was repeated with the refined

increments. This procedure continued until the increments were less than a specified precision.

The second portion of the program calculated the fractional contributions of each range group according to Eq. 16 of the theory.

The data were empirically fit with a function of the form of Eq. 14 of the theory

$$\text{FLUX}_j = \sum_{i=1}^N B_i e^{-(z_j/r_i)^2}, \quad N \leq 10 \quad (\text{G-1})$$

As stated above, the best fit criterion was that

$$\text{ERROR} = \sum_{j=1}^M \frac{1}{W_j^2} \left(\sum_{i=1}^N B_i e^{-(z_j/r_i)^2} - \text{FLUX}_j \right)^2, \quad M \leq 20 \quad (\text{G-2})$$

be a minimum.

The program required, in addition to the experimental data and their respective positions, initial estimates for a specific number of parameters. The program had a capacity for up to 20 data points and 10 terms in the summation of Eq. G-1. These input data were read into the machine along with the program deck on one-word load cards. Each one-word load card contained a particular constant or initial value and its specified storage location. Table 23 lists the various input data needed for this program.

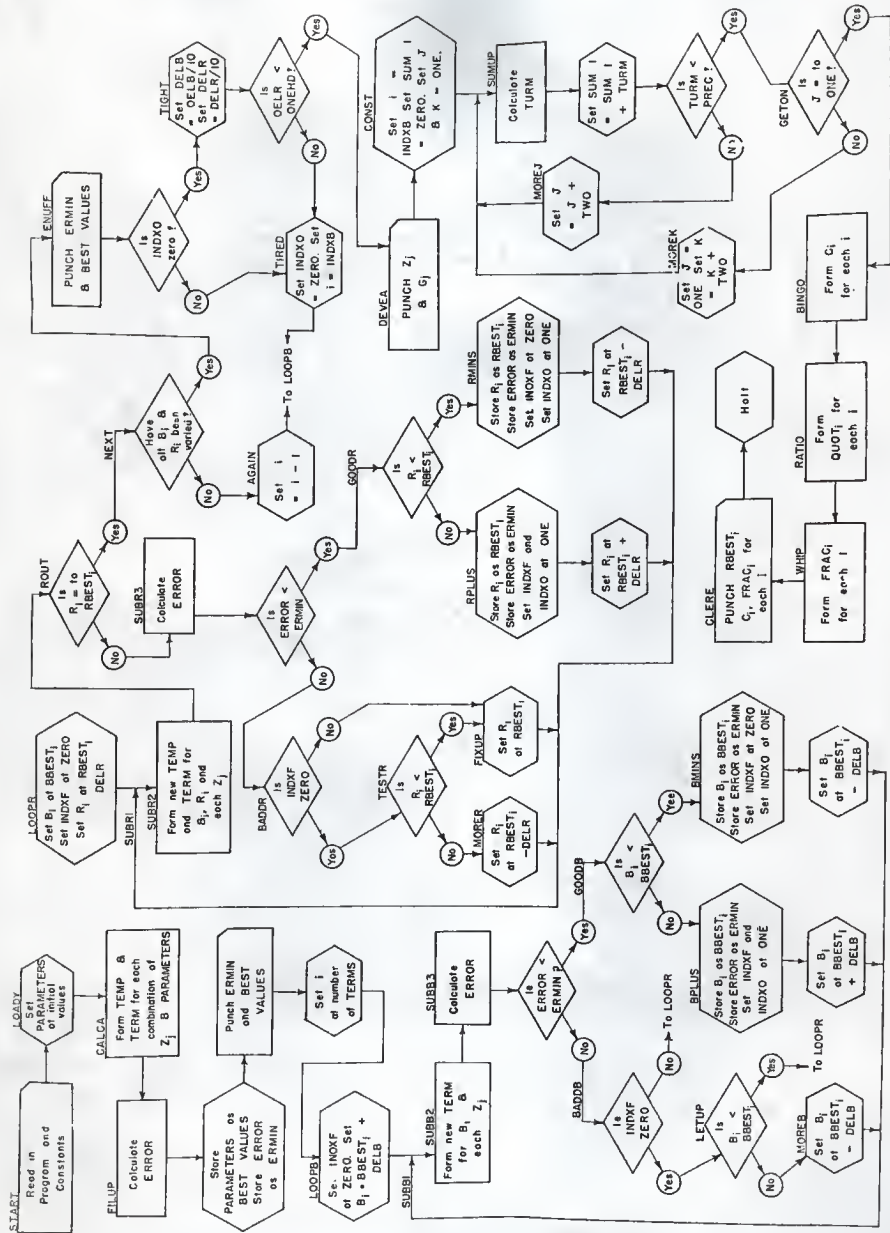
Table 23. Input data required for use of the IBM-650 program which empirically fits experimental data with several terms of Gaussian form.

Symbol	Explanation	Storage location
ZERO	0.00	0059
FPONE	1.00	0096
FPTWO	2.00	0260
FOUR	4.00	0743
TEN	10.00	0436
ONE	Index number 1	0292
EIGHT	Index number 8	0124
ONEHD	Desired precision of parameter increments	0354
PI	π	0290
SQPI	$\sqrt{\pi}$	0164
PREC	Desired precision in term of series summation	0126
A1	Pile width in x-direction (cm)	0405
A2	Pile width in y-direction (cm)	0211
DELB	Initial increment of the amplitude, B_i	0028
DELR	Initial increment of the Gaussian range, r_i (cm)	0198
INDXA	Number of data points	0077
INDXB	Number of Gaussian terms in empirical fit	0162
Z	Position of j^{th} data point (cm)	12(00+j)
FLUX	Experimental data at j^{th} point	12(20+j)
W	Weighting function of j^{th} piece of data	17(50+j)
	Initial estimate of B_i	13(00+i)
	Initial estimate of r_i (cm)	13(20+i)

The machine yielded an answer card having a capacity of 8 words, a word being a ten digit number and a sign. For the first answer punching operation the machine printed out the initial estimates of the fitting parameters on as many cards as was necessary to accommodate them. The amplitude and range of the first term were printed out in word locations 1 and 2, respectively. The amplitude and range of the second term were printed in word locations 3 and 4, respectively.

After a card was filled to its 8 word capacity it was punched and a new card began to be filled. This procedure continued until all fitting parameters had been punched out. Then a separate card was punched giving in the word 8 location, the value of the sum of the weighted squares of the residuals between the experimental data and the calculated value. Subsequent improvements in the parameters were printed out according to this procedure after each cycle of trying to vary each parameter. When the fitting parameters could not be further improved with the most refined increment specified, the punching out of the best fit parameters and their sum of the weighted squares of the residuals took place according to the procedure previously described. At this time the residual at each point was punched out along with the position of the point. The position of the last point and the associated residual were loaded into word locations 1 and 2, respectively. The position and the residual of the next to last point were loaded into word locations 3 and 4, respectively. This procedure continued until all the residuals and their identifying locations had been punched on as many cards as was necessary.

The machine then calculated the fractional contributions of each range group and printed it out in the word 5 location along with the respective Gaussian range in the word 7 location.



LOGIC DIAGRAM - APPENDIX G

				EMPIRICAL FIT OF RESONANCE DATA			
BLR	1200	1780	3	0000	00	0000	0000
BLR	1951	1960	3	0000	00	0000	0000
BLR	1957	1985	3	0000	00	0000	0000
SYN	START	1999	4	0000	00	0000	0000
SYN	7	1200	5	0000	00	0000	0000
SYN	FLUX	1220	POSITION	6	0000	00	0000
SYN	G	1240	ACTIVATION	7	0000	00	0000
SYN	B	1350	DEVIATION	8	0000	00	0000
SYN	B	1350	AMPLITUDE	9	0000	00	0000
SYN	RBEST	1375		10	0000	00	0000
SYN	RBEST	1200	RANGE	11	0000	00	0000
SYN	RBEST	1290		11	0000	00	0000
SYN	RINIT	1300	INITIAL	12	0000	00	0000
SYN	RINIT	1310	ESTIMATE	13	0000	00	0000
SYN	TEMP	1320		14	0000	00	0000
SYN	TERM	1590	SUM TERM	15	0000	00	0000
SYN	FRAC	1720	CONSTANT	16	0000	00	0000
SYN	FRAC	1730	FRACTION	17	0000	00	0000
SYN	DOT	1740	F TO X	18	0000	00	0000
SYN	W	1750	WEIGHT	19	0000	00	0000
SYN	W	1750	F TO X	20	0000	00	0000
EDOE4	STL	AAA1	SUBROUTINE	21	0006	20	0011
EDOE4	STL	AAA2		22	0014	20	0011
EDOE4	STL	AAA3		23	0014	20	0011
EDOE4	STL	AAA3	Y FOR CALC	24	0028	60	0019
EDOE4	STL	AAA3		25	0023	39	0026
EDOE4	STL	AAA5		26	0076	38	0029
EDOE4	STL	AAA5		27	0025	38	0029
EDOE4	STL	AAA5		28	0069	38	0029
EDOE4	STL	AAA14		29	0049	39	0019
EDOE4	STL	AAA3		30	0119	38	0132
EDOE4	STL	AAA3		31	0099	39	0019
EDOE4	STL	AAA3		32	0169	38	0172
EDOE4	STL	AAA1		33	0149	39	0019
EDOE4	STL	AAA11		34	0819	38	0229
EDOE4	STL	AAA1		35	0199	39	0019
EDOE4	STL	AAA10		36	0869	38	0272
EDOE4	STL	AAA4		37	0249	38	0004
EDOE4	STL	AAA4		38	0007	39	0004
EDOE4	STL	AAA4		39	0054	21	0004
EDOE4	STL	AAA4		40	0057	39	0004
EDOE4	STL	AAA4		41	0104	21	0004
EDOE4	STL	AAA2	AAAG	42	0107	60	0011
EDOE4	STL	AAA2	AAAG	43	0063	46	0000
EDOE4	STL	AAA10		44	0018	60	0272
EDOE4	STL	AAA4	AAAG	45	0154	21	0004
EDOE4	STL	AAA4	AAAG	46	0319	60	0004
EDOE4	STL	AAA10	AAAG	47	0272	10	0272
EDOE4	STL	AAA11	AAAG	48	0222	24	3338
EDOE4	STL	AAA12	AAAG	49	0178	31	9878
EDOE4	STL	AAA13	AAAG	50	0128	38	9137
EDOE4	STL	AAA14	AAAG	51	0072	17	1562
EDOE4	STL	AAA15	AAAG	52	0029	4	3229
EDOE4	STL	AAA16	AAAG	53	0026	69	0000
EDOE4	STL	AAA16	AAAG	54	0026	69	0000
EDOE4	STL	AAA16	AAAG	55	0058	24	0053
EDOE4	STL	AAA16	AAAG	56	0056	24	0053
EDOE4	STL	AAA16	AAAG	57	0012	24	1977
EDOE4	STL	AAA16	AAAG	58	0030	24	1979
EDOE4	STL	AAA16	AAAG	59	0031	24	1979
EDOE4	STL	AAA16	AAAG	60	0032	24	1980
EDOE4	STL	AAA16	AAAG	61	0031	24	1980
EDOE4	STL	AAA16	AAAG	62	0034	24	1982
EDOE4	STL	AAA16	AAAG	63	0036	24	1983
EDOE4	STL	AAA16	AAAG	64	0036	24	1984
EDOE4	STL	AAA16	AAAG	65	0009	00	0000
EDOE4	STL	AAA16	AAAG	66	0100	24	0000
EDOE4	STL	AAA16	AAAG	67	0106	60	0000
EDOE4	STL	AAA16	AAAG	68	0055	39	0000
EDOE4	STL	AAA16	AAAG	69	0150	34	0000
EDOE4	STL	AAA16	AAAG	70	0080	34	0000
EDOE4	STL	AAA16	AAAG	71	0130	66	0003
EDOE4	STL	AAA16	AAAG	72	0037	69	0040
EDOE4	STL	AAA16	AAAG	73	0040	20	0000
EDOE4	STL	AAA16	AAAG	74	0200	24	0153
EDOE4	STL	AAA16	AAAG	75	0156	60	0000
EDOE4	STL	AAA16	AAAG	76	0028	39	0000
EDOE4	STL	AAA16	AAAG	77	0010	21	0000
EDOE4	STL	AAA16	AAAG	78	0250	24	0000
EDOE4	STL	AAA16	AAAG	79	0260	10	0000
EDOE4	STL	AAA16	AAAG	80	0062	88	0001
EDOE4	STL	AAA16	AAAG	81	0068	24	0000
EDOE4	STL	AAA16	AAAG	82	0024	69	0077
EDOE4	STL	AAA16	AAAG	83	0080	88	0001
EDOE4	STL	AAA16	AAAG	84	0086	69	0000
EDOE4	STL	AAA16	AAAG	85	0042	88	0001
EDOE4	STL	AAA16	AAAG	86	0048	69	0000
EDOE4	STL	AAA16	AAAG	87	0112	24	0115
EDOE4	STL	AAA16	AAAG	88	0118	60	0000
EDOE4	STL	AAA16	AAAG	89	0041	21	0115
EDOE4	STL	AAA16	AAAG	90	0168	69	0000
EDOE4	STL	AAA16	AAAG	91	0168	69	0000
EDOE4	STL	AAA16	AAAG	92	0230	59	0001
EDOE4	STL	AAA16	AAAG	93	0136	48	0000
EDOE4	STL	AAA16	AAAG	94	0089	49	0000
EDOE4	STL	AAA16	AAAG	95	0090	60	0115
EDOE4	STL	AAA16	AAAG	96	0069	38	0000
EDOE4	STL	AAA16	AAAG	97	0047	21	0000
EDOE4	STL	AAA16	AAAG	98	0043	39	0000
EDOE4	STL	AAA16	AAAG	99	0140	34	0000
EDOE4	STL	AAA16	AAAG	100	0030	38	0001
EDOE4	STL	AAA16	AAAG	101	0087	21	0000
EDOE4	STL	AAA16	AAAG	102	0074	59	0001
EDOE4	STL	AAA16	AAAG	103	0280	51	0001
EDOE4	STL	AAA16	AAAG	104	0186	40	0000
EDOE4	STL	AAA16	AAAG	105	0350	24	0253
EDOE4	STL	AAA16	AAAG	106	0256	60	0000
EDOE4	STL	AAA16	AAAG	107	0109	69	0162
EDOE4	STL	AAA16	AAAG	108	0165	88	0001
EDOE4	STL	AAA16	AAAG	109	0071	69	0001
EDOE4	STL	AAA16	AAAG	110	0127	81	0001
EDOE4	STL	AAA16	AAAG	111	0083	68	0000
EDOE4	STL	AAA16	AAAG	112	0073	24	0000
EDOE4	STL	AAA16	AAAG	113	0038	69	0000
EDOE4	STL	AAA16	AAAG	114	0093	24	0000
EDOE4	STL	AAA16	AAAG	115	0139	38	0001
EDOE4	STL	AAA16	AAAG	116	0045	50	0000
EDOE4	STL	AAA16	AAAG	117	0001	42	0000
EDOE4	STL	AAA16	AAAG	118	0020	40	0000

CARDZ	PCM 1977			119	0008	71 1977	0177
	LOD RESIT	EOOCL		120	0177	69 0073	0000
WHOPE	PCM 1977			121	0105	71 1977	0287
	LOD	EOOCL		122	0227	69 0330	0056
	LD8 ERMIN			123	0230	69 0330	0236
	STD 1984			124	0236	24 1984	0087
PRIME	PCM 1977	EXET		125	0000	71 1977	0233
	STD TIXE		ROUTINE	126	4000	24 0303	0306
	LOD 8		TO SET	127	0306	69 5260	0013
	STD REBT		TEST	128	0113	24 0703	0013
	LBO R		VALUES OF	129	0123	69 5280	0183
	STD REBT		PARAMETERS	130	0183	69 5280	0183
	LOD INDR		ALL	131	0143	69 0021	0174
	STD ERMIN	TIXE		132	0174	24 0133	0303
	LOD INDR			133	1999	69 0000	0110
START	RAB 8001	LOADY		134	0215	82 8001	0121
	LOD BLNIT		SET	135	0121	69 5260	0013
	STD REBT		PARAMETERB	136	0353	24 5260	0063
	LOD INIT		AT INITIAL	137	0063	24 5270	0173
	STD R		ESTIMATED	138	0173	69 0173	0133
	STD REBT			139	0113	24 5280	0233
	STD REBT			140	0233	24 5290	0153
	RAB 8001			141	0004	69 0004	0288
SETUP	NZB LDADY	SETUP		142	0299	42 0121	0403
	LOD INDX8			143	0303	69 0077	0081
	RAA 8001			144	0081	80 8001	0137
	LOD INDX8			145	0137	69 0164	0263
	RAB 8001			146	0263	82 8001	0171
	MPY 8001		DETERMINE	147	0471	12 8001	0044
	STL INDXC		INDXC	148	0844	20 0039	0092
	RAC 0001			149	0092	88 8001	0098
CALCA	LOD INDXC	CALCA	CALCULATE	150	0098	69 0051	0100
	LOD INDXC	TEMP	TEMP AND	151	0051	69 0051	0200
	BYC 0001		TERM FDR	152	0254	59 0001	0060
	RA 0001			153	0060	69 0001	0060
CALCB	NZA CALCA	CALCB	COMRN	154	0016	40 0098	0080
	LOD INDXA		ATIONS	155	0020	62 0077	0380
	RAA 8001		OF R AND B	156	0380	69 0380	0016
	X88 0001			157	0286	53 0001	0142
	NZB 8001			158	0148	42 0000	0046
FILUP	LOD CALCA	FILUP	DETERMINE	159	0046	62 0345	0240
	LOD	PRIME	INITIAL	160	0349	69 0002	0400
	LOD	PRINT	ERROR	161	0002	69 0155	0350
	LOD INDX8			162	0155	69 0162	0315
	RAB 8001			163	0315	82 8001	0323
	LOD INDXC			164	0221	69 0039	0192
	RAC 8001	LODPR		165	0192	88 8001	0142
LODPR	LOD ZERO			166	0142	69 0142	0212
	STD INDXF			167	0212	24 0365	0218
	RAU 8001		INCREASE B	168	0218	60 0218	0155
	FAD DELR	SUB81		169	0218	32 0028	0225
	STU 8			170	0205	21 5260	0163
	LOD 8007			171	0000	69 0000	0438
	STD CTENP			172	0419	24 0322	0175
	LOD 8006			173	0175	69 0006	0131
	STD BTEMP			174	0131	24 0084	0187
	LOD INDXA			175	0187	69 0077	0430
	RA 8001	SUB82		176	0430	69 0430	0336
	LOD	TMRMM	FORM NEW	177	0336	69 0189	0200
	BYC 0001		TERM	178	0189	59 0001	0095
	X8A 0001			179	0095	53 0001	0111
	NZA SUB82	SUB83	DETERMINE	180	0101	40 0356	0255
	LOD	ERR	TEST ERROR	181	0255	69 0255	0000
	RAU ERMIN			182	0058	60 0133	0237
	F88 ERROR			183	0537	33 0021	0147
	BW 8AD08			184	0447	42 0040	0131
	LOD BTEMP		HAVE	185	0151	69 0084	0287
	RAU 8001		IMPROVED B	186	0287	69 0287	0185
	LOD CTENP			187	0243	69 0322	0225
	RAB 8001			188	0225	88 8001	0121
	RAU REBT			189	0225	69 0225	0275
	F88 8			190	0275	33 5260	0337
BPLUS	BW 8PLUS	BMIN8		191	0337	42 0190	0091
	LOD	PRIME	SET B	192	0190	69 0293	0400
	LOD FPONE		AT BBEST	193	0293	69 0066	0399
	STD INDXF			194	0399	24 0365	0268
	STD INDXO			195	0268	24 0271	0224
	FAD DELR	SUB81	INCREASE B	196	0224	60 5270	0385
	LOD		SET B	197	0225	32 0098	0208
	LOD ZERO	PRIME	SET B	198	0091	69 0094	0400
	STD INDXF		AT BBEST	199	0094	69 0099	0262
	LOD FPONE			200	0262	24 0365	0318
	STD INDXO			201	0318	69 0066	0448
	RAU REBT		DECREASE P	202	0449	24 0271	0274
	F88 DELR	SUB81		203	0274	60 5270	0376
	LOD BTEMP		HAVE NOT	204	0375	33 0075	0185
	RAB 8001		IMPROVED B	205	0450	69 0084	0387
	RAU INDXF			206	0387	82 8001	0343
	NZU LOOPR	LETUP		207	0469	44 0283	0324
	LOD			208	0324	69 0324	0437
	RAB 8001			210	0437	82 8001	0393
	RAU REBT			211	0393	60 5270	0425
	F88 8			212	0425	33 5260	0467
	BW 8AD08	LODPR		213	0427	42 0240	0233
	LOD CTENP			214	0240	69 0240	0358
	RAB 8001			215	0537	82 8001	0443
	LOD BTEMP			216	0443	69 0322	0475
	RAU 8001			217	0475	88 8001	0231
	RAC 8001		DECREASE B	218	0231	60 5270	0525
	RAU REBT	SUB81		219	0525	33 0098	0355
	FAD DELR			220	0223	69 0059	0312
	LOD ZERO			221	0312	24 0365	0368
	STD INDXF		SET B	222	0168	69 0168	0276
	STD INDXO		AT BBEST	223	0273	24 5260	0233
	RAU REBT			224	0233	62 5260	0145
	FAD DELR	SUB81	INCREASE B	225	0145	24 0271	0224
	STU 8			226	0575	21 5280	0263
	LOD CTENP			227	0263	69 0263	0623
	RAC 8001			228	0625	88 8001	0281
	LOD BTEMP			229	0281	62 0084	0587
	RAB 8001			230	0587	69 0084	0493
	LOD INDXA			231	0493	62 0077	0420
	RA 8001	SUB82	FORM NEW	232	0480	80 8001	0376
	LOD	TEMP	TEMP AND	233	0366	69 0239	0100
	BYC 0001	TURNP	TERM	234	0239	69 0242	0200
	X8A 0001			235	0246	59 0001	0246
	NZA SUB82	ROUT		236	0246	53 0001	0304
	LOD			237	0304	40 0366	0108
ROUT	RAU REBT			238	0108	60 5290	0195
	F88 8			239	0195	33 5280	0157
	NZU SUB83	NEXT	DETERMINE	240	0157	44 0061	0362

SUBR3	LDD		ERR	ERROR	241	0061	69	0064	0250
	RAU	ERWIN			242	0064	60	0133	0637
	FBS	ERROR		TEST ERROR	243	0637	33	0021	0137
	S	ADDER	GOODR		244	0201	69	0197	0637
	LDD	STEMP		HAVE	245	0201	69	0084	0687
	RAS	S001		IMPROVED	246	0687	02	0198	0537
	LDD	CTEMP		R	247	0543	69	0322	0675
	RAC	S001			248	0675	98	8001	0331
	RAU	RSEST	B		249	0331	50	5990	0266
	FBS	R	B		250	0245	33	5880	0207
	BWJ	RPLUS	B	RWINB	251	0807	46	0110	0111
	LDD	STEMP		PRIME	252	0256	69	0110	0420
	LDD	FPONE		RSEST	253	0263	69	0096	0499
	STD	INXDF			254	0499	24	0198	0537
	RAC	S001			255	0256	64	0471	0374
	RAU	RSEST	B		256	0374	60	5890	0295
	FAD	DELN	SUBR1	INCREASE R	257	0256	69	0198	0537
	LDD	STEMP		PRIME	258	0111	69	0114	0400
	LDD	ZERO		RSEST	259	0245	69	0096	0499
	S	T			260	0412	64	0365	0468
	LDD	FPONE			261	0468	69	0096	0499
	STD	INXDF			262	0849	44	0271	0420
	RAU	RSEST	B	DECREASE R	263	0424	60	5890	0345
	FBS	DELN	SUBR1		264	0345	63	0198	0537
	RAU	ONEZ		HAVE NOT	265	0500	40	0365	0519
	NZU	FI XUP	TESTR	IMPROVED R	266	0519	44	0323	0474
	LDD	STEMP			267	0474	69	0084	0289
	RAS	S001			268	0737	82	8001	0593
	RAU	RSEST	B		269	0593	60	5890	0395
	FBS	R			270	0395	33	5880	0257
	SWI	MORER		FIXUP	271	0257	46	0160	0323
	LDD	STEMP			272	0160	69	0096	0499
	RAU	S001			273	0257	82	8001	0643
	LDD	CTEMP			274	0643	69	0322	0725
	RAC	S001			275	0725	48	8001	0811
	RAU	RSEST	B	DECREASE R	276	0361	60	5890	0445
	FBS	DELN	SUBR1		277	0445	63	0198	0537
	RAU	RSEST	B	SET R AT	278	0361	60	5890	0575
	FIXUP		SUBR1		279	0361	60	5890	0575
	NEXT	8X5	0003	RSEST	280	0361	60	5890	0575
	NZU	ASIN		ENUFF	281	0318	66	0139	0376
	RAU	CTEMP		REPEAT	282	0321	60	0322	0277
	AGAIN	NZU	INXDF	PROCEDURE	283	0277	11	0202	0124
	STD	CTEMP		FOR NEXT	283	0431	21	0332	0775
	RAU	STEMP		RANGE	284	0775	60	0084	0289
	SWI	ONEZ		EQUIP	285	0289	11	0202	0124
	STD	BTEMP			286	0247	21	0084	0537
	LDD	CTEMP			287	0817	69	0096	0499
	RAC	S001			288	0825	98	8001	0481
	LDD	BTEMP			289	0481	69	0084	0289
	RAS	S001		LOOPS	290	0817	69	0096	0499
	ENUFF	LDD		PRINT	291	0372	69	0673	0350
	RAC	S001			292	0825	60	0079	0530
	NZU	TIRED		TIGHT	293	0925	44	0079	0530
	LDD	INX8		IMPROVED	294	0079	69	0162	0415
	RAT	S001		LAST TIME	295	0415	98	8001	0313
	LDD	INX8		THROUGH	296	0371	69	0039	0342
	LDD	S001		AGAIN	297	0342	68	8001	0388
	LDD	ZERO			298	0298	69	0059	0462
	STD	INX0		LOOPB	299	0462	24	0071	0148
	RAU	DELB		REFINE	300	0530	60	0084	0289
	FOV	TEN		INCREMENTS	301	0333	34	0436	0486
	STD	DELB			302	0486	21	0228	0531
	NZU	DELR			303	0333	60	0084	0289
	FOV	TEN			304	0453	34	0436	0536
	STD	DELR			305	0536	11	0202	0124
	FBS	ONEHO			306	0251	33	0354	0581
	BWJ	DEVEA	TIRED		307	0581	46	0133	0279
	LDD	INX8		EOOCL	308	0134	69	0277	0580
	DEVEA	LDD	INX8	DEVIATIONS	309	0537	69	0077	0580
	RAS	S001		RESET	310	0580	80	8001	0580
	LDD	EIGHT			311	0586	69	0124	0322
	RBS	S001		STUFF	312	0322	83	8001	0383
	LDD	Z	A		313	0383	69	0300	0303
	STD	1985	B		314	0503	24	5983	0088
	LDD	G	A		315	0088	69	0240	0933
	STD	1986	B		316	0693	34	5986	0339
	AXA	0001			317	0339	51	0001	0498
	AKS	0002			318	0498	32	0002	0301
	NZA	MOREG		FINIS	319	0301	40	0404	0305
	MOREG	CARDS		CARDS	320	0404	42	0383	0158
	PCH	S002			321	0158	71	0477	0427
	LDD	RESET		EOOCL	322	0377	69	0586	0650
	PCH	1977		CONST	323	0306	71	0477	0427
	FINIS	LDD	INX8		324	0427	69	0162	0465
	CONST	RAC	S001	SETJK	325	0465	82	8001	0421
	SETJK	LDD	ZERO	CONSTANT C	326	0421	69	0096	0499
	STD	SUM1		BY	327	0512	24	0515	0568
	LDD	FPONE			328	0568	69	0162	0465
	STD	J		SUMMING	329	0568	69	0162	0465
	STD	J		INFINITE	329	0599	24	0052	0355
	STD	K		SERIEB	330	0355	34	0208	0161
	RAU	J		UNTIL	331	0441	60	0096	0499
	FMP	J		LAST TERM	332	0307	39	0032	0102
	FOV	A1		SUMLL	333	0102	34	0258	0102
	FOV	A1		ENOUGH	334	0455	34	0403	0505
	STD	PART			335	0505	21	0210	0313
	FMP	K			336	0313	60	0208	0313
	FMP	K			337	0363	39	0208	0258
	FOV	A2			338	0258	34	0258	0102
	FOV	A2			339	0261	34	0211	0311
	FAD	PART			340	0311	32	0210	0987
	FMP	PI			341	0987	39	0208	0340
	FMP	PI			342	0340	39	0290	0390
	FMP	RSEST	B		343	0390	39	5890	0440
	FMP	RSEST	B		344	0440	39	5890	0490
	FOV	F00R			345	0490	34	0243	0293
	LDD	R003			346	0793	66	0083	0335
	FOV	S002		EOOEA	347	0351	69	0454	0000
	STD	TURV			348	0454	60	0002	0133
	FAD	SUM1			349	0413	21	0618	0471
	FBS	SUM1			350	0471	38	0515	0141
	FBS	SUM1			351	0141	21	0052	0668
	RAU	TURV			352	0668	60	0618	0373
	FBS	PREC			353	0373	33	0126	0353
	BWJ	GETON		MOREJ	354	0553	46	0356	0577
	WMOREJ	FAD	FTWO		355	0357	60	0052	0407
	GETON	RAT	J	SUMUP	356	0407	32	0101	0137
	STD	J			357	1037	21	0052	0161
	STD	J			358	0336	60	0366	0423
	FBS	FPONE		SINGO	359	0457	33	0096	0423
	NZU	MOREK			360	0423	44	0477	0078
	RAU	K			361	0477	60	0096	0423
	FAD	FTWO			362	0463	32	0260	1087

	STU K			363	1087	01	0208	0361
	LOO	FPONE		364	0361	69	0286	0446
	RAU	RUMUP		365	0649	24	0052	0161
RINGO	RAU	RUM1		366	0078	60	0553	0569
	FOV	FOUR		367	0569	39	0743	0413
	FOV	A1		368	0843	34	0405	0555
	FOV	A2		369	0555	34	0251	0413
	FOV	BP1		370	0413	34	0164	0214
	FOV	REEST	R	371	0214	34	5290	0540
	LOO	ZERO		372	0540	21	5040	0273
	XB8	0001	B	373	0473	53	0001	0129
	NZB	BETUX	FRACT	374	0129	48	0021	0423
FRACT	LOO	ZERO		375	0133	69	0559	0362
	STO	DEMON		376	0562	64	0565	0718
	LOO	INDB		377	0718	69	0565	0718
	NAB	0001	SATIO	378	0615	03	8001	0551
RATIO	RAU	REEST	B	379	0521	60	5270	0975
	FOV	C		380	0975	34	5730	0073
	STU	DUDY	B	381	0070	21	5740	0893
	FAO	DEMON		382	0893	38	0000	0301
	STU	DEMON		383	0491	21	0565	0768
	XB8	0001		384	0768	53	0001	0584
	NZB	RATIO		385	0584	42	0594	0128
GDWAN	LOO	INOXB	GDWAN	386	0128	69	0162	0665
	NAB	0001	SNIP	387	0464	69	0584	0284
WNIP	RAU	QUOT	B	388	0574	60	5740	0545
	FOV	DEMOU		389	0545	34	0565	0725
	STU	FRAC	B	390	0715	21	5730	0483
	XB8	0001		391	0483	53	0001	0389
	NZB	WNIP	CLERE	392	0389	42	0571	0943
CLERE	LOO	INOXB		393	0464	69	0584	0284
	NAB	0001		394	0765	62	8001	0621
	LOO	WRITE		395	0621	69	0621	0500
WRITE	LOO	REEST	B	396	0574	69	5290	0993
	STO	1981		397	0993	24	1981	0184
	LOO	C	B	398	0748	69	0584	0323
	STO	1983		399	0323	24	1983	0058
	LOO	FRAC	B	400	0085	69	5730	0513
	STO	1983		401	0533	24	1983	0636
	PCH	1977		402	0636	71	1977	0527
	XB8	0001		403	0527	83	0001	0613
	NZB	WRITE	NALY	404	0383	42	0574	1137
NALY	NALY			405	1137	64	0584	0284
ZERO	00	0000	0000	406	0059	00	0000	0000
INORA	00	0000	0010	407	0077	00	0000	0010
INORR	00	0000	0003	408	0162	00	0000	0003
EIGMT	00	0000	0008	409	0124	00	0000	0008
FPDME	10	0000	0051	410	0096	10	0000	0051
RETRD	00	0000	0051	411	0260	20	0000	0051
ONE	00	0000	0001	412	0298	00	0000	0001
TEN	10	0000	0052	413	0436	10	0000	0052
ONEMO	99	0000	0048	414	0354	99	0000	0048
A1	17	6230	0053	415	0405	17	6230	0053
A2	17	6230	0053	416	0211	17	6230	0053
P1	31	4152	0053	417	0220	31	4152	0053
FOUB	40	0000	0051	418	0743	40	0000	0051
PSEC	10	0000	0046	419	0126	10	0000	0046
BPPI	17	7245	0051	420	0164	17	7245	0051
DELB	10	0000	0053	421	0028	10	0000	0053
DELR	10	0000	0051	422	0198	10	0000	0051
Z1	66	3000	0081	423	0201	66	3000	0081
Z2	15	8800	0052	424	1202	15	8200	0052
Z3	25	9600	0052	425	1204	25	9600	0052
Z4	38	1000	0052	426	1205	38	1000	0052
Z5	46	3100	0052	427	1206	46	3100	0052
Z6	58	4800	0052	428	1206	58	4800	0052
Z7	66	1800	0052	429	1207	66	1800	0052
Z8	76	7800	0052	430	1208	76	7800	0052
Z9	88	8400	0052	431	1209	88	8400	0052
Z10	97	1200	0052	432	1210	97	1200	0052
				433	1221	32	6230	0052
				434	1222	26	7380	0055
				435	1223	18	3350	0055
				436	1224	10	6170	0055
				437	1225	56	7300	0054
				438	1226	25	7600	0054
				439	1227	11	5900	0054
				440	1228	47	0700	0053
				441	1229	21	2500	0053
				442	1230	92	9000	0052
				443	1231	84	6400	0054
				444	1232	10	6010	0055
				445	1233	17	6400	0054
				446	1234	11	5600	0054
				447	1235	12	2500	0054
				448	1236	23	5000	0053
				449	1237	64	3000	0052
				450	1238	41	0000	0052
				451	1239	40	0000	0052
				452	1240	37	2000	0052
				453	1241	49	3000	0053
				454	1242	21	7800	0053
				455	1243	11	1120	0055
				456	1244	65	4400	0052
				457	1245	36	9400	0052
				458	1246	27	3100	0052

APPENDIX H

Consideration of Perturbations and Corrections Encountered
in Experiments Using Finite Foils and Sources

In order to determine indium foil activations free from self-perturbations or experimental limitations, it is possible to consider the following:

- (a) activation of indium by higher energy resonance neutrons
- (b) absorption of epithermal neutrons in cadmium filter
- (c) finite size of source and detector
- (d) difference in foil weights or size
- (e) unequal activation of two sides of foil
- (f) flux depression in vicinity of foil
- (g) self-shielding of the center of the foil by its outer layers
- (h) mutual shadowing of neighboring foils
- (i) hardening of the neutron spectrum through the foil
- (j) obliquity of foil with respect to the source.

If there is need for an estimate of the absolute flux in medium or physical situation that differs from the standardizing medium or the standardizing physical situation, these factors should be considered. Factors (a) through (e) have been considered in this pile standardization.

Activation of Indium by Higher Energy Resonance Neutrons

This section considers the correction factor that must be applied to indium foil measurements made near high energy neutron sources, because of activation of the indium by resonance neutrons about 1.44 ev. (19, 41).

According to Hill, Roberts and McCammon, (19), at points close to a source of high energy neutrons in graphite, a good part of the foil activation is due to absorption of neutrons above an energy of 1.44 ev. Farther from the source, the perturbation due to higher resonances becomes less so that this correction factor becomes negligible.

The experimental technique for determining the correction factor to be applied to the measured activity of the cadmium covered indium foils consists of comparing the activity of indium foils covered by both cadmium and indium with the activity of foils covered by cadmium. Since the resonances of indium 115 above 1.44 ev are weak compared with the resonance at 1.44 ev, the self-shielding of the high energy resonances is small compared with that of the 1.44 ev resonance. Consequently, covering the foils with indium will have little effect on the activation by neutrons of higher energy, but will decrease the activation at 1.44 ev by a large factor.

At distances less than $\sqrt{\tau}$ from the source (41), the total activation of cadmium covered foils is

$$A_{\text{CdInCd}} = A_{1.44 \text{ ev}} + A_{\text{higher energy}}. \quad (\text{H-1})$$

At distances of two or three times $\sqrt{\tau}$ from the source, the activation by high energy neutrons is negligible so that the activation is

$$A_{\text{CdInCd}} = A_{1.44 \text{ ev}} \quad (\text{H-2})$$

For the case in which the foils are covered with both indium and cadmium, Eqs. (H-1) and (H-2) can be written, respectively

$$A_{\text{CdInInInCd}} = g_0 A_{1.44 \text{ ev}} + A_{\text{higher energy}} \quad (\text{H-3})$$

$$A_{\text{CdInInInCd}} = g_0 A_{1.44 \text{ ev}} \quad (\text{H-4})$$

where g_0 is a shielding factor for the indium foils at the 1.44 ev resonance. Equations (H-2) and (H-4) may be used to obtain g_0 and then Eqs. (H-1) and (H-3) may be solved simultaneously to obtain $A_{\text{higher energy}}$ from known measured values of A_{CdInCd} and A_{CdInCd} .

Additional experimental measurements were made by enclosing the detecting indium foil on each side with similar indium foils in addition to the usual cadmium cover. Cadmium covered indium foil measurements made by Steichen (39) were used for the unshielded measurements after verifying that Steichen's measurements could be reproduced.

Table 24 lists the experimental results of foil measurements and the ratio of the indium foil activities when covered with indium plus cadmium to the activities when covered only with cadmium. Fig. 27 is a plot of this ratio.

Table 24. Summary of data and results on resonance correction factor.

Distance from source	$A_{\text{CdInCd}}(39)$ counts in 27 minute counting period	A_{CdInInCd} counts in 27 minute counting period	Ratio	Per cent cor- rection to A_{CdInCd}
5.63	35,034 ± 92	15,101 ± 206	0.4310 ± 0.0060	6.73
15.82	27,536 ± 101	11,199 ± 73.3	0.4067 ± 0.0017	2.73
25.96	18,456 ± 42	7,325 ± 75.3	0.3969 ± 0.0042	0.82
36.11	10,706 ± 34	4,089 ± 63.0	0.3819 ± 0.0060	0.14
46.31	5,668 ± 35	2,230 ± 52.7	0.3934 ± 0.0096	
56.45	2,550 ± 32.9	1,104 ± 62.0	0.4329 ± 0.0250	
66.15	1,174 ± 27.8	470.4 ± 30.0	0.4008 ± 0.0271	
76.78	469 ± 26.2	178 ± 32.6	0.3795 ± 0.0725	

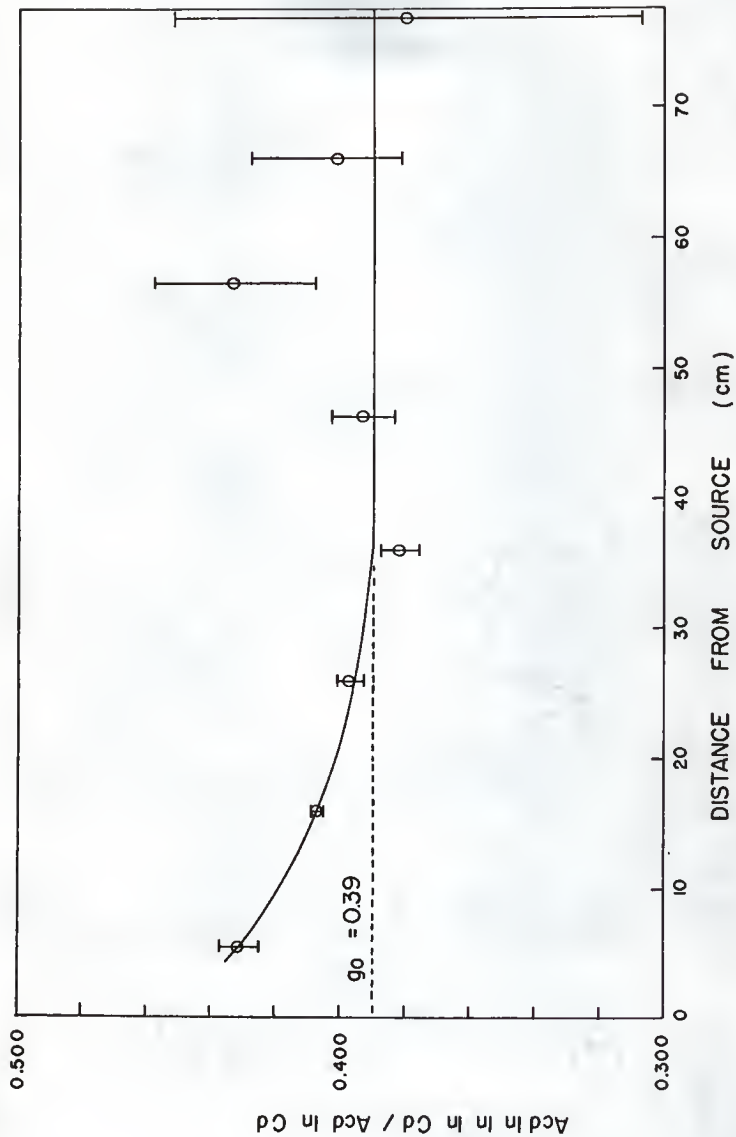


Fig. 27. Ratio of indium foil activities when covered with indium plus cadmium to the activities when covered with cadmium.

By assuming that the ratio will approach the constant shielding factor, g_0 , at points away from the source, a line representing this shielding factor has been approximated. With this approximation, a correction factor has been determined and plotted in Fig. 28 along with the results of other work done with this correction factor (19,41).

Absorption of Epithermal Neutrons in the Cadmium Filter

This correction factor, designated by F_{cd} , considers the absorption of epithermal neutrons in the cadmium foil covering. It is a function of both the thickness of the cadmium covering and the thickness of the foil. For the particular foils and covers used in this work, F_{cd} was 1.16. The graph from which it was obtained is available in many references, (2, 18, 28, 40).

This factor was measured by Tittle (40) by a technique that used successively different thicknesses of cadmium covering for a particular foil thickness, the correction factor being found from an extrapolation to zero cadmium thickness.

Finite Size of Source and Detector

To correct for the finite sizes of the source and detector, the following equation may be used for a circular source of radius a_1 and a circular detector of radius a_2 ,(41).

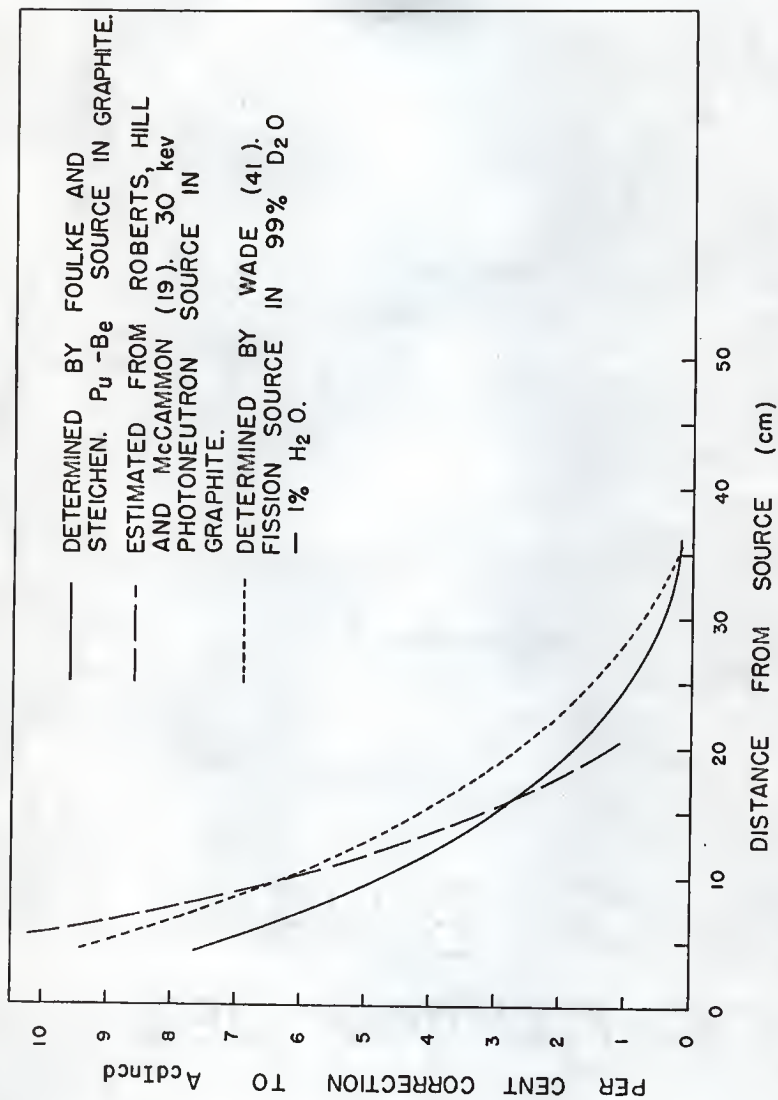


Fig. 28. Correction of indium foil activity for high energy neutron absorption.

$$A(r_0) - A_m(r_0) = - \left(\frac{a_1^2 + a_2^2}{4r_0} \right) \left(\frac{dA}{dr} \right)_{r=0} \quad (\text{H-5})$$

$A_m(r_0)$ is the observed activity at the distance r_0 between the centers of the source and detector. $A(r_0)$ is the ideal activity of a point source.

Steichen (39) has determined this correction factor for resonance neutron measurements. It is given in Fig. 29. It was applied to the resonance measurements made in this work. This factor would vary with the diffusing medium.

Variation in Foil Weights or Sizes

Graves and Froman (16) point out that for thick foils, variation in weight has a small effect so long as the foil area is constant from foil to foil. They state that only the activity of a thin foil is proportional to the mass of the foil, and that a correction for variation of foil mass is difficult to make for a foil of sufficient thickness to be usable. They feel that it is better to control the manufacture of the foils such that the variation in weight from foil to foil is very small.

In the fitting of the resonance activations described in the analytical portion of the work, it was found that consideration of the variation of the foil weights improved the results of the resonance data fit considerably. The average foil weight was 0.4592 grams with a maximum deviation of one per cent by any foil.

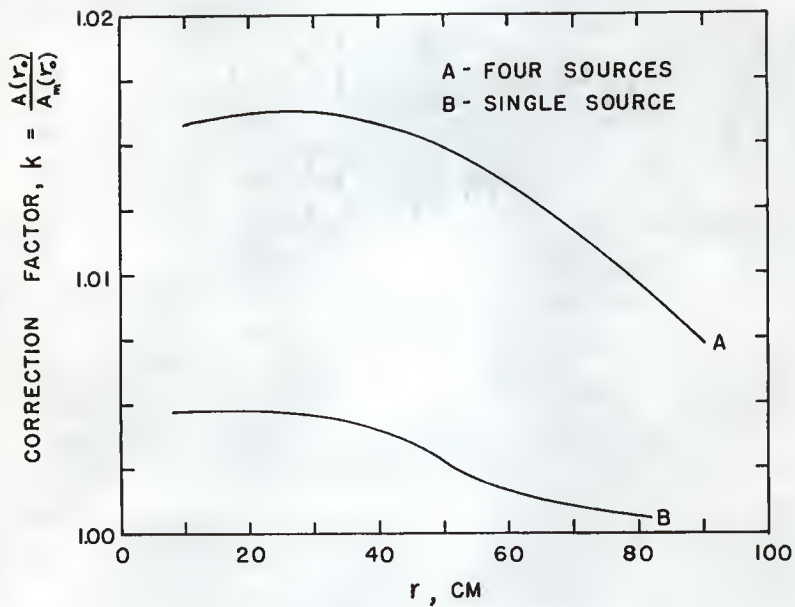


Fig. 29. Source and detector geometry correction factors for the single source and four source resonance distributions.

Unequal Activation of Two Sides of Foil

Since foils are seldom thin for neutrons or for the electrons produced by induced activation, the activity measured on different sides of the foil may be different. This difference depends upon the flux gradient in the neighborhood of the foil, (16). It is generally agreed (2, 16) that whenever the diffusion approximation is adequate to describe the neutron flux, the average of the measurements on both sides of a foil is proportional to the flux.

All foil data reported in this work is the average of measurements made on both sides of the foils.

Flux Depression in the Vicinity of the Foil

A flux detecting foil absorbs neutrons which would otherwise be able to scatter back and bolster the flux at the foil position. The magnitude of this flux depression depends upon the properties of the foil, the angular distribution of the neutrons in the foil vicinity, and the mean free path of neutrons in the surrounding medium (30).

This factor need not be considered when measurements with the standardized detector are made in the standardizing medium. If the standardized detector is used in other mediums, this factor may be easily determined from formulas given in various references, (28, 31, 34).

This correction for flux depression need not be considered for measurements of slowing down density at indium resonance energy. Absorption of an epithermal neutron does not remove a neutron which

could be scattered back to bolster the flux; since in order for the neutron to be scattered back to the detector position, the neutron must suffer an energy degrading collision. Thus the neutron may not have the resonance energy and would not be eligible to bolster the resonance energy flux.

Self-protection of the Foil by Its Outer Layers

This consideration takes into account the fact that atoms in internal layers of a thick detector are exposed to a neutron flux smaller than that impinging on the surface of the foil. The self-protection ratio is the ratio of the gross activation of the foil to the quantity calculated by multiplying the macroscopic cross section for activation by the surface flux (31). Determination of this self-protection ratio is outlined in reference (31).

This factor does not depend upon foil position and may be considered a constant for any medium and position. It is a function of only the foil material and thickness, and the nature of the flux. It would be necessary to apply this correction factor if a collimated flux were being measured. For the assumed isotropic flux in this work, this correction factor has not been considered.

Mutual Shadowing of Neighboring Foils

It is possible to irradiate resonance detectors near enough to each other to cause an effect by one foil upon the other. Approximate values for the fractional loss of resonance activations due to the presence of a neighboring foil are given in reference (30). For the particular

foils and foil spacings used in this work, the effect of one foil on the other was estimated to be negligible.

Hardening of the Neutron Spectrum through the Foil

The correction for the hardening of the spectrum arises from the fact that neutrons of lower energy are preferentially absorbed in the first few layers of a thick foil. Thus the neutrons reaching the internal layers of the detector will be of higher average energy and will be subject to different capture cross sections.

Amaldi (2) and Hughes (20) give complete discussions of this effect. It has not been considered in this work.

Obliquity of Foil with Respect to the Source

Even though the direction of most of the neutrons through the foil does not affect the activation directly, it does affect the correction factors that depend on foil thickness since the effective foil thickness is a function of obliquity, (20).

All experimental work in this paper was performed with the normal to the foil surface area facing the source. If need arises to irradiate the foil in a different manner, it might be of interest to experimentally determine the magnitude of this effect.

No effort to further systematize these foil correction factors has been made in this work. It might be desirable to have a more complete study of these factors. A determination of the absolute, unperturbed flux from absolute foil counting would require application of many of the factors introduced.

KSU PILE STANDARDIZATION AND STUDY OF
SLOWING DOWN AND DIFFUSION MODELS

by

LARRY RAY FOULKE

B. S., Kansas State University, 1960

AN ABSTRACT OF A THESIS

submitted in partial fulfillment of the

requirements for the degree

MASTER OF SCIENCE

Department of Nuclear Engineering

KANSAS STATE UNIVERSITY
Manhattan, Kansas

1961

The Kansas State University Graphite Pile was calibrated for absolute thermal neutron flux with a one curie Pu-Be neutron source, thus standardizing indium foils, a BF_3 probe and a scintillation probe. The sensitivities of these detectors to thermal and indium resonance neutrons are given.

Based on the neutron emission rate of the source, absolute values of the measured slowing down density at indium resonance energy were obtained from the volume integral of the slowing down density over a pile of assumed infinite height. The absolute thermal neutron flux was then obtained from the thermal diffusion equation using as a source condition the absolute slowing down density at indium resonance energy extended to the absolute slowing down density at thermal energy by use of Fermi slowing down theory.

The standardized detectors were used to test experimentally the validity of the diffusion equation in a finite pile geometry, using as a source condition to the thermal diffusion equation: (a) the solution to the Fermi age equation evaluated at thermal energy, (b) a thermal point neutron source, and (c) the analytical expression for the slowing down density at thermal energy as found from the standard pile measurements.

The techniques used in accurate foil activation measurements are discussed. Inconsistent values of various diffusion parameters for graphite are pointed out. IBM-650 programs are given to fit empirically the indium resonance foil activations, to calculate the thermal flux from a fast point source in an infinite column, to calculate the thermal flux from a fast point source in a finite medium, and to calculate the thermal flux from a thermal point source in a finite medium.